CELLULAR AND CIRCUIT MECHANISMS OF ANTI-NMDA RECEPTOR AUTOIMMUNE ENCEPHALITIS

Pavel Švehla

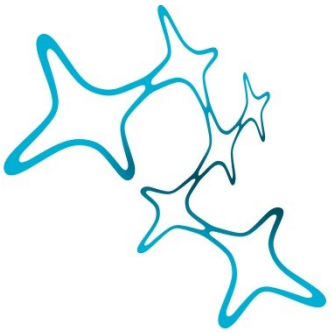

Graduate School of
Systemic Neurosciences

LMU Munich

Dissertation at the
Graduate School of Systemic Neurosciences
Ludwig-Maximilians-Universität München

February 2022

Supervisor
Dr. Dr. Sabine Liebscher
Institute of Clinical Neuroimmunology
University hospital and Biomedical Centre of the
Ludwig-Maximilians-Universität München

First Reviewer: Dr. Dr. Sabine Liebscher
Second Reviewer: Prof. Dr. Martin Kerschensteiner
External Reviewer: Dr. Christoph Schmidt-Hieber

Date of Submission: February 11, 2022
Date of Defense: May 24, 2022

Dinge erscheinen unmöglich.
Bis man sie tut.

Table of Contents

List of Abbreviations

AD	Alzheimer's disease
ALS	Amyotrophic lateral sclerosis
AMPAR	α-amino-3-hydroxy-5-methyl-4-isoxazolepropionic acid receptor
APV	(2R)-amino-5-phosphonovaleric acid
BBB	Blood brain barrier
CA	Cornu ammonis
CaM	Calmodulin
CaMKII	Calmodulin-dependent protein kinase II
CNMF	Constrained non-negative matrix factorization
COM	Centre of mass
CPP	3-[(R)-2-carboxypiperazin-4-yl]-propyl-1-phosphonic acid
CSF	Cerebrospinal fluid
DG	Dentate gyrus
EAE	Experimental autoimmune encephalomyelitis
EEG	Electro-encephalogram
FOV	Field of view
GABA	Gamma-aminobutyric acid
GFP	Green fluorescent protein
HM	Henry Molaison
HSV	Herpes simplex virus
LEC	Lateral entorhinal cortex
LTD	Long-term depression
LTP	Long-term potentiation
ME	Mean error
MEC	Medial entorhinal cortex
MOG	Myelin oligodendrocyte glycoprotein
NGS	Normal goat serum
NMDA	N-methyl-D-aspartate
NMDAR	N-methyl-D-aspartate receptor
PBS	Phosphate buffered saline
PCA	Principal component analysis
PCR	Polymerase chain reaction
PFA	Paraformaldehyde
POV	Population vector
PSD	Post-synaptic density
PV	Parvalbumin
REM	Rapid eye movement
ROI	Region of interest
SD	Standard deviation
SEM	Standard error of the mean
SST	Somatostatin
STED	Stimulated emission depletion
SWR	Sharp-wave ripples

List of Figures

List of Tables

Abstract

Anti-N-methyl-D-aspartate receptor (NMDAR) autoimmune encephalitis is a rare but severe disease of the central nervous system (CNS). Patients suffering from this antibody-mediated disease experience cognitive and memory deficits, which, if untreated, can progress to severe neurological symptoms and even to death. The aim of this PhD project was to investigate cellular and circuit mechanisms of NMDAR encephalitis in a mouse model of the disease, employing passive transfer of recombinant monoclonal NMDAR antibodies into the brain with minipumps over 18 days. Specifically, I focused on structural and functional alterations of neurons in the CA1 layer of the hippocampus. Using confocal imaging in *ex vivo* preparations of hippocampal pyramidal neurons and interneurons expressing GFP, I show that NMDAR antibodies alter dendritic spines, the structural correlates of learning and memory, with interneurons affected differentially than pyramidal neurons in CA1. While dendritic spine density of pyramidal cells remained unchanged, dendritic spine density of interneurons was increased. Moreover, all spines were affected morphologically. These results demonstrate that interneurons may be more sensitive to NMDAR signalling perturbations. I next addressed how NMDAR antibodies affect neuronal function and thus performed *in vivo* two-photon Ca^{2+} imaging in animals performing a spatial navigation task, to investigate the stability and plasticity of hippocampal spatial representations thereby assessing memory and cognition in the mouse. Interestingly, animals that received NMDAR antibodies were not impaired in performance of the spatial navigation task, when compared to control animals. Furthermore, these animals did not exhibit differences in place cell coding, with spatial information content, place field size, reliability and place field shift comparable to controls. However, as a result of the chronic infusion of NMDAR antibodies, place cell activity became more confined, as indicated by a lower number of place fields per place cell, and became more stable, as indicated by a higher correlation of place fields between sessions and higher place cell recurrence. These findings corroborate earlier reports arguing for an increase in place cell stability upon pharmacological NMDAR blockade, thus emphasizing the pathophysiological role of compromised NMDAR function in NMDAR encephalitis. Importantly, the representational drift of place cells was reduced, possibly as a result of LTP decay inhibition and PV interneuron activity decrease. Taken together, these results demonstrate the effect of NMDAR antibodies on structure and

function of CA1 neurons in a mechanism consistent with reduced NMDAR signalling caused by NMDAR antibodies.

Zusammenfassung

Die Anti-N-Methyl-D-Aspartat-Rezeptor (NMDAR) Autoimmunenzephalitis ist eine seltene, aber schwere Erkrankung des Zentralnervensystems. Patienten, die an dieser Antikörper-vermittelten Krankheit leiden, haben kognitive Defizite und Gedächtnisdefizite, die unbehandelt zu schweren neurologischen Symptomen und sogar zum Tod führen können. Das Ziel dieser Doktorarbeit war die zellulären Mechanismen der NMDAR-Enzephalitis in einem passiven Transfer-Mausmodell mit rekombinanten monoklonalen NMDAR-Antikörpern zu untersuchen. Insbesondere konzentrierte ich mich auf strukturelle und funktionelle Veränderungen von Neuronen in der CA1-Schicht des Hippocampus. Unter Verwendung der konfokalen Mikroskopie in *ex vivo* Präparationen von hippocampalen GFP-exprimierenden Pyramidenneuronen und Interneuronen zeige ich, dass NMDAR-Antikörper dendritische Dornen, die strukturellen Korrelate erregender Postsynapsen, verändern, wobei Interneurone in CA1 anders beeinflusst werden als pyramidale Neurone. Während die dendritische Dornendichte von Pyramidenzellen unverändert blieb, war die dendritische Dornendichte von Interneuronen erhöht. Darüber hinaus waren alle Dornen morphologisch betroffen. Diese Ergebnisse zeigen, dass Interneurone empfindlicher auf NMDAR-Signalstörungen reagieren können und legen nahe, dass die Plastizität des dendritisches Dornen durch NMDAR-Antikörper beeinflusst werden kann. Mittels *in vivo* Zweiphotonen-Ca^{2+}-Imaging durchgeführt in Tieren, während sie eine Navigationsaufgabe ausführen, untersuchte ich die Stabilität und Plastizität von ‚Ortszellen' (engl. place cells), welche dadurch charakterisiert sind, dass sie aktiv werden, wenn sich das Tier an einer bestimmten Position in einer Umgebung befindet. Interessanterweise waren Tiere, die NMDAR-Antikörper erhielten, in der Ausführung der Navigationsaufgabe im Vergleich zu Kontrolltieren nicht beeinträchtigt. Darüber hinaus unterschieden sich die Ortszellen in Antikörper-infundierten Tieren nicht hinsichtlich Informationsgehalt, Feldgröße, Feldverschiebung und Zuverlässigkeit im Vergleich zu Kontrolltiere. Nach der chronischen Infusion von NMDAR-Antikörpern wurde die Ortszellaktivität jedoch definierter und wies eine geringere Anzahl von Ortsfeldern auf. Zudem erhöhte sich die Stabilität der Antworteigenschaft dieser Ortszellen, was durch eine erhöhte Korrelation der Ortsfelder und eine grössere Wiederholungsrate nachweisbar war. Pharmakologische Untersuchungen mit NMDAR Blockern kamen interessanterweise zu ähnlichen Ergebnissen und legen somit nahe, das der pathophysiologische Mechanismus

des Autoantikörper-vermittelten Kognitionsdefizits primär auf einer funktioneller Einschränkung des NMDAR beruht (Hayashi, 2019; Silva et al., 2015). Wichtig ist, dass die Dynamik (repräsentationale Drift) der Ortszellen abnahm, möglicherweise als Folge prolongierter Langzeitpotenzierung (LTP) und der Abnahme der PV-Interneuronenaktivität. Zusammengefasst zeigen diese Ergebnisse die Wirkung von NMDAR-Antikörpern auf Struktur und Funktion von CA1-Neuronen in einem Mechanismus, der mit einer durch die NMDAR-Antikörper verursachten reduzierten NMDAR-Signalgebung konsistent ist.

1. INTRODUCTION

1.1. AUTOIMMUNE ENCEPHALITIS

The term encephalitis first came into public awareness during the 1917-1926 pandemic of encephalitis lethargica, also known as sleepy sickness. It was a devastating and mysterious disease that killed approximately 500,000 people worldwide and left many more with permanent symptoms such as parkinsonism or psychosis. Given that it coincided with the 1918 Spanish flu pandemic, many contemporary hypotheses were developed around the infectious origin of encephalitis lethargica (McCall et al., 2008). A recent study in patients presenting with similar symptoms brought forward the idea that it may have been caused by autoimmune processes targeting deep grey matter neurons (Dale et al., 2004).

The example of encephalitis lethargica illustrates how enigmatic manifestations of autoimmunity can be. Autoimmune encephalitis is a disease characterized by brain inflammation caused by autoimmune processes. It is no longer a rarity but rather gaining on importance, as the prevalence of autoimmune encephalitis is comparable to infectious encephalitis (13.7/100,000 and 11.6/100,000 for autoimmune and infectious encephalitis, respectively), and the detection of autoimmune encephalitis is still increasing (Dubey et al., 2018).

1.1.1. Anti-N-methyl-D-aspartate Receptor (NMDAR) autoimmune encephalitis

History

Anti-N-methyl-D-aspartate receptor (NMDAR) autoimmune encephalitis was originally identified in four young women with ovarian teratoma, who developed acute psychiatric symptoms, seizures, memory deficits, decreased level of consciousness and hypoventilation. Cerebrospinal fluid (CSF) samples from these patients hinted at inflammatory abnormalities and when researchers incubated the serum or CSF with live hippocampal neurons, antibodies bound to an antigen expressed at the cytoplasmic membrane (Vitaliani et al., 2005). Thus, the initial report suggested that this disorder is directly antibody mediated.

Direct proof came several years later, when Dalmau et al. (2007) demonstrated that CSF and serum from encephalitis patients contained antibodies that reacted with NMDAR. All teratomas examined in that study contained nervous tissue and strongly expressed NMDAR and reacted with patients' antibodies. Autopsies of NMDAR encephalitis patients showed extensive microgliosis, rare T-cell infiltrates, and neuronal degeneration predominantly in the hippocampus (Dalmau et al., 2007).

Although initially described as a female disease linked to ovarian teratoma, it has been since appreciated that men can also be affected by the disease and the symptoms may develop in the presence of a tumour as well as without it. Nevertheless, this disease affects mostly young female patients - female to male ratio is 8:2 and 37% of patients are younger than 18 years at presentation of the disease (Dalmau et al., 2019).

Clinical course

The disease manifest clinically in several distinct stages: Initially, patients typically present with a viral prodrome lasting several weeks, which deteriorates into psychiatric symptoms, such as hallucinations, mania, agitation and confusion (Figure 1). In most cases, the disease progresses into severe neurological symptoms (hypoventilation, stereotypical movements, seizures, coma), often requiring intensive care unit hospitalization (Dalmau et al., 2008). Typical treatment strategies involve tumour resection (if identified), aggressive immunosuppression with steroid treatment and B cell depletion with rituximab (Prüss, 2021). This strategy achieves overwhelmingly positive outcomes, 80% of patients fully recover and only 12% of patients relapse within 2 years (Titulaer et al., 2013). Although diagnosis of NMDAR encephalitis is challenging at symptom onset, it has become clinically recognizable and effective treatment is available. It is diagnosed through IgG antibody detection in the CSF using a commercially available essay (Euroimmun) and is often accompanied by oligoclonal bands. Best predictor of the clinical outcome are antibody titres in the CSF rather than in the serum (Gresa-Arribas et al., 2014).

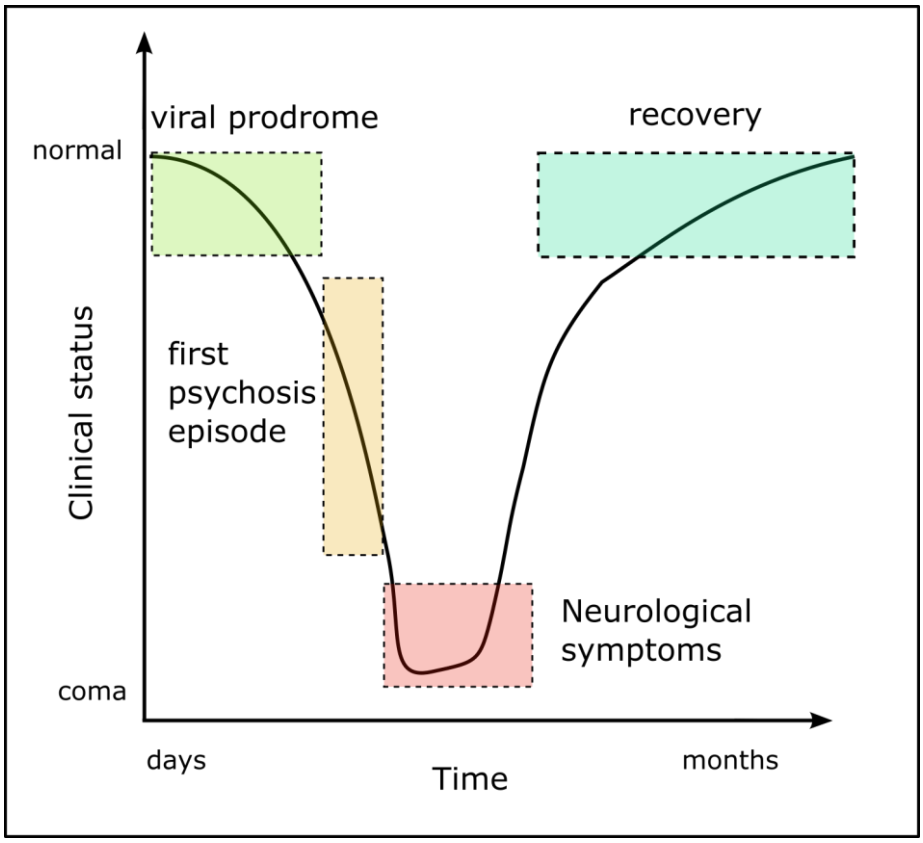

Figure 1. **Clinical course of NMDAR encephalitis.** Initial symptoms include a viral-like prodrome followed by a first psychosis episode, characterized by agitation and confusion. Symptoms progress into serious neurological symptoms such as seizures and coma. Available treatment is effective with 80% patients reaching full recovery. If untreated, NMDAR encephalitis could be fatal. Modified after Kayser and Dalmau (2016).

Knut

Probably the most famous patient with NMDAR encephalitis was Knut the polar bear (Ursus maritimus), who drowned in 2011 in the Berlin Zoological Garden following a seizure. Using the diagnostic criteria applied to human patients, Knut was shown to have suffered from NMDAR encephalitis. A high concentration of NMDAR antibodies was detected in Knut's CSF and his brain showed plasma cell infiltration with minimal neuronal loss. Knut was the first non-human case of this disease, and this finding suggested that it might be a disease relevant to other mammals (Prüss et al. 2015). The unfortunate tale of Knut helped to raise public awareness of new autoimmune diseases.

1.1.2. Cellular and molecular mechanisms of NMDAR encephalitis

Mechanism of humoral (auto)immunity

Since its discovery 14 years ago, it has become widely accepted that NMDAR encephalitis is predominantly antibody mediated. The origin of autoantibody producing autoreactive B cells has been a subject of intensive research. B cells undergo positive and negative selection, while developing in the bone marrow to ensure proper development, both

involving B cell receptors on the cytoplasmic membrane. Negative selection occurs through the presentation of self-antigens to the B cell; if it reacts to the self-antigen, then the B cell undergoes one of three fates: clonal deletion (apoptosis), receptor editing or anergy (dormant state). B cells further mature in germinal centres after antigen-mediated activation and undergo clonal expansion, affinity maturation and class switch to become memory B cells or plasma cells (Abbas et al., 2021). During B cell development, antibodies are assembled by random gene segment reassortment to produce a vast number of specificities. Interestingly, most of all antibodies expressed by immature B cells are self-reactive and are removed at central and peripheral checkpoints during B cell development (Wardemann et al., 2003). Such mechanisms of immune system tolerance ensure that mature B cells do not bind self-antigens.

The risk of developing autoreactive antibodies lies in the disruption of checkpoint regulation, which could lead to autoreactive clones evading the checkpoints. This has been proposed as a possible cause of several autoimmune diseases, in some cases associated with primary immune system deficiency, but not in the case of NMDAR encephalitis (Prüss, 2021). Therefore, NMDAR encephalitis probably occurs as a correct reaction to an incorrectly placed antigen (i.e., tumour).

T cells appear to be important for NMDAR encephalitis as well, as indicated by the perivascular T cell infiltrates, primarily CD4+ T helper cells, in patient autopsies (Tüzün et al., 2009). Indeed, presence of mature T helper cells is necessary for disease development in mice (Jones et al., 2019). This highlights the importance of T cell – B cell interaction in antibody mediated autoimmunity. Specifically, there could be a role of NMDAR-specific T helper cells in the generation of mature B cells producing NMDAR-specific antibodies (Dao et al., 2021). In addition, antigen-specific T cells could stimulate the maturation of autoreactive B cells in a scenario where B cells present the antigen to T cells (e.g., a viral protein) together with an autoantigen (Sanderson et al., 2017). This mechanism could explain the strong link between infection and autoimmunity.

The variable clinical manifestation of the same pathogenic antibody in individual patients may be attributed to several factors, such as affinity of the antibody for its epitope or glycosylation of NMDAR receptor interfering with antibody access, but most likely the biggest source of variability is the amount of intrathecal synthesis of antibodies by plasma cells (Prüss, 2021).

Antibody-mediated receptor internalization

NMDARs are heterotetrameric receptors composed of two obligatory GluN1 subunits in combination with two GluN2 (further subtypes GluN2A-D) and/or GluN3 subunits (Monyer et al., 1992). While all combinations are possible, most frequent compositions of subunits are two GluN1 with two GluN2A or GluN2B. GluN2A-NMDARs are predominantly anchored at the postsynaptic density of synapses, whereas GluN2B-NMDARs are usually located in the extrasynaptic portion of the cytoplasmic membrane (Papouin et al., 2012).

The main pathological effect of autoantibodies is mediated by reversible internalization of NMDARs, both synaptic as well as extrasynaptic receptors, while sparing other glutamate receptors and post-synaptic density proteins (Hughes et al., 2010; Planagumà et al., 2015). In case of the GluN1 antibody, internalization occurs through antibody binding to asparagine in 368. position on the extracellular amino-terminal domain of GluN1 leading to crosslinking of the receptors, which targets them for internalization and lysosomal degradation (Kreye et al., 2016). Loss of NMDARs from the cytoplasmic membrane is positively correlated with antibody titre (Hughes et al., 2010) and antibodies are solely responsible for receptor internalization, since their depletion from the CSF abrogates these effects. *In vitro* studies of NMDAR internalization have shown that antibody effects begin to take place 2 hours after the exposure, with the peak of NMDAR reduction at 12 hours after exposure. After that, there is a steady state of NMDAR levels for as long as the neurons are exposed to the antibody. This may reflect a population of receptors unaffected by the antibodies or represent a state of equilibrium between internalization and insertion of NMDARs. This internalization effect is independent of NMDAR activity since no difference was observed after agonist addition. Decrease in available receptors does not induce compensatory changes in glutamate receptor gene expression (Moscato et al., 2014).

Treatment of cultured neurons with NMDAR antibodies decreases NMDA evoked currents, which is mediated by removal of functional receptors from the membrane (Moscato et al., 2014) rather than by direct allosteric blockade (Jones et al., 2019). As a consequence of NMDAR current reduction, synaptic plasticity is impaired as evidenced by a reduction of long-term potentiation (LTP) in cultured hippocampal neurons (Mikasova et al., 2012) as well as *in vivo* (Rosch et al., 2018). These effects do not seem to be specific to a neuronal population since both excitatory and inhibitory neurons are affected to the same degree (Moscato et al., 2014). Although neurons are impaired

functionally, their structure remains largely normal, since the number of synapses and dendritic structure or survival of cultured hippocampal neurons is not affected (Hughes et al., 2010). However, a decrease in inhibitory synapse density on excitatory neurons has been reported (Moscato et al., 2014). This could result in increased excitability, and is complemented by the increase of extracellular glutamate upon antibody injection into the brain (Manto et al., 2010).

Receptor trafficking dysregulation

NMDARs interact with many scaffolding proteins and binding partners, one of which is the Ephrin type B2 receptor (EphB2R). EphB2R is a tyrosine kinase receptor that modulates synaptic plasticity through stabilization and clustering of NMDAR in the postsynaptic membrane. This effect is dependent on the ephrin-B2 ligand binding to EphB2R and is mediated through conformational changes of the receptor (Dalva et al., 2000). At synapses, antibodies cause a rapid dispersion of GluN2A-NMDAR preventing their synaptic retention through blockade of NMDAR-EphB2R interaction. In contrast, extrasynaptic GluN2B-NMDAR trafficking is reduced, consistent with receptor crosslinking and subsequent internalization (Mikasova et al., 2012), suggesting that NMDARs with different subunit composition are differentially affected by the antibodies. This finding proposed an additional mechanism of pathology though antibody-mediated disruption of NMDAR stabilization at synapses by EphB2R, in addition to the antibody-mediated internalization of NMDARs (Hughes et al., 2010).

Planagumà et al. (2016) demonstrated the effectiveness of ephrin-B2 in antagonizing the deficits in the mouse model of NMDAR encephalitis by co-infusing ephrin-B2 intrathecally together with patient antibodies. They showed that all antibody-mediated effects, ranging from impaired behaviour to reduced synaptic plasticity, can be prevented or mitigated by the administration of soluble ephrin-B2. The authors hypothesise that antibody binding to NMDAR directly interferes with EphB2R interaction, which results in a reduction of the fraction of synaptic NMDARs as well as a reduction in phosphorylation of NMDAR through the kinase activity of EphB2R. This study also extended the understanding of the pathophysiology of NMDAR encephalitis by showing that changes are specific to the post-synapse: in contrast to severe LTP reduction, paired-pulse facilitation was unaffected, suggesting largely intact presynaptic release mechanisms (Planagumà et al., 2016).

Further studies focusing on binding partners of NMDARs showed that dopamine receptor D1 dynamics are altered by NMDAR antibodies through surface crosstalk between

NMDAR and D1 (Gréa et al., 2019). These synaptic receptor dynamics alterations by NMDAR antibodies from patient CSF have disruptive effects on dopamine signalling and cause changes in cell-surface dopamine receptor cluster density (D1R decrease, D2R increase; Carceles-Cordon et al., 2020).

Taken together, two pathological mechanisms conveyed by autoantibodies have been proposed: receptor internalization and trafficking disruption. Moreover, these findings show a delicate interplay of synaptic receptors and proteins through mutual stabilization in post-synaptic complexes, the disruption of which has detrimental effects on neuronal function.

1.1.3. Relevance of antibodies in health and disease

There has been an ongoing discussion about the relevance of circulating anti-NMDAR antibodies in healthy people and patients suffering from various psychiatric diseases. This section recapitulates the shifting views in the field over the past decade.

NMDAR antibody immunoglobulin classes

The initial description of NMDAR encephalitis identified IgG antibody class as the main mediator of the disease, and IgG antibodies were seen as the hallmark of the disease as well as a predictor of clinical outcome (Dalmau et al., 2007; Hughes et al., 2010). The picture of the disease with IgG as the main culprit was challenged when a large study (> 5000 individuals) described 20 % seroprevalence in the general population, regardless of the clinical status (i.e., healthy or diseased). When seroprevalence of individual immunoglobulin subtypes was investigated, all immunoglobulin classes were found (except IgE) with a prevalence of IgA > IgM > IgG, and seroprevalence significantly increased with age and was higher in men than women (Hammer et al., 2014). *In vitro* internalization essays showed functionality of all investigated antibodies, thereby suggesting that all naturally occurring antibodies against the NMDAR have pathogenic potential irrespective of the epitope and immunoglobulin class (Castillo-Gómez et al., 2017).

To account for the pathogenicity of NMDAR antibodies in the disease, it was suggested that the blood brain barrier (BBB) plays a decisive role in enabling access of antibodies to the brain parenchyma. This central role of BBB was supported by the finding that antibodies cause deficits only in ApoE mutant mice (leaky BBB), as well as schizophrenic patients with history of birth complications or neurotrauma having more severe symptoms, indicating past or present BBB insufficiency. Therefore according to this

hypothesis, naturally occurring NMDAR antibodies must cross the BBB for exerting pathological effects or antibody must be secreted intrathecally by B cells (Hammer et al., 2014).

Remarkably, not only humans, but also other mammals, such as dogs, cats, mice, rats and monkeys, show high seroprevalence of NMDAR antibodies, with Ig class distribution comparable with humans. Functionality of all antibodies across species was again verified by NMDAR endocytosis essays and a positive correlation between antibody titre and age was shown for different species and antibody classes (Pan et al., 2018).

NMDAR antibodies in healthy population

The origin of the disease is also subject of a heated debate. An association was uncovered between influenza antibody and NMDAR antibody seropositivity, suggesting molecular mimicry could play a role (Hammer et al., 2014). The same authors hypothesise that one of the driving factors is chronic stress, supporting their view on the loss of seroprevalence age dependence in monkeys (long life in captivity is a proven stressor) and human migrants (described by the authors as suffering from 'unfriendly environment'; Pan *et al.*, 2018). A further link between the NMDAR encephalitis and infection is provided by the finding that 27% patients with herpes simplex virus 1 (HSV) encephalitis develop autoimmune encephalitis, often associated with NMDAR antibodies (Armangue et al., 2018; Prüss et al., 2012).

The absence of evidence of brain inflammation in the passive transfer mouse models of NMDAR encephalitis, such as T-cell infiltration (Planagumà et al., 2015) or microgliosis (Pan et al., 2018), led some authors to conclude that antibodies do not cause encephalitis but only shape behavioural phenotype upon entering the brain (Hammer et al., 2014). Further speculations emerged that NMDAR antibodies may have a detrimental effect on the immune system itself by modulating B and T cell function via their surface NMDARs, and NMDAR encephalitis could be a result of such a dysregulation of the immune system (Ehrenreich, 2018). Some authors go as far as casting doubts on whether NMDAR encephalitis is a separate disease entity and should be treated as such (Ehrenreich, 2018, 2017).

NMDAR antibodies in psychosis

On the other hand, a much smaller study by Jézéquel et al. (2017), comprised of 48 schizophrenic patients and 102 controls, reported the presence of circulating IgG NMDAR antibodies in about 20% of psychotic patients diagnosed with schizophrenia and only

very few healthy subjects. By employing a sophisticated imaging technique able to track a single molecule using quantum dot nanoparticles, they show that antibodies from patients, but not healthy subjects, specifically alter surface dynamics and nanoscale organisation of NMDAR. They show increased motility of synaptic NMDARs, which leads to higher exchange rate between synaptic and extrasynaptic compartments and thus decreased fraction of available NMDAR at the post synaptic density. Moreover, antibodies from patients and controls do not compete for the binding site on NMDAR, suggesting they target different epitopes with potentially different relevance for pathology. Importantly, they show that psychotic patient antibodies cause synaptic plasticity deficits, while antibodies from healthy controls have no effect. Taken together, they suggest a pathogenically relevant role of NMDAR antibodies in schizophrenic patients and so the term 'autoimmune psychosis' was coined (Jézéquel et al., 2017).

Another study of 300 patients contradicted these findings by showing that none of the schizophrenic patients had NMDAR antibodies of the IgG class. Moreover, only IgG NMDAR antibodies are highly specific for NMDAR encephalitis and cause a decrease of NMDAR levels. In contrast, IgA or IgM antibodies occur infrequently and non-specifically in other diseases and do not alter the receptor levels (Hara et al., 2018). Several other studies attempted to replicate the high seropositivity of psychotic patients for NMDAR antibodies and reported that these cases in psychotic patients are extremely rare (Bien et al., 2021; Kelleher et al., 2020). Consequently, the newly emerged field of autoimmune psychosis was once again disproved (Graus and Dalmau, 2021).

Untangling inconsistencies

Untangling apparent inconsistencies in the published literature is not an easy task, and further research is needed to reconcile the opposing opinions in the field and shed more light on the significance of NMDAR antibodies in various diseases and the contribution of different immunoglobulin classes to NMDAR encephalitis phenotype (Figure 2). The discrepancies may be assigned to the detection techniques used in different studies, such as immunofluorescence with live or fixed cells expressing NMDARs, serum incubation with rat brain sections or more sophisticated essays (single molecule imaging). Nonetheless, specificity of some of these essays might be questioned. Samples used for NMDAR antibody detection (i.e., CSF or serum) also varied between the studies, highlighting the importance of CSF analysis for reliable detection of autoantibodies. Indeed, CSF-only reactivity has been shown for ~25 % cases of NMDAR encephalitis (Gresa-Arribas et al., 2014).

The presence of germline antibodies against NMDARs in NMDAR encephalitis patients indicates that tolerance induction against the NMDAR protein is incomplete or absent (Kreye et al., 2016). Under physiological conditions and without access to the brain the presence of peripheral antibodies may not pose a risk. In case of NMDAR exposure to the immune system through a tumour, this may trigger positive selection and expansion of high-affinity NMDAR-reactive B cells. When these affinity-matured cells access the brain and get activated through exposure to the autoantigen, these memory B cells then induce and fuel full-blown encephalitis.

Current status of the field

A following summary can be drawn: Antibodies to central nervous system antigens, such as NMDAR antibodies, may be a part of the normal immune repertoire of mammals. They may be converted to immunogens via exposure to brain antigens outside the central nervous system (teratoma or through cell injury/death), infection (HSV, influenza) or chronic life stress. However, the key fact remains: patients with NMDAR antibodies in CSF have NMDAR encephalitis and suffer from severe psychiatric symptoms, which is compatible with the glutamate hypothesis of psychosis and schizophrenia given the molecular mechanism of antibody-mediated receptor internalization.

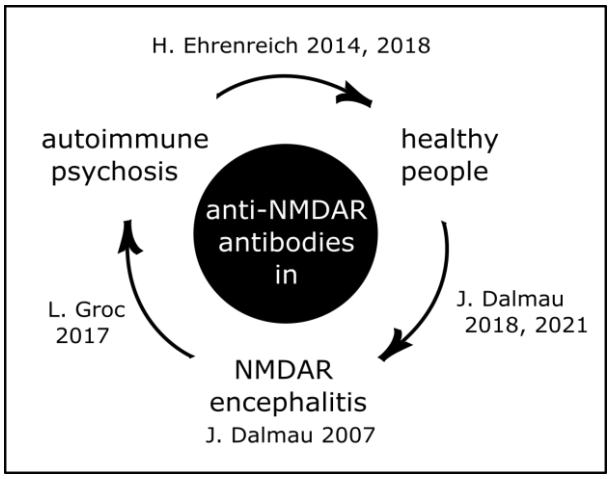

Figure 2. **Shifting views in the field of NMDAR encephalitis.** Since the initial discovery of NMDAR encephalitis 14 years ago, investigations of NMDAR antibodies have gradually shifted from NMDAR encephalitis patients to psychotic patients, suggesting an autoimmune origin of many psychiatric diseases. This was later disproved. Broad seroprevalence of NMDAR antibodies in healthy individuals was also suggested and doubts were cast about relevance of antibodies in disease. Due to low specificity of autoantibodies detected in healthy people, studies refocused on first onset psychosis patients, which subsequently leads back to NMDAR encephalitis. Key publications with senior authors and respective print years are highlighted.

1.1.4. Mouse models of NMDAR encephalitis

Passive transfer mouse model

The mouse model of NMDAR encephalitis was initially reported by Planagumà et al. (2015). In this model of passive transfer of human antibodies, CSF from patients or healthy controls was infused into mice using an intracerebroventricular catheter connected to subcutaneously implanted osmotic minipumps that continuously delivered

CSF over 14 days. Mice infused with patient CSF developed reversible memory deficits, anhedonic and depressive-like behaviour, without affecting their locomotor activity or social behaviour. Mice were examined for brain bound human antibodies and prominent deposits were found in hippocampi of mice infused with patient CSF, which were confirmed to target NMDAR subunits. Patient CSF infused mice had decreased NMDAR cluster density in the hippocampus, while post-synaptic density (PSD) protein-95 and α-amino-3-hydroxy-5-methyl-4-isoxazolepropionic acid receptor (AMPAR) density remained unaffected (Planagumà et al., 2015). This work was a cornerstone in the investigation the effect of NMDAR antibodies and was since adapted a number of times.

Monoclonal antibodies

Another breakthrough came when direct pathogenicity of NMDAR antibodies was proven (Kreye et al., 2016). A recombinant NMDAR antibody was generated from memory B cells isolated from CSF of patients through cloning of immunoglobulin genes from single B cells. The recombinant antibody recapitulated the NMDAR downregulation and NMDAR current reduction, the hallmark effects of patient CSF application in cultured neurons. Further evidence of the vital contribution of NMDAR antibodies in the disease pathology was brought forward when the monoclonal NMDAR antibody was shown to recapitulate all behavioural symptoms associated with the mouse model of patient CSF infusion (Malviya et al., 2017).

Active immunization

Since then, several mouse models employing an active immunization approach were developed. Mice infected with HSV spontaneously developed antibodies against NMDAR (Linnoila et al., 2019), providing a further link between NMDAR encephalitis and HSV infection in humans (Prüss et al., 2012). Spontaneous development of the disease in mice can also be achieved through active immunization with whole, conformationally stabilized NMDARs (Jones et al., 2019) or extracellular peptides of GluN1 subunit (Ding et al., 2021; Pan et al., 2018). While passive transfer of patient antibodies has been proven useful in isolating specific pathological effects of the recombinant antibody, mouse models employing active immunization are better suited for the investigation of disease mechanisms, since they better recapitulate the complete clinical picture, including neuroinflammation and immune cell infiltration (Jones et al., 2019). An advantage of the active immunization model can be its combination with immunosuppression, similarly to human therapy. Moreover, such a mouse model is an analogy to experimental

autoimmune encephalomyelitis (EAE), a well-established animal model for multiple sclerosis research (Robinson et al., 2014).

1.1.5. Autoimmune encephalitis spectrum

NMDAR encephalitis is currently the most common autoimmune encephalitis. Over the past decade, the field rapidly expanded with publications describing new pathological autoantibodies and distinguishing new disease entities. Several other antibodies target synaptic proteins and receptors, such as metabotropic glutamate receptor 1 (mGluR1; Smitt et al., 2000), aquaporin-4 (Lennon et al., 2005), AMPAR (Lai et al., 2009), myelin oligodendrocyte glycoprotein (MOG; Brilot et al., 2009), leucine-rich glioma activated 1 (LGI1; Lai et al., 2010), contactin-associated protein-like 2 (CASPR2; Irani et al., 2010) and mGluR5 (Spatola et al., 2018). Currently, 25 antibodies implicated in autoimmunity are known and new antibodies are being discovered, with respective clinical pictures varying widely from cognitive impairment and stereotypical movements to epileptic seizures.

Changing clinical practice

These discoveries have significantly improved clinical routines – several commercial diagnostic essays allow for routine testing for the presence of any of these autoantibodies, thus enabling faster diagnosis and more efficient and earlier treatment initiation. Therefore, research of underlying mechanisms of these diseases will bring important insights and further improvement of clinical practice. Several innovative therapies have already been brought forward. Chimeric autoantibody receptor T cells can be engineered to detect and deplete B cells specific to a given autoantibody (such as NMDAR antibody), via extracellular presentation of the target antigen (receptor protein containing the known binding site). Another novel strategy is ‘aquaporumab’, an aquaporin-4 selective antibody, which lacks the binding site for complement, the mediator of its cytotoxicity, which can outcompete the pathogenic patient autoantibody (Prüss, 2021).

Autoantibodies in neurodegenerative diseases

The existence of so many antibodies targeting synaptic proteins and receptors brings forward the interesting notion, that immune system interference in brain function may be more widespread than previously thought. Some antibodies can manifest symptoms similar to those of neurodegenerative diseases: LGI1 antibodies can resemble the typical clinical picture of Alzheimer’s disease (Marquetand et al., 2016). Antibodies specific to

voltage gated potassium channels can mimic frontotemporal dementia (McKeon et al., 2007). Gamma-aminobutyric acid (GABA) receptor b antibodies can mirror amyotrophic lateral sclerosis (ALS), suggesting the intriguing possibility that antibody-mediated autoimmunity could be one of several pathways leading to the ALS phenotype (Schumacher et al., 2019). On top of these 'phantom' diseases, which are antibody-mediated and highly immunosuppressant responsive, an association exists between autoantibodies and diseases of proven neurodegenerative origin. In ALS, antibodies against cortical motoneurons may contribute to neurodegeneration (May et al., 2014).

It seems conceivable that subthreshold levels of pathogenic antibodies in individuals suffering from mild cognitive impairment, subclinical psychotic episodes or age-related cognitive decline can have an autoimmune origin. Although a study looking for 8 different autoantibodies in psychotic patients produced no hits (Bien et al., 2021), antibody levels may still be below the detection or clinically relevant threshold and therefore this possibility cannot be fully excluded. The fact that a significant fraction of the healthy population carries NMDAR antibodies of unknown specificity (Hammer et al., 2014) suggests that antibodies to synaptic structures could influence neuronal function and thus cognition and memory.

It may be necessary in the future to screen even asymptomatic patients for autoantibodies. For instance, asymptomatic mothers with autoantibodies could endanger the development of their unborn children. Antibodies from pregnant mothers seropositive for NMDAR encephalitis could cross into the foetus through placenta and accumulate in the developing brain. These quantities can be sufficient for neurodevelopmental abnormalities and increased offspring mortality in animal models (Jurek et al., 2019). However, these experimental findings may not be fully translatable to human patients, as observed mortality rates and developmental impairments in children of NMDAR patient mothers are not nearly as severe (Dalmau, 2020). Nevertheless, these findings illustrate the potential necessity to screen the general population for pathogenic autoantibodies.

1.2. HIPPOCAMPUS

The hippocampus has the highest expression of NMDARs in the brain. For this reason, the hippocampus is in the centre of NMDAR encephalitis pathophysiology. Indeed, highest NMDAR antibody binding is observed in the hippocampus and key NMDAR encephalitis symptoms are consistent with hippocampal function disruption, such as impaired

memory and cognition. This chapter introduces the hippocampus, which is one of the most thoroughly investigated structures in the brain. The discovery of place cells, grid cells and time cells established that the hippocampus plays a critical role in memory formation by providing spatiotemporal map that integrates various sensory information. The hippocampus allows the experience to be stored in such a way that it allows later for conscious recollection of that experience.

Extensive knowledge about the hippocampus originated from lesion studies in humans. The case of the best known and the most studied patient in neuroscience, Henry Molaison (HM), brought about a significant understanding of the role of hippocampal formation in episodic memory. It was described in a seminal publication (Scoville and Milner, 1957), which is one the most cited articles in modern medical literature.

HM had both of his hippocampi together with adjacent areas removed in a bid to cure his debilitating epilepsy. There was a profound change in his behaviour following the surgery, as he developed a severe amnesia. His cognitive abilities and personality remained intact as was his working memory, however he was unable to consolidate any information into his long-term memory. Interestingly, HM's motor learning skills were intact which he demonstrated through increased performance of a task; only he was oblivious to having trained such task (Corkin, 1968). Researchers concluded that nondeclarative learning relies on memory circuits separate from hippocampal formation and that it does not require conscious memory processes.

HM was only one of many patients that developed severe amnesia after hippocampal resection, because the hippocampus is highly susceptible to epilepsy, stroke, or encephalitis. Research on these patients helped shape modern neuroscience and establish the notions of episodic and semantic memory as subcategories of declarative memory. Episodic memory seems to be dependent on the hippocampus, whereas semantic memory appears to reside in anterior temporal lobes. Patients with hippocampal damage have episodic memory deficits but are perfectly able to form semantic memories (factual knowledge). Given that amnesia of HM and other patients with hippocampal lesions was only anterograde, i.e., patients were able to retain old memories, the hippocampus seems to be involved in forming new memories. This important insight suggested that memories over time become independent of the hippocampus, presumably by moving into cortical areas.

1.2.1. Hippocampal function

According to the original work by O'Keefe and Nadel (1978), the hippocampus supports memory for items or events in a spatiotemporal context. Indeed, studies have shown that populations of spatially tuned neurons, dubbed place cells, form a spatial map of an environment whereas another population of cells map the temporal dimension of that environment, hence called time cells (O'Keefe and Nadel, 1978). Therefore, episodes are spatially and temporally discrete events. Consistently with this idea, both temporal and spatial boundaries of a task strongly modulate hippocampal activity (Bird et al., 2010). There is also considerable evidence suggesting that the hippocampus contributes to a broad range of behaviours beyond spatial cognition. In animals, these include cells selective for odour and auditory cues (Aronov et al., 2017), landmark views and goals (Gauthier and Tank, 2018; Rolls and O'Mara, 1995). Interestingly, the hippocampus plays a role in mapping of dimensions entirely dissociated from physical space, such as social space (Tavares et al., 2015).

It is a generally acknowledged fact that the hippocampus is essential for episodic memory, however, it is still not clear to what extent spatial navigation depends on the hippocampus. People with bilateral hippocampal lesions can retain spatial memories and are even able to navigate the streets of London as taxi drivers (Maguire et al., 2006). In contrast, lesions to other brain regions, such as the retrosplenial cortex, seem to have much more profound effects on spatial memory and navigation (Takahashi et al., 1997). Rodents with hippocampal lesions are impaired in the Morris water maze task, but their ability to navigate physical space is intact (Pearce et al., 1998). Patients with hippocampal lesions are impaired in imagining scenes (Hassabis et al., 2007), suggesting they are unable to access or create the cognitive map necessary for such a task. These studies illustrate our limited understanding of the role of the hippocampus in complex cognitive behaviours.

Importantly, the hippocampus does not seem to encode a global cognitive map but rather a series of maps, each tied to a specific context or modality (Eichenbaum, 2015, 2014). Even multiple maps of the same environment can stably coexist in the hippocampus, suggesting a level of redundancy or different attractor states. Often upon repeated entry of an animal to a linear track arena, the pre-existing spatial map can be recalled in a flipped orientation, possibly representing disorientation of the animal (Sheintuch et al., 2020). Our brains construct individual, overlapping spatial maps that might not compete with each other. Often, we form maps of indoor environments, without necessarily

connecting them to the global map (outdoors), further supporting the notion that the hippocampus constructs multiple episodic maps each tailored to the requirements of a specific episode or task.

It can be concluded that the hippocampus uses space and time as primary dimensions for defining contexts or episodes, however other dimensions can be incorporated into the map if they are determined to be relevant in the event-defined context.

1.2.2. Hippocampal structure

Hippocampus in humans is an elongated structure, buried deep within the medial temporal lobe and its shape resembles that of a seahorse, hence the name *hippocampus*. In rodents it is a prominent structure situated right underneath the cortex. A cross section of the hippocampus reveals the classic laminar structure consisting of dentate gyrus (DG) and cornu ammonis (CA) 1-4 (Figure 3).

The main input from cortex comes from the entorhinal cortex through the subiculum of the hippocampus, giving rise to the name 'perforant pathway' due to its laminar pattern. These glutamatergic projections terminate in the DG, CA1 and CA3 regions of the hippocampus. The DG projects into CA3 via the 'mossy fibre' pathway, which in turn projects into CA1 through the 'Schaffer collateral' pathway. Finally, CA1 projects back to the entorhinal cortex, completing the loop. Together, these 3 pathways form what is known as trisynaptic circuit (Schultz and Engelhardt, 2014).

The functioning of the trisynaptic loop was traditionally proposed to be contained within cross section (radial) axis composed of largely independent sections stacked on the longitudinal axis. We now know that the hippocampus is interconnected also on the longitudinal axis, and individual segments may perform parallel computations. Traditional categorization of pyramidal neurons into individual layers, e.g. CA1, CA2 and CA3, disregards the fact that these are heterogeneous populations of neurons, which can be further subdivided along the longitudinal axis (anterior and posterior in humans or dorsal and ventral in rodents), along the transversal axis (proximal and distal) as well as along the radial axis (deep and superficial). The mounting evidence for the heterogeneity of its pyramidal neurons and diversity of information processing the hippocampus is involved in suggests that pyramidal cell identity is a spectrum rather than a discrete category.

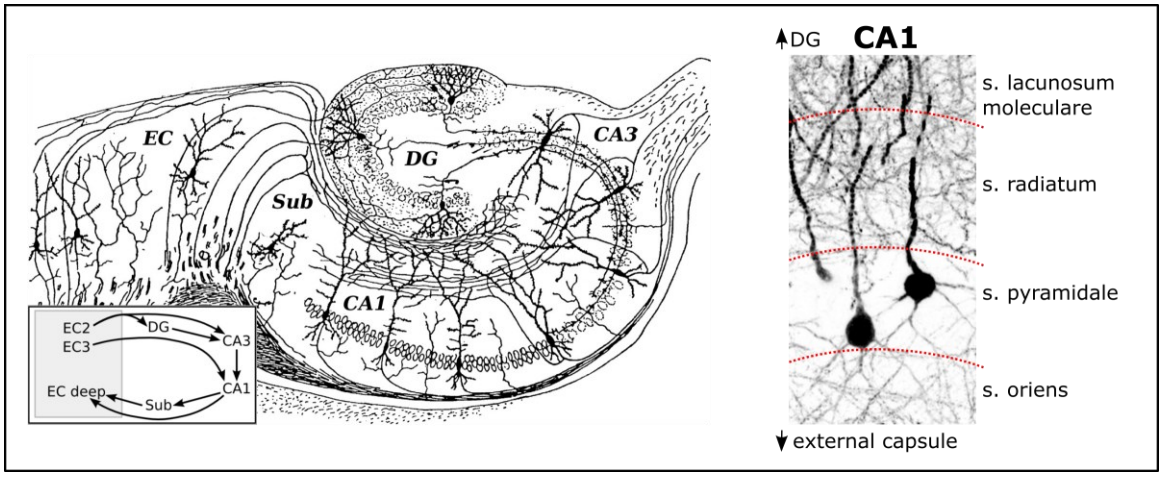

Figure 3. **Hippocampal structure.** Left, original drawing by Ramon y Cajal (1901). DG, dentate gyrus; CA, cornu ammonis; Sub, subiculum; EC, entorhinal cortex. Right, schematized depiction of individual sublayers (stratum) in CA1. Adapted from Ramon y Cajal (1901) under the Public Domain License.

Structure of hippocampal neurons

CA1 pyramidal neurons receive direct input from the entorhinal cortex, whose perforant path projections target CA1 apical dendrites in stratum lacunosum moleculare, the region furthest from the soma towards DG. Input from Schaffer collateral projections of hippocampal CA3 pyramidal neurons target CA1 apical dendrites in stratum radiatum, closer to the soma and below stratum lacunosum moleculare. Cell bodies of CA1 pyramidal neurons are located in the stratum pyramidale. Basal dendrites of these neurons are located in stratum oriens, which stretches from stratum pyramidale towards the external capsule. These apical and basal dendrites of hippocampal pyramidal neurons branch extensively into secondary, tertiary, and fourth-degree dendrites, and the complexity of the dendritic arbour itself plays an important role in neuronal function. Firstly, computational processes are performed through local dendritic action potentials (Sheffield and Dombeck, 2015). Secondly, the branching pattern physically restrict biochemical signal spreading from activated synapses, serving as one of the key factors that define the biochemical signalling pattern (Yasuda, 2019).

In the hippocampus, 10-15 % of neuronal population are GABAergic interneurons. Contrary to excitatory, glutamatergic pyramidal neurons that are located in compact layers with orthogonal dendrites, hippocampal interneurons are dispersed throughout all subfields and have diverse morphology. Although traditionally categorized morphologically into groups such as Chandelier cells, basket cells or bistratified cells (Freund and Buzsáki, 1996), hippocampal interneurons are morphologically diverse population. The morphology may be tightly linked with their function, with some interneurons forming only local connections while others possess long-range projections.

Interneurons provide inhibitory synaptic input that plays a critical role in regulation of single cell excitability and timing of action potentials, thereby synchronizing circuits and facilitating oscillatory activity. Interneurons are further classified based on the expression of various molecules into parvalbumin- (PV), somatostatin- (SST), cholecystokinin- and vasoactive intestinal peptide-positive interneurons (Pelkey et al., 2017).

1.2.3. Hippocampal circuits

The incoming information from all sensory and motor association cortices enters the hippocampus via the perforant path, goes through the trisynaptic loop and is returned back to the entorhinal cortex by CA1 projections. However, the information flow in the trisynaptic circuit is also not unidirectional as once was widely believed. Although most projections terminate on granule cells of the DG, the perforant pathway projects also directly to CA1 and CA3. In addition, CA3 cells provide feedback to granule cells in DG. Entorhinal cortex provides topographically different inputs into the hippocampus. The medial entorhinal cortex (MEC) is associated with spatial processing, whereas lateral entorhinal cortex (LEC) is associated with item recognition and emotions (Schultz and Engelhardt, 2014). MEC-CA1 collateral contacts mostly deep pyramidal neurons in the proximal part of CA1, whereas LEC-CA1 contacts superficial neurons located in the distal part of CA1 (Masurkar et al., 2017). This differential input is reflected in CA1 neuron properties: deep pyramidal neurons have higher spatial information content and larger fraction of place cells compared to superficial neurons (Danielson et al., 2016).

Dorsal and ventral hippocampus is differentially involved in spatial information processing versus emotional memory and cognition. The ventral hippocampus is highly connected to prefrontal cortex and amygdala, whereas the dorsal hippocampus contains highest resolution spatial map. In humans, the hippocampus appears broadly subdivided into an anterior segment that supports emotion, stress and sensorimotor integration, and a posterior part dedicated to declarative memory and cortex-supported cognition.

Place cells

The hippocampus has been most studied in experiments regarding spatial navigation and spatial memory. Place cells are hippocampal pyramidal cells that fire when the animal is in a specific location (O'Keefe and Dostrovsky, 1971). Place cells line up the spatial dimensions of the environment with their firing fields (place fields) at largely uniform distribution, thus creating a spatial map for that environment. Position of the animal can

be predicted/decoded from activity of many cells with considerable accuracy (Stefanini et al., 2020). Place cells provide a framework for allocentric memory, serving as a reference map for the animal while navigating. They are active in light and dark conditions, suggesting place cells are not dependent on a single modality such as visual input, and neither somatosensory input since self-motion information alone is insufficient to generate stable firing fields (Zaremba et al., 2017). Therefore, place cells integrate complex inputs into their spatial selectivity.

Pyramidal cells across all hippocampal fields have place fields, and their properties vary, suggesting that individual hippocampal areas perform different computations related to encoding of space (Hainmueller and Bartos, 2018). The same place cells participate in encoding of different environments, but the relationship between their firing fields varies from one environment to the next (O'Keefe and Nadel, 1978), a feature known as remapping (Fyhn et al., 2007; O'Keefe and Nadel, 1978). When an animal experiences an environment for the first time, place cells rapidly form place fields along its dimensions to form a new place map for the novel environment, a phenomenon known as remapping. Remapping is manifested as a change of firing rates in the presence of a stable place code, known as rate remapping, and under certain conditions as a complete reorganization of the hippocampal place code in which both place and rate of firing changes, known as global remapping (Fyhn et al., 2007).

Destruction of DG has little effect on CA1 place fields (McNaughton et al., 1989). These findings suggested that most of the spatial information exhibited by place cells is conveyed from cortex through other pathways than the traditional trisynaptic circuit, most likely through direct projections from the entorhinal cortex to CA1 and CA3. Although vast majority of experimental evidence comes from animal studies, the existence of spatially tuned cells has also been demonstrated in the human brain. Patients with intracranial electrodes navigating a virtual town experienced distinct locations to which some of the hippocampal neurons became tuned (Ekstrom et al., 2003). This suggests that mechanisms of space encoding are largely conserved across mammals.

It has long been known that place cells form an association with a physical location (O'Keefe and Nadel, 1978), however the direct implication of place cells in driving spatial navigation was not demonstrated until recently by Robinson et al. (2020). In a virtual spatial navigation task in mice, the authors selectively manipulated a group of neurons associated with a reward location, i.e., a particular zone of the virtual arena in which a reward was delivered. When activating a small group of these reward zone place cells,

mice exhibited licking behaviour normally associated only with the reward zone. Thus, this study demonstrated a causal role for place cell activity in guiding spatial navigation and supporting spatial memory. Surprisingly, activation of a very small fraction of the total place cell population produced a detectable change in behaviour. This suggest that the neural representation is both sparse and efficient. Moreover, the effect of such small and selective CA1 stimulation could be amplified through attractor dynamics in downstream regions (Robinson et al., 2020).

During spatial learning, place fields in the CA1 region of the hippocampus reorganize to represent new goal locations. The stabilization and successful retrieval of these newly acquired CA1 representations of behaviourally relevant places is NMDAR-dependent and necessary for subsequent memory retention performance. Thus, remembering newly learnt goal locations requires NMDAR–dependent stabilization and enhanced reactivation of goal-related hippocampal assemblies (Dupret et al., 2010).

Spatial firing selectivity of place cells is thought to rely upon two interacting mechanisms: sensing the position of the animal relative to familiar landmarks and measuring the distance and direction that the animal has travelled from previously occupied locations. This process, known as path integration, is an evolutionarily conserved strategy that allows an individual to maintain an internal representation of its current location by integrating time over distance and direction travelled (Jayakumar et al., 2019).

Time cells

In striking similarity to place cells, existence of time cells in the hippocampus has been demonstrated (Manns et al., 2007). These cells fire when an animal is at a particular time in a temporally structured task. Therefore, these cells encode time, rather than space, and are limited by the temporal dimensions of the experience - that is, by temporal cues (beginning and end of an episode) and are marked by critical intervals. Time cells therefore behave just as place cells, which are be governed by spatial cues and spatial dimensions of the environment (Eichenbaum, 2013).

Increasing evidence suggests that firing sequences of time cells develop with learning, are memory specific and predict the accuracy of subsequent memory across a broad variety of tasks. Finally, time cells and place cells are the same neurons and form the same neuronal ensembles, which can encode the temporal and spatial organization of experiences (Eichenbaum, 2014). In humans, a similar function has been attributed to temporal parietal junction which thus represent the ‘when’ pathway in the human brain (Davis et al., 2009).

Reward cells

Reward cells are specialized neurons in CA1 and subiculum that encode the location of a reward in mice performing a goal-oriented spatial learning task. The same cells are active near multiple reward sites in different environments during global remapping and their identity is fully conserved, that is, reward cells always encode for reward and never for a place (Gauthier and Tank, 2018). Reward also modulates the entorhinal spatial coding: grid cells increase firing rate in fields near the reward and non-grid spatial cells shift their fields towards the reward location, thus enriching the reward location (Butler et al., 2019). The discovery of reward cells provided a cellular correlates of goal memory located in the hippocampal–entorhinal cortex circuit. The dopaminergic system is thought to be implicated in reward signalling (Sosa and Giocomo, 2021). Reward cells represent one opportunity to assess cognition of the animal, contrary to the 'automatic' navigation system provided by place cells and grid cells. Indeed, when a reward is omitted in a familiar environment, reward cells fire to signify the animal's expectation of a reward in that location (Gauthier and Tank, 2018). Moreover, selective stimulation of reward cells elicit reward associated behaviour (Robinson et al., 2020) and the overrepresentation of the goal location in the place cell population has been shown to correlate with learning performance (Dupret et al., 2010).

Theta rhythm and sharp-wave ripples

In rodents, hippocampal electro-encephalogram (EEG) is dominated by oscillations of about 8 Hz (known as theta oscillation) when the animal is locomoting, exploring or in the rapid eye movement (REM) stage of sleep. When rodents are engaged in non-exploratory behaviour or in the non-REM stage of sleep, hippocampal EEG is dominated by sharp-wave ripples (SWR), characterized by large irregular activity caused by synchronized activity discharges. Hippocampal cells are strongly modulated by theta phase and fire bursts that are phase locked to the theta rhythm (O'Keefe and Recce, 1993). Place cells show a phenomenon known as theta phase precession: as the animal moves through the place field, the phase locking of action potentials shifts backwards to earlier theta phases. This provides a precise information about animal's position in a large firing field. Moreover, theta phase precession allows sequences of place cell firing to be reactivated in a compressed manner with each theta cycle, representing the animal' past and future trajectory (Wilson and McNaughton, 1993).

Hippocampal theta yields two patterns before navigational decisions. First, when the animal pauses at a maze junction and looks in each direction, theta sequences project ahead of the animal in directions of the different choices, first one direction and then the other. This is thought to help the animal evaluate each path (Johnson and Redish, 2007). Second, during movement before a maze junction, future choices are represented on alternating theta cycles, thereby encoding multiple possible scenarios (Kay et al., 2020). Future-signalling spikes occur on late phases of theta, whereas spikes signalling the current or past location occur on the early phases (Kay et al., 2020; Sosa and Giocomo, 2021). Therefore, place cells can fire in a sequence that represents a future trajectory of an animal to a goal location, even before it moves. This may be involved in the animal's planning of routes and evaluating behavioural choices.

Trajectory replay events

During SWR, place cells fire with each theta cycle to form activation sequences similar to those manifested when the animal is navigating. These sequences, called trajectory replay events or replays, can represent place cell sequences in an order in which their place fields were recently visited, since trajectory replays require previous experience for their formation. NMDARs are required for replay sequence encoding but not for the retrieval of trajectory replay events (Silva et al., 2015).

However, it has been demonstrated that, in an environment that has been previously sampled, the hippocampus is able to generate replays of place cell sequences in an order that has never been experienced before. Moreover, replay sequences can represent not yet experienced trajectories, such as a novel path to a remembered goal location (Pfeiffer and Foster, 2013). These findings suggest an intriguing possibility that place cells have a role in navigational planning. Replay sequences could represent constructive attempts to read out information from an existing cognitive map and apply such information to a future navigational behaviour, such as finding more efficient way to a reward. Alternatively, replay sequences may be involved in the systems consolidation process, as a mechanism whereby the events recently experienced by the animal are replayed to the neocortex in order to update the permanent, neocortical memory stores (Diba and Buzsáki, 2007).

Pattern separation & pattern completion

To distinguish between similar objects and events that have different relevance for behaviour, the brain needs to transform similar inputs into well separated neuronal

representations of memory. Conversely, different objects that have identical behavioural relevance need to be grouped into a common representation. These processes are known as pattern separation and pattern completion, respectively, and the hippocampus is engaged in these tasks (Knierim and Neunuebel, 2016).

Recurrent CA3-CA3 synapses are thought to be the synaptic mechanism for pattern completion, where neural representations fall into one of the attractor states that are robust to incomplete input information (Guzman et al., 2016). The opposite operation, pattern separation, is mediated by the DG through input information decorrelation, i.e. reduction in correlation of two representations (Allegra et al., 2020). DG constantly performs pattern separation, thereby pushing the downstream network to remap, while CA3 through its attractor dynamics counteract this process with pattern completion computation (Knierim and Neunuebel, 2016).

In the framework of attractor dynamics of neural networks, the structure of synaptic connectivity defines an energy landscape, which determines the attractor states (local energy minima) the network may converge to when the animal is encountering an environment. This synaptic structure ensures that the network possesses a set of stable attractors that are localized in the space of neuronal variables reflecting their synaptic interactions, rather than their physical location in the hippocampus (Tsodyks, 1999). Long-term changes in excitability and/or synaptic connectivity may alter this energy landscape of the network, thus leading to gradual changes in spatial representations and the probability of a given representation to recur (Sheintuch et al., 2020). Therefore, as described above, the neural representation of an environment in the CA1 is a result of these upstream attractor dynamics, allowing to recall a representation of a familiar environment or, when the environments are sufficiently distinct, trigger global remapping into a new representation.

Mixed selectivity

It is possible to predict the activity of a neuron from the activity of all the other neurons, regardless of how well that neuron encodes position. Therefore, correlation patterns in CA1 only partially arise from position encoding. Some components of the correlation pattern encode the internal state of the animal. Understanding of neuronal activity may not only require knowledge about the external variables but also about the internal state of the organism (Meshulam et al., 2017).

Each variable can be encoded by a group of highly specialized neurons. However, this significantly limits the number of possible combinations of network responses. Instead,

when variables are mixed nonlinearly, the neural representation can be high-dimensional. Mixing position encoding with head direction and other variables may lead to poor spatial tuning of most individual cells, but it vastly increases the computational capacity of the network. Therefore, a distributed code can reliably represent multiple combinations of variables. Correlated activity between neurons has been shown to convey information, since destruction of correlation between the neurons leads to information loss from the network (Stefanini et al., 2020). Modelling suggests that pairwise correlations accounts for only 10% information (Schneidman et al., 2006), whereas higher order correlation models reveal around 20% information (Pillow et al., 2008).

Neuronal ensembles

Already in 1949, D. Hebb predicted the existence of cooperative activity of groups of neurons and postulated that these form basic units of perceptive integration (Hebb, 1949). Thanks to advances in neuronal activity recording and data science, today we know that neurons form ensembles with temporally correlated activity between them. Brain activity is characterized by a limited set of spatiotemporal coactivity patterns, which occur spontaneously under no stimulation and upon a visual stimulus presentation are recruited into the stimulus representation (Carrillo-Reid et al., 2015). This is consistent with the hypothesis that pre-existing Hebbian cell ensembles may be the substrate for microcircuit sensory processing in primary visual cortex (Hamm et al., 2017). Recruitment of individual neurons into existing ensembles can be variable, with several neurons forming the core ensemble and other neurons participating sporadically or participate in several ensembles (Carrillo-Reid et al., 2015), further suggesting mixed selectivity of neuronal responses.

Engram cells

Memory consolidation is a process whereby a newly formed memory transitions from fragile to a stable, long-term state. This is thought to be conveyed by selective stabilization of neurons encoding an experience, also called engram cells (Goode et al., 2020). By employing learning-dependent cell labelling, it is possible to tag a specific group of neurons encoding a memory. When an ensemble of neurons representing a given context was artificially activated during conditioning in a distinct context, animals formed a hybrid memory representation. Reactivation of the network within the conditioning context was sufficient for driving future recall of a contextual fear memory, and thus

represent a component of a distributed memory engram (Garner et al., 2012). Moreover, memory consolidation is accompanied by an increase in synaptic strength and dendritic spine density specifically in engram cells (Ryan et al., 2015). These findings suggest that a specific pattern of connectivity of engram cells may be crucial for memory storage and that strengthened synapses in these cells critically contribute to the memory retrieval process.

1.2.4. Dendritic spines

In the central nervous system of vertebrates, dendritic spines are mushroom-like protrusions on dendrites of neurons, harbouring most of the excitatory postsynapses in the brain. According to some estimates, there are 100 trillion of spines in the human brain. The spine density varies greatly depending in the brain region and neuron type, ranging between 1 and 10 spines per micrometre (Yuste, 2010). The main characteristic of spines is the spine head, with a volume up to 1 μm^3, containing synaptic proteins forming a disc-shaped PSD that clusters glutamate receptors with other receptors and signalling molecules into the postsynaptic membrane. PSD is positioned opposite of the presynaptic terminal, which can in some cases consist of multiple presynaptic sites. The spine head forms a functional compartment and is connected to the dendritic shaft via a narrow neck, approximately 0.2 μm wide, which acts as a diffusion barrier and thus influences spine's electrophysical and metabolic properties. Mature spines can contain intracellular structures such as mitochondria, ribosomes and vesicular clusters, to support material requirements for synaptic transmission (Kasai et al., 2021).

Dendritic spine morphology

Spines grow and shrink, spines are formed and eliminated throughout the life of an individual. In addition, there is a large variability in spine shapes even on a single dendrite. It has long been known that spine head size positively correlates with PSD size and synaptic strength (Bosch and Hayashi, 2012), which is suggestive of a tight coupling between spine structure and its function. These morphological changes are mediated by cytoskeleton formed by F-actin filaments, which serve both as a structural framework as well as regulator of protein and vesicular trafficking (Matus, 2000).

Although spine morphology is tightly linked with activity, spines undergo significant fluctuations in size even when activity is entirely suppressed, or when the network develops in absence of synaptic transmission (Kasai et al., 2021). Under baseline conditions *in vivo*, spine volume fluctuate by more than 10%. Interestingly, stable spines

are not spared of morphology fluctuations (Steffens et al., 2021). To put that in perspective, LTP-associated changes are around 21 % (Wiegert et al., 2019). According to some estimates, spontaneous baseline fluctuations in spine size can account for up to 50% of the overall variability (Dvorkin and Ziv, 2016). This is suggesting that dendritic spines are intrinsically dynamic entities. Although spines morphologically respond to synaptic activity, the spontaneous morphological dynamics are almost as great. The intrinsic changes may be a result of ongoing biological and metabolic processes.

Dendritic spines are classically categorized based on their morphology into stubby (short without a prominent neck), thin (long without a prominent head) and mushroom spines (with head and neck). However, such a categorization is purely arbitrary and spine morphology is rather a spectrum of morphological features. An extreme case of thin spines are filopodia, which lack an actual spine head. Filopodia are transient structures with a short lifetime (less than 4 days) which were thought to be precursors of newly form spines. However, recent evidence from super-resolution microscopy argues against this preconception and therefore filopodia may have a different, yet unknown physiological role (Steffens et al., 2021).

Morphological changes associated with synaptic activity

Spines that undergo synaptic plasticity display a corresponding change in morphology. Specifically, LTP achieved with repetitive stimulation of spines through glutamate uncaging results in rapid and selective enlargement of stimulated spines, which is associated with AMPAR-mediated currents and is dependent on NMDAR activity and actin polymerization (Wiegert et al., 2019; Yuste, 2010). Furthermore, this effect is more pronounced in small spines than in large mushroom spines, suggesting that small spines may be preferential sites for LTP induction whereas large, already potentiated spines represent physical traces of long-term memory (Matsuzaki et al., 2004). Moreover, stimulation of a dendritic shaft with glutamate induces a location specific, *de novo* spine growth (Kwon and Sabatini, 2011). Conversely, long-term depression (LTD) induced through chemical or electrical means leads to shrinkage or loss of dendritic spines (Okamoto et al., 2004).

In addition to the morphology changes, LTP promotes spine survival whereas LTD destabilizes synapses. When plasticity inducing events follow in a sequence, the effect of last event dominates over earlier stimulation. Increase in spine volume correlates well with LTP 30 minutes after induction, however spines return to pre-LTP volumes within 24 hours. Nevertheless, a long-lasting, synapse-specific memory of the potentiation event

is maintained, since potentiated spines have increased survival rates for at least 7 days (Wiegert et al., 2019). These findings show that synaptic strength and synaptic morphology can be dissociated, although they are to some extent correlated. Thus, the precise role of morphological changes of spines in synaptic transmission and plasticity still remain an open question.

Protein signalling associated with synaptic plasticity

During the induction of LTP or LTD, firing of action potentials leads to pulses of calcium influx a few milliseconds long, which are subsequently translated into signalling that lasts for many hours. This 'slow signalling' has far-reaching consequences, and it adds another layer of complexity into synaptic plasticity. The incoming Ca^{2+} binds to Ca^{2+} binding proteins, the most important of which is calmodulin (CaM). CaM in turn signals to other molecules, such as CaM-dependent kinase II (CaMKII), which acts as a slow integrator of Ca^{2+} influx and mediates spine volume increase. On the other hand, spine volume decrease is mediated by calcineurin, a CaM-dependent phosphatase (Kasai et al., 2021). CaMKII, calcineurin and other CaM-dependent kinases/phosphatases activate or deactivate a host of downstream signalling molecules which then diffuse on a micrometre scale. Their spatial spreading is a function of diffusion and inactivation rate, and depends on physical factors, such as spine neck or dendrite diameter (Yasuda, 2019). In this way, neighbouring spines can share signalling molecules normally associated only with the potentiated spine.

Indeed, it has been shown that spines neighbouring to a selectively stimulated spine are subjected to changes in synaptic plasticity. In an *in vitro* single spine LTP induction, increase in spine volume is modestly mirrored in spines less than 5 micrometres away. Similarly, these nearest neighbour spines have increased survival rates, a feature normally associated with the potentiated spine. Although LTP changes in neighbouring spines are scarcely reported, it is an important evidence for spreading effect of synaptic changes (Wiegert et al., 2019). Shrinkage and pruning (removal) of neighbouring spines on the other hand is much more pronounced and it can extend up to 15 micrometres from the stimulated spine. This is likely due to higher spreading of calcineurin, which has a destabilizing effect on F-actin and thus results in spine shrinkage (Hayama et al., 2013). Moreover, previously potentiated spines are protected against pruning. Many proteins that regulate spine shrinkage and enlargement also regulate F-actin dynamics (Kasai et al., 2021).

Whether a spine will follow LTD or LTP depends on the magnitude of intracellular Ca^{2+} elevation. Activation of CaMKII and calcineurin occurs in Ca^{2+} nanodomains, which are cytosolic areas within 10 nm of open NMDARs, where peak Ca^{2+} concentration can exceed 10 μM. While high frequency stimulation leads to sharp increase in intracellular Ca^{2+} concentration (100-1000x) and subsequent CaMKII activation, low frequency stimulation only leads to moderate Ca^{2+} concentration and thus calcineurin activation. A critical role in deciding which synaptic pathway should a spine go is mediated by GABA receptors which regulate the intracellular Ca^{2+} concentration. GABAergic neuron activity has been shown necessary for LTD induction (Nishiyama et al., 2010). Thus, spine growth and shrinkage are determined by spine intracellular Ca^{2+} levels mediated by NMDAR, and inhibitory neurons play a key role in determining these levels.

Spines and memory

As outlined above, small spines are preferential target to LTP and subjects of greater morphological fluctuations. It is therefore believed that small spines play a central role in creation of new memories (Kasai et al., 2003). Large spines are stable, presumably maintaining pre-existing connections with little interference. Small spines are unstable, and responsible for new memory acquisition and retention by transforming themselves into large spines. Large spines are rarely eliminated, whereas small spines undergo constant remodelling, formation and elimination, particularly during intense neuronal activity and LTP. Distribution of spines in the brain is left-skewed and approximately 80% of spines are small (Kasai et al., 2021). This gives rise to the enormous storage capacity of the brain. Small spines are close to the pruning threshold and their lifetime is short, consistent with short lifetime of most new memories. Thus, it is believed that memory lifetime corelates with synaptic structure, with large spines being the structural basis for long-term memory.

This hypothesis is supported by the observation that individuals with schizophrenia, who often have short-term memory deficits, have reduced spine density driven by selective decrease in small spines while density of large spines is maintained (MacDonald et al., 2017). Moreover, mice with selective knock-out of calcineurin, important pruning regulator, have schizophrenia-like symptoms accompanied by selective loss of small spines (Okazaki et al., 2018).

Proteins crucial for spine structure and function have been implicated in autism spectrum disorder. Consistently, mice lacking an important PSD scaffold protein SHANK1 have overall reduced spine size together with weaker synaptic transmission. Remarkably,

these mice have increased performance in a spatial learning task, however their long-term memory retention of this task is impaired (Hung et al., 2008). This provides an additional evidence for the role of small spines in encoding new memories. In another mouse model of autism spectrum disorder, altered spine morphology is not the main driver of cognitive disabilities. Instead, increased spine turnover rates have been shown to be responsible for memory deficits, and this originates from intrinsic changes in spine dynamics rather than from altered activity levels (Nagaoka et al., 2016). Thus, not only reduction in spine size but also increased spine turnover rates have been shown to result in impairment of long-term memory formation.

Consistently, network modelling has suggested the largest effectivity when operating with highly skewed synaptic weights (i.e., spine size), which also maximizes the capacity of the network to retain stable activity patterns (Chen et al., 2010). This mostly theoretical framework has been confirmed by experiments, which showed that a small fraction of strong connections accounts for neuronal stimulus-specific responses in cortical microcircuits (Cossell et al., 2015).

1.2.5. Methodological advances

In vivo visualization of neurons and their processes has been a major milestone in neuroscience and was enabled by the advent of two-photon excitation laser scanning microscopy. Living tissue is a difficult environment for the traditional microscopy techniques such as wide-field or confocal microscopy, due to their sensitivity to scattering and photobleaching.

The principle of two-photon excitation was originally proposed by the Nobel laureate M. Göppert-Mayer in her doctoral thesis (Göppert-Mayer, 1931). 60 years after this initial proposition, two-photon excitation microscopy was invented by W. Denk (Denk et al., 1990). Until then, only electrophysiological recordings were used to investigate neuronal activity *in vitro* (e.g., patch-clamp) and *in vivo* (e.g., tetrodes). Optical recordings of neuronal activity have several advantages over electrophysiological recordings. First, microscopy allows for large-scale recordings and reveals also entirely silent cells as well as different cell populations (e.g., interneurons). Second, optical approach is generally less invasive for the recorded cell than electrodes and allows for long-term, chronic assessment of the same neurons. Since its discovery more than 30 years ago, thousands of publications employed two-photon imaging approaches for investigations of structural

and functional plasticity of neurons, and significantly advanced our understanding of the brain.

Two-photon excitation microscopy

In two-photon fluorescence, two low-energy photons emitted by a femtosecond pulsing laser (e.g., Ti:Sapphire) arrive simultaneously at the fluorophore, thereby causing a higher-energy electronic transition in a fluorescent molecule (Figure 4). Two-photon excitation is a nonlinear process: absorption rate depends on the second power of the excitation light intensity, which is highest at the focal plane and drops quadratically above and below. As a result, fluorophores are excited almost exclusively in a diffraction-limited volume. This represents the first of three key advantages of two-photon microscopy: low-density scattered excitation photons will not excite the fluorophore. The consequence of this excitation localization is a three-dimensional contrast and resolution which eliminates the need to reject out-of-focus light with a pinhole. When excitation photons enter tissue, they are scattered through collisions with tissue molecules and their paths are altered. Scattering in adult brain is about twice as high as in juvenile tissue, and approximately half of the incident light is scattered every 200 μm. The far-red or infrared wavelengths used in two-photon imaging constitute the second advantage, since these low-energy, long-wavelength photons penetrate better through the tissue. This improved penetration is due to reduced scattering and reduced absorption by endogenous chromophores (Oheim et al., 2001). The last key advantage of two-photon microscopy is that all photons captured by the detector contribute to the signal. Given that the majority of excitation light is scattered deep in tissue, these photons will not cause a signal and therefore will not contribute to the background (Denk et al., 1990).

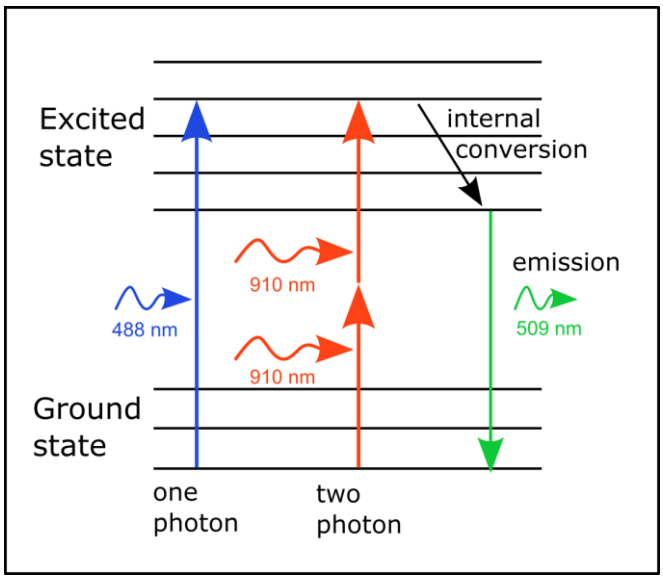

Figure 4. **Jablonski diagram of the two-photon fluorescence process of a green fluorescent protein (GFP) molecule.** In case of one photon excitation process (blue arrow), a single photon excites the fluorophore. In case of two photon excitation (red arrow), two photons of twice the wavelength arrive simultaneously at the fluorophore. In both cases, excitation leads to a single photon emission (green arrow). Higher orders of excitation (e.g., three/four photon) are also possible.

Although photon scattering can be compensated for by increasing laser power, the imaging depth is ultimately limited by the out-of-focus fluorescence signal generated at the surface of the sample. After this point is reached, increasing excitation light will enhance background and signal equally. Two-photon imaging can reach to a depth of 1 mm (Theer et al., 2003), however the record imaging depth stands at 1.6mm and reaches the limit set by excitation of out-of-focus fluorescence (Kobat et al., 2011).

The above-mentioned depth limitation of two-photon imaging can be circumvented by higher-order photon excitation, such as three-photon excitation imaging. Subcortical structures, such as vasculature and red-fluorescent protein labelled neurons, have been imaged in an intact mouse brain with the excitation wavelength 1,700 nm (Horton et al., 2013). Though imaging of deep brain structures with three-photon excitation is technically feasible, its use is cost prohibitive.

Genetically encoded Ca^{2+} indicators

Electrical activity of cells in living tissue can be assessed noninvasively using genetically encoded Ca^{2+} indicators, which react to changes in intracellular Ca^{2+} concentration with changes in fluorescence. Ca^{2+} is one of the most ubiquitous messengers in cellular biology, and diverse extracellular signals and intracellular events are encoded into spatiotemporal Ca^{2+} dynamics. These dynamics are involved in vital processes, such as metabolism, transcription and apoptosis. Action potentials are characterized by strong increase in intracellular Ca^{2+} concentration. Influx of Ca^{2+} into the cytoplasm follows membrane depolarization and occurs through cytoplasmic membrane receptors (voltage-gated Ca^{2+} channels and NMDARs; Hodgkin and Huxley, 1952) and intracellular

Ca^{2+} stores such as endoplasmic reticulum and mitochondria (Bootman and Berridge, 1995). Thus, intracellular Ca^{2+} levels are an excellent proxy for neuronal activity. Consequently, efforts have been undertaken to develop molecular tools to monitor and quantify the spatiotemporal dynamics of intracellular Ca^{2+} (Lin and Schnitzer, 2016). Fluorescent imaging with Ca^{2+} indicators has achieved rapid progress in visualizing Ca^{2+} at the levels of cell populations, single cells or subcellular compartments.

Over the past two decades, optical visualization of neuronal activity has become a standard research approach in animal models, transforming brain research in the process. GCaMP is a genetically encoded calcium indicator initially developed by Nakai et al. (2001). It is a synthetic fusion of the green fluorescent protein, calmodulin, and M13, a peptide sequence from myosin light-chain kinase. When bound to Ca^{2+}, GCaMP exhibits green fluorescence with excitation wavelength peak of 480 nm and emission wavelength peak of 510 nm (Nakai et al., 2001). The GCaMP-family of genetically encoded calcium indicators has since been improved, with every generation bringing an improvement in signal-to-noise ratio and a range of temporal kinetics. To date, the most widely used versions are GCaMP6f and GCaMP7, which have the ability to resolve single action potentials in brain tissue with a half rise and decay time of 140 ms and 550 ms, respectively (Lin and Schnitzer, 2016). GCaMP can be delivered to cells by a viral vector (such as adeno-associated virus), either through a local injection directly into the tissue of interest or by intracerebroventricular injections. Downside of local injections of viral vectors are the highly variable expression depending on the concentration of virus particles. Overexpression in a subset of cells can lead to intracellular aggregation, nuclear filling and potentially even to cell death (Yang et al., 2018).

Hippocampal window

Imaging in the hippocampus is inherently difficult, given that the hippocampus lies more than 1 mm below the skull. Unrestricted optical access to hippocampal neurons *in vivo* was achieved by the development of a hippocampal window. This procedure involves the removal of the overlying cortex through a craniotomy followed by insertion of a microendoscopic lens or a steel cannula with a glass coverslip. This technique was pioneered by Mizrahi et al. (2004) and allowed observation of hippocampal dendritic spines for several hours. Chronic imaging over several months was later accomplished (Attardo et al., 2015; Gu et al., 2014).

The impact of cortex removal or damage to the hippocampus is a concern when using hippocampal windows. Following the surgery, mice exhibit transient microgliosis and

astrogliosis which is limited to ipsilateral hemisphere and declines within a few weeks. Moreover, the surgical procedure does neither affect the survival of hippocampal neurons nor of dendritic spines (Gu et al., 2014). Mice that underwent hippocampal window surgery exhibit normal behaviour, as their fear conditioning performance, spatial learning performance and locomotor behaviour remains intact (Gu et al., 2014; Hainmueller and Bartos, 2018). Therefore, surgical procedures involved in hippocampal window preparations do not affect the brain function to a greater degree, since other brain regions potentially substitute for the removed cortical areas. It provides an excellent opportunity to investigate hippocampal neurons *in vivo*.

1.3. HIPPOCAMPUS-ASSOCIATED DISEASES

As described in Section 1.1.1, NMDAR encephalitis is characterized by psychotic symptoms, namely delusion and hallucinations, and was in the past often misdiagnosed as schizophrenia (Kayser and Dalmau, 2016). These symptoms are consistent with disruption of hippocampal function (see Section 1.2.1) and are caused by antibody-mediated disruption of NMDAR signalling. The following chapter describes other hippocampus-associated diseases and illustrates experimental approaches that are used in conjunction with research of hippocampal function in animal models.

1.3.1. Schizophrenia

Glutamate hypothesis of schizophrenia

The basis of the glutamate hypothesis of schizophrenia builds on the long-standing observation that interference with NMDARs in humans and animals through pharmacological or genetic means leads to psychotic symptoms (Balu, 2016). For more than two decades, antagonists of NMDAR (ketamine, phencyclidine) have been used to generate animal models of schizophrenia and psychosis (Hamm et al., 2017). Similarly, administration of NMDAR antagonists in schizophrenic patients cause aggravation of symptoms (Malhotra et al., 1997). These findings put the spotlight on NMDAR in research of schizophrenia pathophysiology.

Evidence from patients and animal models

Impairment of cognition and declarative memory is a key symptom of patients with schizophrenia, and the severity of these deficits serves as one of the best predictors of patient outcome (Murray and Van Os, 1998). Changes in anatomy, blood perfusion, and

neuronal activity have been reported in the hippocampus of schizophrenic patients (Tamminga et al., 2010). Extensive post-mortem study of brains of schizophrenic patients revealed evidence for morphological alterations of dendrites of glutamatergic neurons and reduced general levels of presynaptic terminals in cortex. Moreover, several key components of glutamate metabolism have altered expression in schizophrenia, though there is no clear evidence of reduction of mRNA expression of glutamate receptors (Hu et al., 2015). Hypofunction of the glutamatergic system could interfere with the mnemonic role of the hippocampus, namely with the pattern completion function of the CA3 and pattern separation function of the DG. It is believed that psychosis is caused by an imbalance between internally generated predictions and actual sensory input, which could result in illusory experiences and decrease an individual's ability to discriminate between past and present memories, thus creating cognitive 'mistakes' leading to psychotic events (Tamminga et al., 2010).

Specific morphological alterations of CA1 have been reported in schizophrenia patients, such as CA1 deformity possibly reflecting shrinkage, which might result from neuronal hyperactivity (Zierhut et al., 2013). These results suggest a potential primary role of this area in the disease pathophysiology. Deficits in CA1 may be directly involved in the pathogenesis of hallucinations and delusions, core symptoms in schizophrenia.

Supporting evidence for the glutamate hypothesis of schizophrenia came from an animal model with reduced levels of the NMDAR co-agonist D-serine (serine racemase knock-out mice), in which impaired long-term potentiation, reduced dendritic spine density, reduced hippocampal volume, and impaired memory was shown. Upon administration of D-serine, the electrophysical and cognitive deficits were normalized (Balu et al., 2013). Moreover, there is extensive and direct evidence of alterations of glutamate signalling in the brains of schizophrenic patients; it was shown that schizophrenic patients have elevated levels of glutamate in the medial prefrontal cortex (Poels et al., 2014). Schizophrenia is a highly heritable disorder, and the genetic risk is conferred through a large number of alleles. Variations in genes involved in glutamate signalling, including NMDAR, and the immune system have been reported (Ripke et al., 2014), providing a link between the immune system and psychosis.

Our understanding of NMDAR functionality has been extended by single molecule imaging studies, which have shown that NMDARs are highly mobile structures and their trafficking between synaptic and extrasynaptic areas is a highly regulated process (Groc et al., 2009). Numerous synaptic proteins have been suggested to interact with NMDARs

as scaffolding partners, such as dopamine receptors, nicotinic receptors, EphB2R (Petit-Pedrol and Groc, 2021), or to regulate NMDAR membrane trafficking, such as protein kinase C, stress hormones or PDZ domains (Groc et al., 2009, 2004; Mikasova et al., 2017). Some of these binding partners of NMDARs have been shown to play a role in schizophrenia, such as disrupted in schizophrenia 1 (DISC1; Brandon and Sawa, 2011). Consequently, a theory of synaptic disorganization has been developed around the intriguing idea that NMDAR dysfunction could arise from alterations of the molecular environment rather than from a direct effect on ionotropic function of the receptor through mutations or allosteric regulation.

A substantial support for the glutamate hypothesis of psychosis is provided by the severe psychiatric symptoms presented in NMDAR encephalitis patients and the rapid improvement of symptoms after removal of NMDAR antibodies (Dalmau et al., 2007). Based on this fundamental observation of immune system-mediated NMDAR hypofunction and elaborating on the synaptic disorganization hypothesis, a search has been ongoing to identify NMDAR antibodies in psychotic patients with various illnesses. Indeed, pathogenic antibodies have been identified in psychotic patients (Jézéquel et al., 2017), however, subsequent studies failed to reproduce this finding (Bien et al., 2021; Kelleher et al., 2020).

Discoordination hypothesis

According to the discoordination hypothesis in schizophrenia, NMDAR hypofunction leads to impaired coordination of neuronal ensemble activity which in turn leads to information processing impairment (Szczurowska et al., 2018). This may form the basis for cognitive deficits in psychosis (Phillips and Silverstein, 2003). Increase in theta modulation of CA1 neuron firing and a resulting increase of pairwise correlation of neuronal activity after a psychotomimetic dose of dizocilpine (MK-801) was demonstrated in the hippocampus (Szczurowska et al., 2018). The authors hypothesize that the neuronal discoordination is driven by alterations of GABAergic interneuron activity, in line with previous findings showing disproportional sensitivity of GABAergic interneurons to NMDAR antagonists (Li et al., 2002). Interestingly, a genetic model of partial ablation of the GluN1 subunit of NMDAR in corticolimbic GABAergic interneurons in mice resulted in symptoms partially resembling those of NMDAR antibodies, including memory deficits and anhedonic behaviours (Belforte et al., 2010). Indeed, a central role of GABAergic interneurons in the context of NMDAR hypofunction in schizophrenia has been repeatedly suggested (Nakazawa and Sapkota, 2020).

Taken together, an extensive body of research in schizophrenic patients and animal models suggests that NMDAR dysfunction is at its core. The strongest argument in favour of the glutamate hypothesis of schizophrenia comes from the ability of NMDAR antagonists and NMDAR antibodies to induce psychotic symptoms in animals and in men. Emerging evidence points towards GABAergic interneurons as the prime target of NMDAR dysregulation.

Genetic models of schizophrenia

Deletions in the 22q11.2 portion of the human chromosome 22 result in sporadic cases of schizophrenia in 30 % of carriers, and represents the highest genetic risk factor in schizophrenia (McDonald-McGinn et al., 2015). Investigations in a mouse model of 22q11.2 deletion syndrome revealed that mutant mice have reduced performance in a goal-oriented learning task, and exhibit compromised stability and plasticity of hippocampal spatial maps during navigation. Specifically, the place cell fraction in mutant mice was 25 % smaller than in controls, and spatial tuning of individual place cells is less diffuse as indicated by fewer place fields per place cell. Furthermore, hippocampal spatial maps were less stable in mutant mice, as a significantly smaller fraction of place cells recurred from day to day in mutant mice, and place cells displayed a greater shift in preferred firing locations on subsequent days as assessed by centre of mass (COM) shift. Stability of place cell ensembles (recurrence probability and COM shift) correlates with learning performance in the goal-oriented learning task in control animals while the correlation is lost in mutant mice. In mutant mice, the place cell enrichment in goal location was absent in a striking difference to controls. Thus, place cell enrichment supports learning of the new goal location, and the lack of place cell enrichment may be associated with significantly worse performance during the goal-oriented learning task in mutant mice. This may be mediated through a lack of place field shift in mutant mice toward the reward location. Thus, these findings demonstrate that disrupted spatial representations underline the cognitive deficits in schizophrenic mice (Zaremba et al., 2017).

Mutations in the Disc1 gene, which encodes a scaffolding synaptic protein, is associated with schizophrenia and the Disc1-L100P mouse strain exhibit schizophrenia-like symptoms with working memory deficits accompanied by LTP deficits in the CA1 (Cui et al., 2016). Mutant mice have intact spatial coding, and their place cell properties are largely indistinguishable from control mice. However, mutant mice show a decrease in the number of place fields per place cell and a decrease in hippocampal theta power.

Moreover, there is a higher number of active interneurons in mutant mice and these interneurons fire with faster action potential kinetics. Furthermore, mutant mice have a reduced density of PV-interneurons in CA1 (Mesbah-Oskui et al., 2015). Alterations in interneuron activity and PV-interneuron density are consistent with reports of aberrant GABAergic signalling in schizophrenia (Li et al., 2002). The precise role of hippocampal interneurons in spatial working memory is yet to be understood and will help understand the cellular correlates of cognitive impairment in schizophrenia.

1.3.2. NMDAR ablation

Knock-out mouse models

Different subunits confer distinct physiological and molecular properties to NMDARs. Knock-out rodent models of the many genes comprising NMDARs have been generated to dissect their respective contribution to synaptic plasticity and learning. These findings are summarized in Table 1.

Table 1. NMDAR deletions in rodent models of NMDAR hypofunction.

Gene	**Region**	**Phenotype**	**Reference**
GluN2A	Whole brain	Impaired spatial working memory and spatial novelty preference	Sakimura et al., 1995
GluN2B	Cortex + CA1	Impaired hippocampal LTD, impaired learning and memory	Brigman et al., 2010
GluN2B	Hippocampus	Impaired spatial working memory	von Engelhardt et al., 2008
GluN1	CA3	Larger place fields in novel environment, impaired acquisition of novel spatial memories	Nakazawa et al., 2003
GluN1	CA1 + DG	Impaired LTP, impaired spatial discrimination, impaired pattern separation	Bannerman et al., 2012
GluN1	DG	Impaired LTP, impaired spatial working memory	Niewoehner et al., 2007
GluN1	CA1	Impaired LTP, impaired spatial memory, altered place field specificity and size, decorrelated place cell activity	McHugh et al., 1996

GluN2A knock-out mice show moderate deficiency in spatial learning, such as spatial working memory and novelty preference (Sakimura et al., 1995). Knock-out mice lacking GluN2B in pyramidal neurons in cortex and CA1 have normal LTP in the hippocampus while LTD is impaired. Mutants are impaired on cortico-hippocampal learning and memory tasks (Brigman et al., 2010). Mice lacking GluN2B in the forebrain are impaired on a range of spatial and nonspatial memory tasks. In contrast, hippocampus-specific GluN2B ablation spares hippocampus-dependent memory (hidden-platform water maze) but induces a selective, spatial working memory deficit for recently visited places (von Engelhardt et al., 2008). Mice with selective deletion of the GluN1 subunit in CA3 pyramidal cells are impaired in the rapid acquisition of novel spatial memories but their

ability to recall previously acquired memories is intact. CA1 place cells in the CA3-specific GluN1 knock-out mice had significantly larger place fields in novel environments, but normal place fields in familiar environments (Nakazawa et al., 2003). DG specific GluN1 knock-out mice displayed impaired LTP in the perforant path and have impaired spatial working memory. Mutant mice acquire spatial reference memory as well as controls, however they have deficits in using that information in a forced choice task (Bannerman et al., 2012; Niewoehner et al., 2007).

CA1-specific GluN1 knock-out mice lack NMDAR-mediated postsynaptic currents and LTP in the CA1 region. Also, these mice show impaired spatial memory (measured in the hidden platform version of the Morris water maze) but display good performance in nonspatial learning tasks. Remarkably, CA1-KO neurons display clear spatial selectivity despite the complete lack of NMDAR dependent synaptic plasticity. While fields in CA1-KO mice are present and stable, there are significant alterations of the quality and size of individual fields and spatial information carried by neuronal ensembles. Moreover, activity of CA1-KO neurons is significantly decorrelated, since neurons tuned to similar locations do not fire together (McHugh et al., 1996).

Pharmacological blockade

Several studies investigating the role of NMDARs in spatial learning and hippocampal function using NMDAR antagonists reported relatively normal place cell function (Hayashi, 2019; Kentros et al., 1998). These studies showed that long-term stabilization of newly formed place fields is NMDAR-dependent, suggesting the spatial learning process may be related to LTP, while formation and short-term stability of place fields is independent of NMDARs. Interestingly, NMDAR blockade by 3-[(R)-2-carboxypiperazin-4-yl]-propyl-1-phosphonic acid (CPP) does not affect place cell properties such as field size, information content, reliability, firing rate (Kentros et al., 1998). However, intrinsic dynamics of place cells, such as survival rates or activity differences between sessions, have been shown to be supressed by chronic treatment with CPP (Hayashi, 2019). On the level of behaviour, chronic intracerebroventricular infusion of the NMDAR antagonist (2R)-amino-5-phosphonovaleric acid (APV) with subcutaneously implanted osmotic minipumps resulted in selective deficits in spatial learning but not spatial navigation. Moreover, NMDAR antagonism with APV impaired the encoding of new spatial information but did not disrupt the retrieval of previously acquired spatial information (Morris et al., 2013).

This evidence from region-specific NMDAR knock-out mice and pharmacological blockade of NMDAR argue that NMDAR-dependent mechanisms participate directly in spatial learning. Importantly, impairment on the behavioural level is not due to sensorimotor disturbances since other forms of learning and navigation are intact (Morris et al., 2013). The changes of place cell properties appear rather mild compared to the behavioural deficits of NMDAR supressed mice. However, even small alterations of spatial coding at the CA1 level may be amplified in the downstream network. Furthermore, the spatial learning deficits in NMDAR supressed mice could arise from decorrelated neuronal activity: Hebbian synaptic plasticity mechanisms in downstream regions may fail to integrate such corrupt input into a robust memory (Tsien et al., 1996). Moreover, it has been hypothesised that changes in functional circuit ensembles rather than simple alterations in response properties of individual neurons generate pathophysiology. Chronic administration of the NMDAR antagonist ketamine results in disruption of neuronal ensemble activations, with a systematic disorganization of neuronal activity wherein the presence of distinct ensembles became less pronounced and recurring ensemble activations became less reliable over time (Hamm et al., 2017).

2. AIM OF THE STUDY

Psychiatric symptoms and cognitive deficits are key manifestations of NMDAR encephalitis and are consistent with hippocampal dysfunction. Moreover, the largest amount of NMDAR antibody binding occurs in the hippocampus, further supporting the central role of the hippocampus in NMDAR autoimmune encephalitis pathophysiology (Kayser and Dalmau, 2016). Research in a mouse model of the disease has shown a reduction in hippocampal NMDAR density and short-term memory deficits (Planagumà et al., 2015). Although initial studies used patient CSF to induce NMDAR encephalitis, the paramount role of NMDAR-specific antibody in NMDAR encephalitis pathophysiology has been demonstrated (Kreye et al., 2016). Building on previously published literature, the overall aim of my PhD project was to investigate cellular correlates of psychiatric and cognitive symptoms associated with NMDAR encephalitis in a mouse model of the disease using a monoclonal recombinant NMDAR antibody.

The NMDAR is a synaptic protein crucial for excitatory synaptic transmission and synaptic plasticity (Vyklicky et al., 2014). Given that NMDAR antibodies disrupt NMDAR signalling at synapses (Section 1.1.2) and that synaptic morphology is tightly coupled with synaptic plasticity (Section 1.2.4), I investigated the impact of NMDAR antibodies on dendritic spines. This forms the first part of my project, and these points were investigated utilizing confocal microscopy:

- Is dendritic spine density changed?
- Are dendritic spines affected morphologically?
- Are excitatory pyramidal neurons and inhibitory interneurons differentially affected by NMDAR antibodies?

NMDAR dysfunction has been implicated in several other neurological diseases, demonstrating compromised response properties of hippocampal neurons (Section 1.3). Thus, in the second part of my project, I investigated the effect of NMDAR antibodies on the function of CA1 hippocampal neurons, particularly focusing on spatially tuned cells (place cells). Research questions in this part were answered employing *in vivo* two-photon imaging in mice and following questions were answered:

- Are neuronal activity rates affected under anaesthesia and in awake mice?
- Are response properties of individual hippocampal place cells affected by NMDAR antibodies?
- Is the long-term stability of spatial representations in the hippocampus affected?
- Is the plasticity of spatial representations in the hippocampus affected?
- Is encoding of space in hippocampal neuronal network compromised?
- What is the impact of NMDAR antibodies on coordinated neuronal activity patterns (ensemble activations)?

3. MATERIALS AND METHODS

3.1. SURGICAL PROCEDURES

3.1.1. Mice

All experiments in this work that involved animals were carried out according to national and institutional guidelines. Experiments were approved by the government of the state of Bavaria under the license number 55.2-2532.Vet_02-18-80. The number of animals together with their genotype and age is summarized in Table 2.

Table 2. Mice used in the study.

Experiment type	Number	Genotype	Gender ratio m:f	Age mean (months) ± SD (days)
Dendritic spines	10	GFP-M	7:3	3.0 ± 31
	13	GAD67	9:4	3.5 ± 10
In vivo imaging	9	PV-cre	3:6	2.2 ± 22
	4	SST-cre	2:2	2.5 ± 5

Mice were bred and kept in-house (CAM facility) and housed in groups of 2-5 animals on a 12-hour light/dark cycle. Animals had free access to food and water. After the surgery, mice were kept individually. Mice for functional imaging experiments were kept on an inverted light/dark cycle and their access to water was limited to 1 ml per day starting one week before the training.

3.1.2. Hippocampal window

30 minutes before the surgery, analgesia (Metacam 1 mg/kg and Metamizol 200 mg/kg) was administered orally. Animals were anesthetized with a mixture of Medetomidine (0.5 mg/kg), Midazolam (5.0 mg/kg) and Fentanyl (0.05 mg/kg) intra-peritoneally. Once the animals were deeply anesthetized, they were removed from the cage and positioned in a stereotactic frame. Body temperature was maintained at 37 °C using a heating pad and eyes were protected against drying by applying an eye ointment (Bepanthen, Bayer). The scalp was washed three times alternating 70 % ethanol and iodine (Betadine) solution. Next, 2 % lidocaine (Xylocaine) was applied on the shaved scalp. After 5-10 minutes, a

longitudinal incision was made, using a sterile scalpel blade. Lidocaine was applied on the exposed skull again for several minutes.

Then, periosteum was removed, and shallow scratches were made onto the exposed skull with the apex of the scalpel blade in order to increase the bonding surface between the dental cement and the skull. The centre location of the window was 2.0 mm posterior from bregma and 2.0 mm lateral from the midline. Using a dental drill (NSK Presto II), a 3 mm diameter circular craniotomy was performed. The dura was gently peeled away using fine forceps. The exposed cortex was then aspired by applying suction through a 27 G blunt needle while the aspired area was continuously flushed with ice-chilled, sterile saline. Whenever any major bleeding occurred, aspiration was paused and a small piece of sterile Gelfoam (Pfizer) was applied until the bleeding stopped. Cortical aspiration was continued until the external capsule of the hippocampus became visible. Bleeding was stopped by applying Gelfoam and the area was cleared of debris and blood clots. Next, viral vectors AAV2/9-syn-jGCaMP7s-WPRE and AAV2/1-CAG-Flex-tdTomato-WPRE-bGH (AddGene) were diluted 1:10 and 1:50 in saline, respectively. The solution was injected into the hippocampus at 3 locations evenly spanning the excavated area. At each location, a thin glass pipette was slowly lowered 0.4 mm into the hippocampus, where 500 nl of virus solution was injected and left to diffuse for 5 minutes before the pipette was retracted. A hippocampal window was then inserted into the craniotomy and sealed around the edges with dental cement (Superbond C&B, Sun Medical). The hippocampal window consisted of a 1.5 mm long stainless-steel cannula of 3 mm in diameter, to which a 3 mm coverslip was glued using a Pattex ultra superglue (Henkel). A small amount of histoacryl tissue adhesive (Braun) was applied on the skull surface.

Once the hippocampal window was secured in place, the surgery proceeded with the insertion of the brain infusion catheter. A brain infusion catheter (brain infusion kit 3, Alzet) was inserted into the contralateral hemisphere (relative to the hippocampal window) at 0.2 mm posterior, 1.0 mm lateral from bregma and 2.2 mm depth from the brain surface. For the brain infusion catheter insertion, a small hole was drilled at the stereotactic location and the catheter was slowly lowered into the brain and secured with dental cement. The brain infusion catheter was connected to a piece of plastic tubing approximately 2 cm long and filled with sterile saline and sealed on the opposite end. The loose end of tubing was inserted into a subcutaneous pocket on the back of the animal. Two skull screws were inserted into the skull to provide further stabilizing points. To

provide an interface for head fixation, a metal head bar was affixed to the skull with dental cement.

The anaesthesia was antagonized with an intraperitoneal injection of Naloxone (1.2 mg/kg), Flumazenil (0.5 mg/kg) and Atipamezole (2.5 mg/kg) mixture. Mice were given a subcutaneous injection of 0.5 ml saline and placed on a heating pad, where they remained until they sufficiently recovered from the procedure. Analgesia (Metacam, 1 mg/kg) was administered orally 24, 48 and 78 hours after the surgery.

Osmotic minipump was implanted on day 0 of the experiment (30-40 days after surgery). After the mice were anesthetized, their backs were shaved and disinfected around the area of the subcutaneously implanted plastic tubing. Through a small skin incision, the plastic tubing was located, the sealed end cut and osmotic minipumps were connected to the open end. Osmotic minipump was inserted into a subcutaneous pocket on the right side of the animal. The skin was sutured, and animals left to recover on a heating pad. Analgesia (Metacam, 1 mg/kg) was given 24, 48 and 78 hours after the surgery.

3.1.3. Brain infusion for *ex vivo* analyses

For animals used for *ex vivo* analysis of dendritic spines, bilateral brain infusion catheter was implanted to deliver human antibodies. For this, animals were given analgesia and anesthetized as described above. Animals were positioned in the stereotax and the skull was exposed through a skin incision. For each hemisphere, a hole was drilled into the skull at 0.2 mm posterior and 1.0 mm lateral from bregma using a dental drill. Brain infusion catheters connected to the osmotic minipumps through a piece of tubing were stereotactically lowered 2.2 mm into the brain and secured with dental cement. Osmotic minipumps were then inserted into subcutaneous pockets on both sides of the animal. The skin was sutured over the entire implant. Anaesthesia was antagonized, mice were rehydrated with 0.5 ml saline injected subcutaneously and allowed to recover on a heating mat. Metacam was administered orally at 24, 48 and 78 hours after the surgery.

3.1.4. Osmotic minipump preparation

The solution for the brain infusion was prepared by diluting the control or NMDAR antibody in sterile saline. For *ex vivo* experiments (no window) and for *in vivo* imaging (with window) a total of 20 μg and 100 μg of antibody was delivered, respectively. The increased dose of antibodies for *in vivo* imaging was necessary due to lower infusion efficiency in these experiments. The delay between brain catheter implantation and

antibody infusion (30-40 days) may have resulted in tissue growth and clogging, thereby limiting the flow through the catheter. Osmotic minipumps were preassembled by connecting the brain infusion catheter through a piece of plastic tubing to the minipump filled with the antibody solution. To prime minipumps before the implantation, assembled minipumps were transferred to sterile saline and kept at 37 °C overnight.

3.1.5. Human antibodies

Recombinant human antibodies used in this work were kindly provided by Dr. Prüß (DZNE, Berlin), the generation of which was reported previously (Kreye et al., 2016). Briefly, single antibody secreting cells and memory B cells were isolated from CSF samples from patients with NMDAR encephalitis. Individual cells were subjected to reverse transcriptase-polymerase chain reaction (PCR), nested PCR and sequencing. Obtained immunoglobulin genes cloned into expression vectors were transfected into HEK cells and antibodies were harvested from the supernatant. Monoclonal antibodies were screened for reactivity on HEK cells transfected with the NMDAR. Out of 170 monoclonal antibodies generated, 9 were identified as NMDAR-reactive. The clone 003-102 was used in this work (refer to Kreye et al. (2016) for further details). The control antibody (mGo53) is a nonreactive human IgG antibody (Wardemann et al., 2003).

3.2. IMMUNOHISTOCHEMISTRY

At the end of the experiment, mice were deeply anesthetized with Ketamine (130 mg/kg) and Xylazine (10 mg/kg) mixture and perfused with 4 % paraformaldehyde (PFA, Sigma Aldrich) through cardiac perfusion. Brains were dissected and further fixed in PFA overnight at 4 °C. Next, brains were embedded in 3 % agarose and cut into 100 µm coronal sections using a vibratome (Leica VT1000). Sections were stored in 0.05 % NaN_3 in phosphate buffered saline (PBS, Sigma Aldrich).

3.2.1. Anti-human IgG staining

Successful antibody infusion was verified by anti-human IgG staining. Sections were transferred into a 48-well plate filled with PBS. Next, Sections were blocked in blocking buffer consisting of 10 % normal goat serum (NGS, Sigma Aldrich), 1 % bovine serum albumin (BSA, Sigma Aldrich), 0.5 % Triton X-100 (Sigma Aldrich) in PBS for 2 hours at room temperature. Sections were washed with PBS and incubated with goat anti-human IgG AF633 (Catalogue number A-21091, ThermoFisher Scientific) diluted 1:500 in

incubation buffer (5 % NGS, 1 % BSA, 0.5 % Triton X-100 in PBS) overnight at 4°C. The next day, sections were washed 3 times with PBS for 5 minutes and incubated with DAPI (1:10,000 in PBS, ThermoFisher Scientific). Sections were mounted with Vectashield mounting medium (Vectashield) on glass slides and edges sealed with nail polish.
Human IgG concentration in CSF and sera samples obtained from mice receiving the infusion was determined using ELISA (Mabtech) according to manufacturer's instructions.

3.2.2. Anti-IBA1 and anti-GFAP staining

Free-floating brain sections were blocked in blocking buffer (see above) for 2 hours at room temperature. Sections were washed with PBS and incubated with rabbit anti-IBA1 (ab178846, Abcam) and rat anti-GFAP (13-0300, ThermoFisher Scientific) antibodies diluted 1:500 in incubation buffer for 24 hours at 4 °C. Then, sections were washed 3 times with PBS for 5 minutes and incubated with goat anti-rabbit AF568 and goat anti-rat AF633 diluted 1:500 in incubation buffer for 24 hours at 4 °C. Sections were washed 3 times with PBS for 5 minutes and incubated with DAPI diluted 1:5,000 in PBS for 30 minutes. Sections were mounted with Vectashield mounting medium (Vectashield) on glass slides and sealed with nail polish.

3.2.3. Anti-PV and anti-SST staining

Free-floating brain sections were blocked in blocking buffer for 2 hours at room temperature, washed with PBS and incubated with rabbit anti-PV (ab11427, Abcam) or rabbit anti-GFAP (HPA019472, Sigma Aldrich) antibodies diluted 1:200 in incubation buffer overnight at 4 °C. The next day, sections were washed 3 times with PBS for 5 minutes and incubated with goat anti-rabbit AF647 diluted 1:500 in incubation buffer overnight at 4 °C. Sections were then washed 3 times with PBS for 5 minutes and incubated with DAPI diluted 1:5,000 in PBS for 30 minutes. Sections were mounted with Vectashield mounting medium (Vectashield) on glass slides and sealed with nail polish.

3.3. CONFOCAL IMAGING

To verify brain infusion efficiency, low resolution overviews of brain sections stained for human IgG were imaged on a confocal microscope (Leica SP8, 20x, 0.75 NA, 0.73x0.73 µm). Sections with positive hippocampal staining were identified and inspected for typical antibody binding pattern (high intensity CA1, low intensity DG). High resolutions

scans were taken to verify presence of synaptic pattern of the antibody staining (63x, 1.4 NA, 0.05x0.05 µm).

For reconstruction of dendritic spines, high resolution images (63x, 1.4 NA, pinhole 0.7 AU, 0.05x0.05x0.05 µm) of GFP expressing neurons were taken with the confocal microscope in the Stratum Oriens of CA1 layer of the hippocampus. The images were deconvolved using Huygens software (Scientific Volume Imaging) using dedicated settings (CMLE, 15 signal to noise ratio, 40 iterations).

Sections stained for IBA1 (microglia) and GFAP (astrocytes) were imaged at confocal microscope (Leica SP8, 40x, 1.3 NA, 0.2x0.2x0.4 µm). IBA1-positive and GFAP-positive cells were manually counted using the cell counter plugin in FIJI.

Sections stained for PV or SST were imaged at confocal microscope (Leica SP8, 20x, 0.75 NA, 0.54x0.54 µm).

3.4. *IN VIVO* IMAGING

3.4.1. Virtual reality task

Three weeks after the surgery, mice were put on a water restriction scheme. Mice received approximately 1 ml of water daily and their average weight was reduced to 85 % of their initial weight. Mice underwent handling and habituation to the head fixation for three consecutive days for 15-20 minutes per day. Once mice were habituated, they began the training in a head-fixed spatial navigation task for 30-60 minutes daily for 7 days. In this task, mice ran on an air supported styrofoam ball, which was restricted to backward and forward movements only with a blocking pin. The movement of the mouse was recorded via a computer mouse (MX-518, Logitech) and translated into the corresponding movement on the virtual track. The virtual reality setup consisted of a toroidal screen made of white paper, on which video feedback was projected though a top mounted projector (Samsung), which covered most of the mouse's visual field. To prevent any stray light reaching the detectors, the projector was operated in a flickering mode at 16 kHz synchronized in antiphase to the laser scanning.

The virtual track was a 3-metre corridor containing proximal and distal visual cues along the entire length, which were covered with textures. Mice collected 10 µl water rewards at determined locations marked by a prominent visual cue, which were delivered through a lick port. Once the mouse reached the end of the track, the screens were blanked for 2 seconds, and the mouse was teleported back to the beginning. Two linear tracks were

presented to the mouse at each imaging timepoint: a familiar context and a novel context. The novel track was visually different from the familiar one but consisted of similar shapes and textures. The number and locations of rewards was different on each track. Mice alternated between runs in the familiar and novel tracks in a random order. Mice were habituated to the imaging setup for 2-3 days and then trained in the virtual spatial navigation task for at least 7 consecutive days. By the end of the training period mice were proficient at the task and achieved at least 1 trial per minute. Mice not passing this threshold were excluded from the experiment. During the 7-day training period, only the familiar environment was presented to the mouse. On each imaging session, a new novel environment was presented.

3.4.2. Optical recording of activity

While mice performed the task in the virtual environment, activity of neurons was monitored through somatic fluorescence of the calcium indicator GCaMP7s. Data were collected on a two-photon microscope (Hyperscope, Scientifica) operated using the SciScan software (Scientifica). Field of views (FOV) measured 250 by 250 μm (512 by 512 pixels) with a single imaging plane for early experiments or several imaging planes for later experiments, in which volumetric imaging was performed. Volumetric scanning was achieved by using a piezo module, mounted onto the objective, allowing for fast vertical movement of the objective resulting in 4 imaging planes. Imaging data was acquired at 30 Hz using a resonant scanner. A Ti:sapphire laser (Mai Tai, Spectra Physics) was operated at 950nm to simultaneously excite GCaMP7s (green) and TdTomato (red). Green and red channels were isolated using a dichroic and 2 bandpass filters (525/625 nm, ThorLabs) and detected using GaASP photo-multiplier tubes (PMTs, Hamamatsu). Typical laser power underneath the objective (16x, 0.8 NA, Nikon) was 20-30 mW and was adjusted according to the signal detected by the PMTs. Imaging session typically lasted 15-20 minutes.

3.4.3. Behavioural recording

During the two-photon imaging data acquisition, pupil diameter and position, whisking and licking were recorded using an infra-red camera (DMK 22BUC03, ImagingSource), while running speed and position on the track were recorded using the computer mouse sensor. Synchronization of the behavioural data, reward timing and two-photon image timing was achieved by triggering all data acquisitions by the laser shutter opening times.

3.4.4. Imaging under anaesthesia

Mice were induced with 3 % isoflurane (vol/vol, in pure O_2) for 1-2 minutes. Then, mice were positioned under the objective and their eyes were protected with eye creme. Constant body temperature and breathing rate were monitored with a physiological monitoring station (Harvard apparatus). In order to achieve stable anaesthesia depth, isoflurane was reduced to 1.5 % and maintained for 20 minutes, and then further lowered to 1 % for another 10 minutes. After this period, the respiration stabilized at about 100-130 breaths per minute. Respiration rate was used as a readout for anaesthesia depth and was adjusted whenever the respiration rate was outside the desired range. Once the respiration rate stabilized, the recording of spontaneous activity was started.

3.4.5. Imaging data processing

Analysis of *in vivo* calcium imaging data was performed in FIJI (Schindelin et al., 2012) and MATLAB (R2018a, MathWorks) using custom written scripts. Motion artefacts of the imaging data were corrected with fast Fourier transform-based rigid transformation of individual frames relative to a selected template, which typically was the average of the first 5 frames. Whenever two channels were simultaneously recorded, motion artefacts were estimated using the red channel (TdTomato) and used for global motion artifact correction. When multiple imaging planes were acquired simultaneously, motion correction was performed independently for each plane. Processed data was visually inspected for motion artefacts and discarded whenever excessive z-drift was apparent. Next, motion corrected and time averaged data for each imaging session were aligned to sessions from the same FOV using image transformation.

Pyramidal cells in CA1 were segmented into regions of interest (ROIs) by outlining their cell bodies. Segmentation of individual neurons was achieved automatically using the constrained non-negative matrix factorization (CNMF) framework (Pnevmatikakis et al., 2016). This method identifies cell bodies based on their spatiotemporal correlation and simultaneously de-mixes overlapping components. ROIs extracted using the CNMF algorithm were visually inspected and manually corrected whenever necessary. Next, ROIs that corresponded to the same neurons were manually matched across imaging sessions. ROIs were carefully inspected at each imaging session to make sure that they were clearly visible throughout the entire imaging series. ROIs corresponding to PV or SST interneurons were identified by their TdTomato expression.

Calcium fluorescence traces were obtained from each ROI by frame-wise averaging of all pixels in a given ROI, resulting in a vector of mean fluorescence over time. Significant Ca^{2+} transients corresponding to single action potentials or bursts of neuronal firing were identified in fluorescence traces according to published methods (Dombeck et al., 2019). Briefly, Ca^{2+} traces were corrected for a baseline drift by subtracting the 8^{th} percentile of the fluorescence value distribution in a 10s sliding window. Next, Ca^{2+} traces were smoothed with a 2 Hz low pass filter. Baseline fluorescence was obtained by subtracting the 8^{th} percentile from the raw fluorescence trace in a 1 s sliding window. The filtered fluorescence trace was divided by the median of 50^{th} percentile of the baseline value which yielded a normalized (dF/F) trace. Candidate Ca^{2+} transients were fitted with an exponential fit using an autoregressive model (Friedrich et al., 2017). This denoised trace was then used for Ca^{2+} transient detection. Ca^{2+} transients were defined as peak events, which exceeded 6 times the baseline value (median of the entire trace), with a minimum threshold of 20% of the normalized trace. This threshold ensured that low signal-to-noise ratio events were excluded from the analysis. Minimal distance between Ca^{2+} transients was 1 s. Multiple transient peaks within a single, long lasting Ca^{2+} transient were considered only if there was a further increase of 3 times the baseline value within a single Ca^{2+} transient. Result of this procedure was a binarized trace, where all values that did not contain a Ca^{2+} transient were masked to zero.

3.5. QUANTIFICATION AND STATISTICAL ANALYSIS

3.5.1. Rate maps

For the place field analysis, only epochs in which the mouse ran more than 1 cm/s for at least 1 s were considered. Each track was divided into 100 spatial bins and the time spent in each bin and the number of Ca^{2+} events per bin were computed. The resulting maps ('occupancy' and 'Ca^{2+} event number') were smoothed using a Gaussian kernel (12 bins). Next, the activity rate map was calculated for each neuron by dividing the smoothed map of Ca^{2+} event numbers by the smoothed map of occupancy.

3.5.2. Identification of spatially tuned cells

Spatial information content in bits per Ca^{2+} event was calculated for all active cells (Ca^{2+} transient frequency > 0.05 Hz) according to the formula below (Markus et al., 1994):

$$Spatial\ Information\ = \sum_i p_i \left(\frac{r_i}{\bar{r}}\right) log_2 \left(\frac{r_i}{\bar{r}}\right)$$

where p_i is the probability of the mouse to be in the i-th bin (time spent in i-th bin/total running time), r_i is the Ca^{2+} event rate in the i-th bin and r is the overall mean Ca^{2+} event rate. For significant place cell detection, each fluorescence trace was subjected to a two-step permutation to generate a shuffle distribution: the trace was cut into segments containing a single Ca^{2+} transient (e.g., trace containing 10 Ca^{2+} transients results in 10 segments) and these segments were permuted in a random order. Next, permuted trace was circularly shifted by a random amount. 1000 distinct shuffles were generated for each trace, and the spatial information was calculated for each iteration. This process yielded the p-value of the real spatial information relative to the shuffled data. Cells with spatial information higher than that of 95% of their shuffle distribution were considered significant place cells. The fraction of place cells in each session was defined as the number of significant place cells out of the number of all cells in that session.

3.5.3. Place field properties

Place field width, centre of mass and number of place fields were computed for each place cell. Place field width was defined as the full width at half maximum of the binned rate map (see Figure 16A). Place cells with multiple fields were defined whenever multiple peaks of the rate map exceeded 50 % of the maximal value of the rate map with a drop of at least 25 % between neighbouring fields. The centre of mass (COM) of a place field was defined for each place cell as:

$$COM = \frac{\sum_i^N \Delta F_i x_i}{\sum_i^N \Delta F_i}$$

Where N is the number of bins, ΔF_i is the is the mean fluorescence of the i-th bin and x_i is the distance of the i-th bin from the start of the track. For all cells that had a defined place field in the familiar track during two consecutive sessions, the offset between the place field locations was defined as the distance between the two COMs of the place fields.

3.5.4. Population vector correlations

Similarity between neuronal representations of different environments and/or different imaging sessions was assessed with mean population vector (POV) correlations (Leutgeb et al., 2005). POV of an i-th bin was defined as Ca^{2+} event rate in i-th bin for all place cells having a place field in that session. POV was correlated to the matching location in

another session. This process was repeated for all position bins and the result was a N-by-N cross-correlation matrix, where N is the number of position bins (100).

3.5.5. Rate map correlation

Rate maps represent the binned Ca^{2+} activity rate divided by binned occupancy, smoothed with a Gaussian kernel (see Section 3.5.1). For each place cell, the level of similarity between the representations of familiar and novel environment or between representations of familiar environment on different imaging sessions were determined by calculating the rate map correlation. The stability of a place field was measured as the correlation between rate maps for runs in the familiar environment on two different sessions. Place cell reliability was defined as mean pairwise cross-correlation of rate maps corresponding to individual traversals made on the same track on the same day.

3.5.6. Position decoding

In order to assess spatial coding accuracy of the network, position of the animal on the virtual track was predicted using the recorded neuronal activity and compared to actual position of the animal. For position decoding analysis, the Maximum Correlation Coefficient classifier was used, which is a part of the Neural Decoding Toolbox (Meyers, 2013). Rate maps for each traversal of the linear track were randomly split into 70 % training data and 30 % test data (e.g., if total of 10 traversals were made, 7 would be used for training and 3 for testing).

The classifier derives a mean POV (template) for each class from the training data. In this case, each position bin on the virtual track is one class, and the template for each class is generated by averaging all training points within each class (i.e., the bin-wise average of rate maps across all place cells in that session). The classifier makes prediction on the test data by calculating the Pearson's correlation coefficient between a test point and the templates derived from the training set, and the class with the highest correlation value is returned as the predicted label (i.e., the inferred position bin). Model performance was measured by calculating the mean error (ME) rate defined as the mean of absolute difference between the predicted and actual position.

Cross-validation of the model was performed n-times, where n equals the number of traversals in the session, and which generated a distribution of ME values. In each iteration, different trials were assigned to the training and test datasets, which ensured equal contribution of the data to training and testing of the model. The reported value of

model performance is the mean of the ME distribution. The purpose of the cross-validation procedure was to generate a more reliable estimate of the model performance. To estimate chance rates of position decoding analysis, the data was shuffled by randomly permuting the vector of rate maps associated with the vector of positions. Next, the complete procedure described above was repeated and a shuffled distribution of ME values was generated.

3.5.7. Discrimination between contexts

Discrimination between the familiar and the novel context was quantified using the Discrimination Index:

$$Discrimination\ Index = \frac{POV_{Fam1-Fam2} - POV_{Fam-Nov}}{POV_{Fam1-Fam2} + POV_{Fam-Nov}}$$

Where $POV_{Fam1\text{-}Fam2}$ is the mean POV correlation between the first and the second block of 10 runs in the familiar environment and $POV_{Fam\text{-}Nov}$ is the mean POV correlation between all runs in the familiar environment and all runs in the novel environment. Discrimination index value of 0 signify no discrimination between contexts and a value of 1 signify perfect discrimination between the familiar and the novel contexts.

3.5.8. Identification of neuronal ensembles

Neuronal ensemble activations were defined as frames with significant levels of coactivity (Carrillo-Reid et al., 2016; Hamm et al., 2017).

Significance of ensemble activations was evaluated through a bootstrapping procedure to identify the chance levels of neuronal coactivations occurring due to uncorrelated variations in firing rates across neurons. First, fluorescence traces of individual neurons were normalized by dividing the entire trace by its maximal value. Normalized fluorescent traces were then averaged across neurons, which yielded a coactivity value for each frame ranging from 0 to 1, representing a fraction of total possible activity of the entire network. To generate the chance distribution of coactivation, each neuron's trace was randomly shifted in time and frame-wise coactivation was calculated for the shuffled dataset; this step was repeated 1,000 times. Ensemble activations were then identified as coactivity levels greater than 99% of the chance distribution. To exclude similarity of adjacent frames, only ensemble activations separated by at least 1.5 s were considered. This procedure was performed for each experiment separately and identified typically between 100-150 ensemble activation frames.

Next, neuronal ensemble activation frames were analysed for recurring patterns of activity. Pairwise Pearson's correlations between ensemble activation frames were calculated, resulting in n-by-n similarity matrix where n is the number of ensemble activation frames. Ensembles recurring significantly above chance were identified with bootstrapping. For this, neuron identity was shuffled 1,000 times within each frame, keeping overall activity constant. In each iteration, pairwise frame-frame correlations were calculated for the shuffled dataset. Significant similarity threshold was defined as 99th percentile of the shuffle distribution and was used to quantify the proportion of significant ensemble repeats and to adjust display of similarity matrices in Figure 20B.
Network state can be represented in an n-dimensional space, where n is the number of simultaneously recorded neurons. Principal component analysis (PCA) of the n-dimensional network state was used to reduce the network state into 3 principal components. k-means clustering on the PCA reduced space was repeated for values of k ranging from 2 to 15 to evaluate the optimal number of clusters. For each iteration of k, the clustering solution was evaluated with silhouette analysis. A silhouette value measures how similar a point is to points in its own cluster, when compared to points in other clusters. High silhouette values indicate that a point is well matched to its own cluster, and poorly matched to other clusters. This step was repeated 100 times to ensure the stability of the solution. k with the highest silhouette value was selected as the best number of clusters. For visual representation in Figure 20C, k-means clustering with k = 4 was performed.

3.5.9. Statistical analysis

Statistical testing in this work was performed in Prism (GraphPad) and MATLAB. Data is presented as mean ± standard deviation (SD) or standard error of the mean (SEM). All statistical tests are described in the figure legends. Where applicable, parametric statistical tests were performed. All comparisons were two-sided, ANOVA tests were one-way or two-way tests. Statistical comparison of bootstrapped means (Figure 7J and Figure 8J) was performed by drawing 2 random samples from the pooled data and calculating the difference of their means; this procedure was repeated 10,000 times. The resulting p-value is expressed as the fraction of values equal to or more extreme than the true value.
Although data presented here is of a nested nature (animals – recording sessions – neurons), single neurons were chosen as statistical units in accordance with established

conventions in the field (Hainmueller and Bartos, 2018; Silva et al., 2015). Moreover, statistical analysis of pooled neurons represents a unique opportunity to investigate changes in statistics distributions.

4. RESULTS

4.1. PASSIVE TRANSFER MOUSE MODEL OF NMDAR ENCEPHALITIS

To induce NMDAR encephalitis, I employed chronic passive transfer of human antibodies into the cerebral ventricles of mice using osmotic minipumps (Figure 5A). The antibodies diluted in sterile saline were continuously infused into the brain through bilateral intracerebroventricular catheters over 14 days, after which the minipumps became fully exhausted. For the following 4 days (days 15-18), the antibody further diffuses from the ventricular system and reaches the peak in brain immunopositivity 18 days after the infusion was started (Planagumà et al., 2015). For this reason, animals were sacrificed at day 18 of the experiment (Figure 5B). Mice were perfused, their brains sectioned and stained for presence of human IgG (see Section 3.2). Brains infused with NMDAR but not control antibody showed clear human IgG immunopositivity throughout the brain (Figure 5C). The staining pattern of animals that received brain infusion resembled the staining pattern of sections directly incubated with the NMDAR antibody (Figure 5D). This binding pattern was consistent with NMDAR expression throughout the brain (Planagumà et al., 2015). The strongest antibody binding was in the hippocampus, while other brain areas such as the cortex and cerebellum showed approximately 20 % of that of the hippocampus.

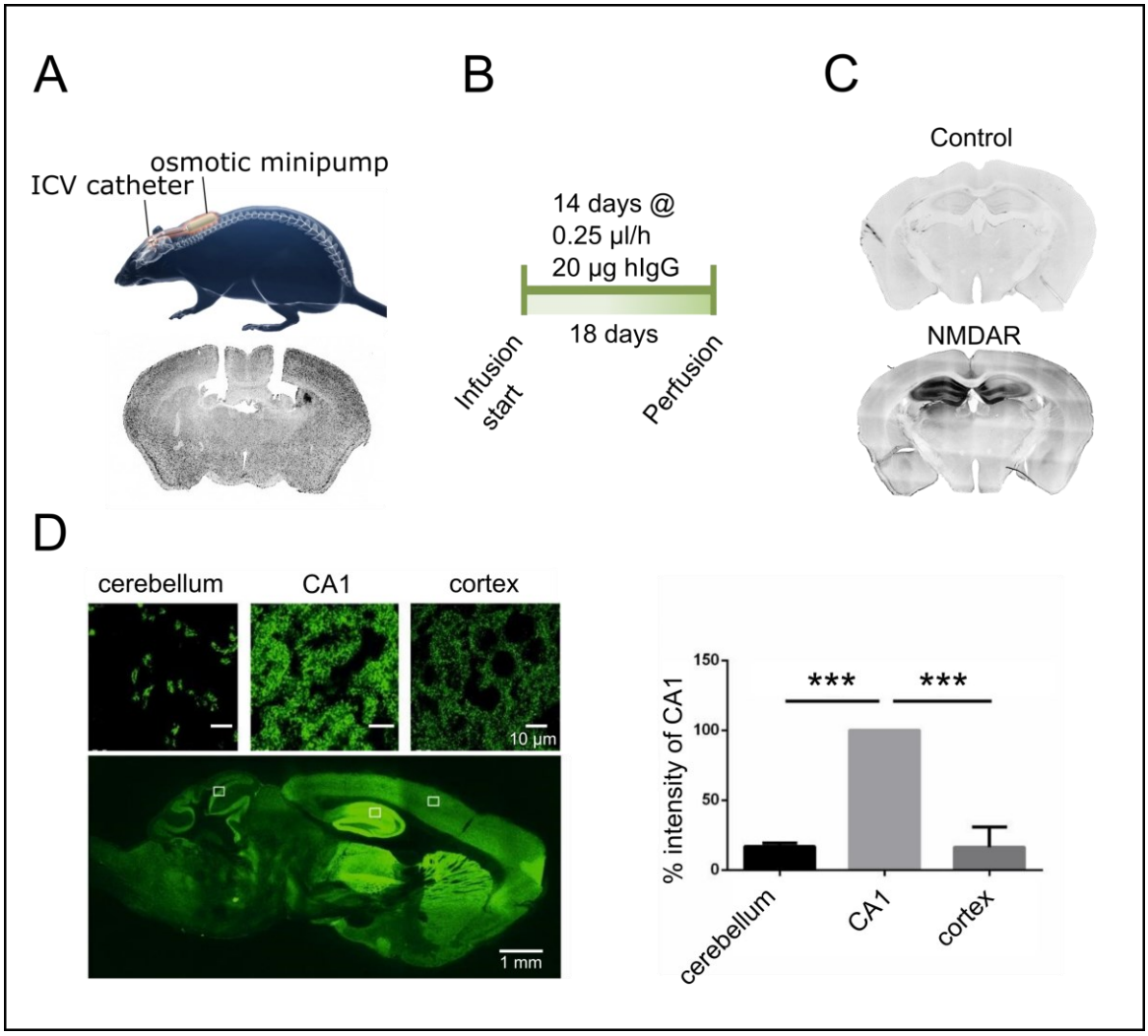

Figure 5. **Passive transfer of human monoclonal IgG antibodies into mice. A**, Schematic of the brain infusion setup consisting of intracerebroventricular catheters connected through a piece of tubing to subcutaneously implanted osmotic minipumps (top). Antibody solution was delivered bilaterally (bottom). **B**, A timeline depicting the experimental procedure. **C**, Anti-human IgG-stained sections of control and NMDAR infused mice (black area corresponds to high antibody deposits). **D**, Quantification of a relative staining intensity of brain sections incubated directly with NMDAR antibody. Images were taken with identical laser power and a mean intensity of a standardized area was computed. Values are normalized to CA1 levels. Significance was evaluated with one-way ANOVA. n = 4 sections from 4 mice. Data is mean ± SD. *** $p < 0.001$.

Next, I asked the question what the extent of tissue damage and neuroinflammation associated with the cannula insertion and the intracerebroventricular delivery is. Low impact on the brain function is critical for *in vivo* imaging of neuronal structure and function. For this, a group of mice (n = 5) received intracerebroventricular saline infusion for 14 days, after which the mice were sacrificed, and their brains were analysed for neuroinflammation by quantifying the number of microglia (IBA1) and astrocytes (GFAP). Numbers of immunopositive cells were quantified in the ipsilateral and contralateral cortices in the immediate vicinity of the insertion site (Figure 6A). This analysis showed a trend towards higher IBA1-positive cell counts on the ipsilateral cortex

next to the insertion side of the catheter, compared with cell counts obtained from a sham animal that received no intracerebroventricular infusion (317 cells/mm^2 and 349 cells/mm^2 IBA1-positive cells for sham and minipump group, respectively). GFAP-immunopositive cell counts were significantly increased on the ipsilateral hemisphere (104 cells/mm^2 and 366 cells/mm^2 GFAP-positive cells for sham and minipump group, respectively). Importantly, both IBA1 and GFAP-immunopositive cells remained at baseline levels on the contralateral cortex.

Quantification of IBA1 and GFAP-immunopositive cell counts in the CA1 layer of the hippocampus did not show any significant increase compared to the baseline levels (258 cells/mm^2 and 254 cells/mm^2 IBA1-positive cells, 407 cells/mm^2 and 450 cells/mm^2 GFAP-positive cells for the sham and minipump group, respectively; Figure 6B). Together, these results show that intracerebroventricular catheters are associated with a significant increase in GFAP-immunopositive cell counts in the immediate vicinity (0.5-1.0 mm) of the cortical insertion site. Furthermore, the neuroinflammation does not extend to the hippocampus, particularly the CA1, further warranting the use of the model for hippocampal neuron investigations.

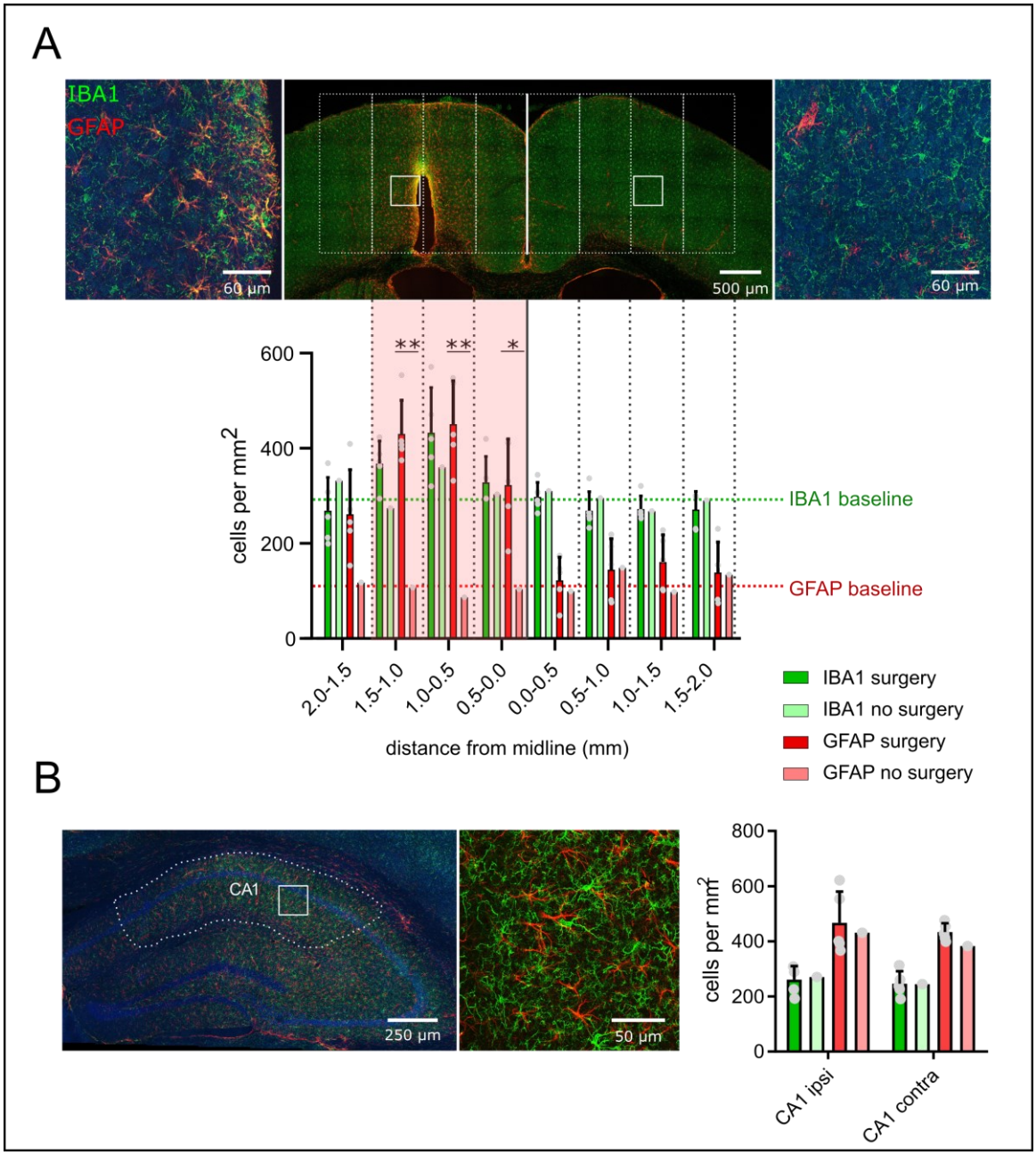

Figure 6. **Assessment of inflammation caused by intracerebroventricular infusion. A**, Overview of a coronal section stained for microglia (IBA1, green) and astrocytes (GFAP, red). Below, quantification of IBA1 and GFAP-immunopositive cells in areas with varying distance from midline (white rectangles). **B**, Quantification of IBA1 and GFAP-immunopositive cells in CA1 layer of the hippocampus. $n_{(surgery)}$ = 5 animals, $n_{(no\ surgery)}$ = 1 animal. Statistical comparison was performed with Bonferroni corrected one sample t-tests against cell counts of the animal that had received no surgery. * $p < 0.05$, ** $p < 0.01$.

4.2. STRUCTURAL ALTERATIONS OF CA1 NEURONS

Data presented in this chapter were obtained together with Sebastian Ehrt (Figure 7) and Anna Brauer (Figure 8), MD students in the Liebscher lab. To investigate structural alterations of dendritic spines in excitatory neurons, GFP-M animals were implanted with osmotic minipumps. 18 days later, mice were sacrificed and their brains inspected for antibody deposits using a confocal microscope (Figure 7A, B). Neuronal somata in the CA1 region of the hippocampus (Figure 7C, F) were located and their basal dendrites in stratum oriens were imaged at high resolution (Figure 7D, G). Typical branches were 100-150 µm long, and images of dendrites starting at the neuronal soma were acquired.
Quantification of dendritic spines (Figure 7E, H) revealed an increase in spine density as a function of distance to the soma, which plateaued at 80-100 µm from the neuron soma (Figure 7I). For this reason, I focused the analysis on this portion of dendritic arbour for each neuron investigated. The comparison of two main morphological parameters of dendritic spines, head diameter and spine length, showed identical spine head diameters between the groups (Figure 7J; $p = 0.13$). However, spines of NMDAR infused mice were significantly longer than spines from the control group ($p < 0.001$). Comparison of overall dendritic spine density revealed no significant difference between the control and NMDAR group (Figure 7K, $p = 0.6$). When classifying dendritic spines based on morphological features into stubby (short with no neck), thin (long with no head) and mushroom (with neck and head), I found no significant differences between the groups (Figure 7L, $p = 0.6$). Together, these results show that NMDAR antibodies do not affect dendritic spine density of excitatory pyramidal neurons in the hippocampus. However, these spines are morphologically affected.

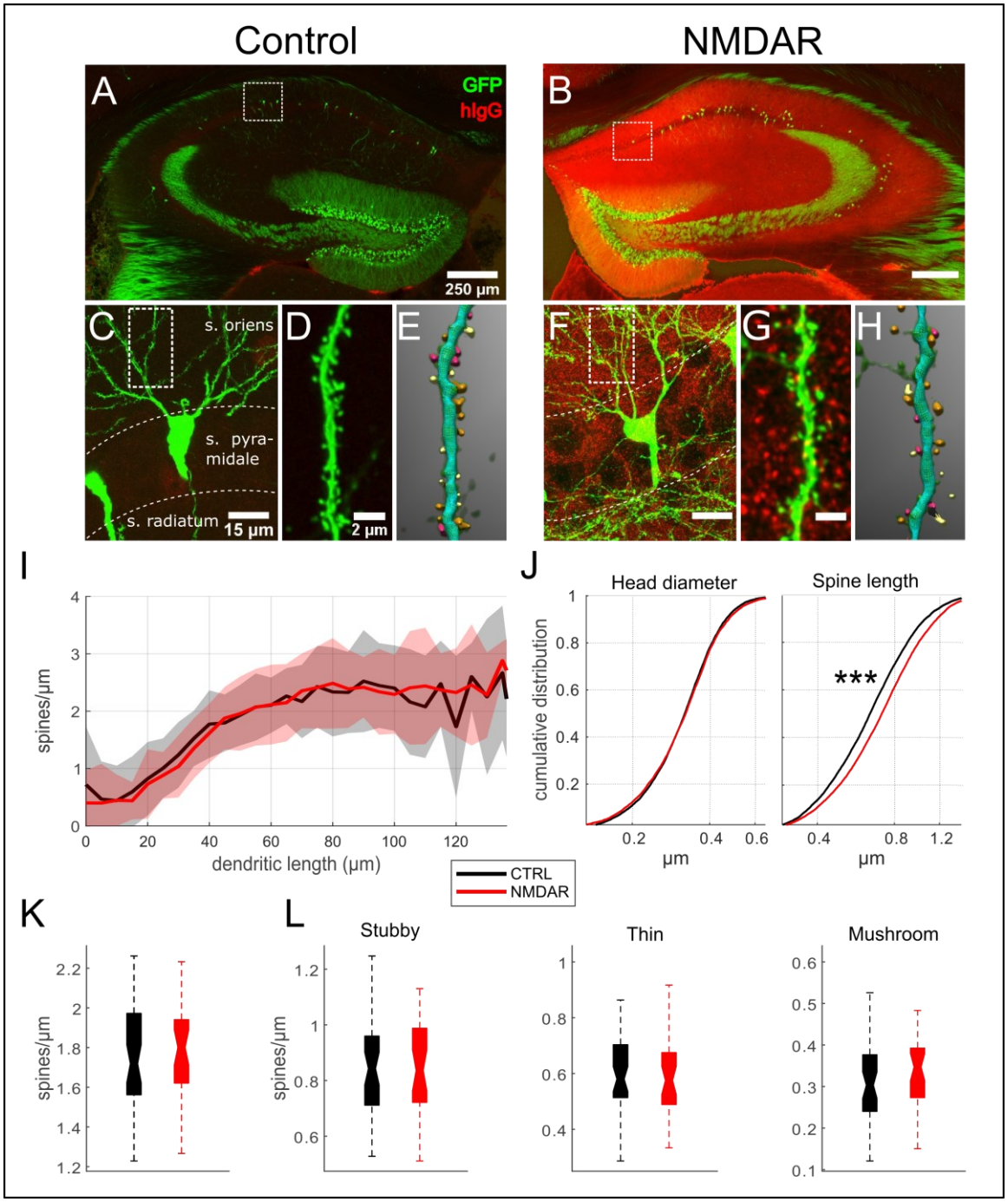

Figure 7. ***Ex vivo*** **analysis of dendritic spines of CA1 pyramidal neurons in GFP-M mice. A** and **B**, overview scans of hippocampi of control and antibody infused mice. **C** and **F**, GFP-expressing pyramidal neurons located in the CA1 layer of the hippocampus. **D** and **G**, dendrites in stratum oriens of these neurons imaged at high resolution. **E** and **H**, 3D reconstructions of dendrites and dendritic spines in D and G. Stubby spines are depicted in red, thin spines in yellow, and mushroom spines in orange. **I**, Dendritic spine density as a function of distance from the neuron soma. Data is represented as mean ± SD. Significance was evaluated with two-way ANOVA; effect of treatment: $F_{(1,1512)} = 0.84$, $p = 0.36$; effect of soma distance: $F_{(28, 1512)} = 60.6$, $p < 0.001$; interaction: $F_{(28,1512)} = 0.90$, $p = 0.62$. **J**, Cumulative distribution function plot of all spine head diameters and spine lengths. $p_{(\text{head diameter})} = 0.13$, $p_{(\text{spine length})} < 0.001$, comparison of bootstrapped means. **K**, Total dendritic spine density. $p = 0.6$, two-tailed t-test. **L**, Spine density of spines classified as stubby, thin and mushroom. effect of treatment: $F_{(1, 228)} = 0.3$, $p = 0.6$; effect of spine type: $F_{(2, 228)} = 248$, $p < 0.001$; interaction: $F_{(2, 228)} = 0.10$, $p = 0.9$, two-way ANOVA with Šidák multiple comparisons test. $n_{(\text{Control})} = 12{,}595$ spines in 45 stretches from 5 animals, $n_{(\text{NMDAR})} = 10{,}226$ spines in 33 stretches from 5 animals, data shown in boxplots with the central mark corresponding to the median, the bottom and top edges to the 25th and 75th percentiles, respectively, whiskers are the most extreme data points.

To further understand the effect of NMDAR antibodies on neuronal structure, I investigated dendritic spines in CA1 neurons in the GAD67 mouse line, which expresses GFP in inhibitory interneurons majority of which are SST interneurons. As previously, GAD67 animals were implanted with osmotic minipumps and sacrificed at day 18 of the intracerebroventricular infusion. Brains of NMDAR antibody-infused mice but not controls showed positive staining (Figure 8A, B). GFP-expressing interneurons in CA1 (Figure 8C, F) were imaged at high resolution (Figure 8D, G). A high variability in spine density was found along the dendritic arbour of these interneurons (data not shown), with majority of dendritic spines located on dendrites further away from the neuron soma. Therefore, I focused my analysis to dendritic stretches starting at 100 µm from the soma and reconstructed dendritic spines in these stretches (Figure 8D, G).

The analysis of dendritic spine density as a function of distance from the soma starting at 100 µm (Figure 8I) showed no dependence on soma distance ($p = 0.19$). This eliminated the soma distance as a confounding factor and warranted the comparison of spine density between the groups. Analysis of morphological parameters revealed significantly shorter spines with smaller spine heads in the NMDAR infused group (Figure 8J; $p_{(\text{head diameter})} = 0.04$, $p_{(\text{spine length})} = 0.004$). Analysis of dendritic spine density showed significant increase in total spine density in the NMDAR group compared to the control group (Figure 8K; $p = 0.04$). When classifying dendritic spines into stubby, thin and mushroom spines, there was a significant increase in stubby spine density in the NMDAR group (Figure 8L; $p = 0.03$). These results show that CA1 interneurons undergo structural changes upon NMDAR antibody exposure, leading to increased overall spine density and decrease in spine size.

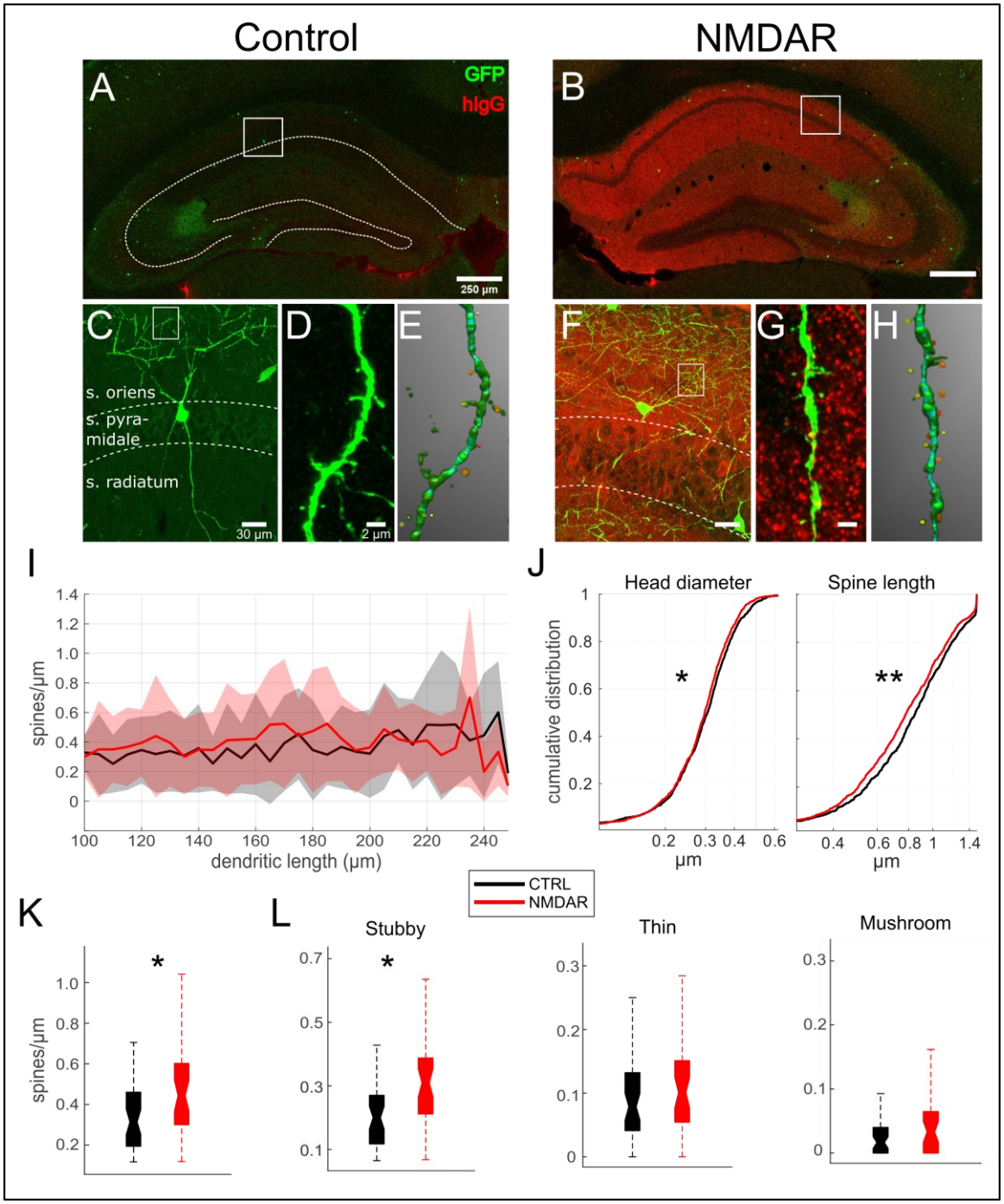

Figure 8. ***Ex vivo* analysis of dendritic spines in CA1 interneurons of GAD67 mice. A** and **B**, overview scans of hippocampi of control and antibody infused mice. **C** and **F**, GFP-expressing interneurons located in CA1 layer of the hippocampus. **D** and **G**, Dendrites in stratum oriens of these neurons imaged at high resolution. **E** and **H**, 3D reconstructions of dendrites and dendritic spines in D and G. Stubby spines are depicted in red, thin spines in yellow, and mushroom spines in orange. **I**, Dendritic spine density as a function of distance from the neuron soma. Data is represented as mean ± SD. Significance was evaluated with two-way ANOVA; effect of treatment: $F_{(1,\ 1011)} = 1.2$, $p = 0.3$; effect of soma distance: $F_{(30,\ 1011)} = 1.2$, $p = 0.2$; interaction: $F_{(30,\ 1011)} = 0.9$, $p = 0.6$. **J**, cumulative distribution function plot of all spine head diameters and spine lengths. Significance was evaluated through bootstrapped means; $p_{(\text{head diameter})} = 0.04$, $p_{(\text{spine length})} = 0.004$. **K**, Total dendritic spine density. $p = 0.04$, two-tailed t-test. **L**, Spine density of spines classified as stubby, thin and mushroom. On each box, the central mark indicates the median, and the bottom and top edges of the box indicate the 25th and 75th percentiles, respectively. The whiskers extend to the most extreme data points. Significance was evaluated with two-way ANOVA; effect of treatment: $F_{(1,\ 252)} = 8.3$, $p = 0.004$; effect of spine type: $F_{(2,\ 252)} = 63.5$, $p < 0.001$; interaction: $F_{(2,\ 252)} = 0.7$, $p = 0.5$. Multiple comparisons were

performed through Šidák test. $n_{(Control)}$ = 1,305 spines in 46 stretches from 7 animals, $n_{(NMDAR)}$ = 1,422 spines in 40 stretches from 6 animals. * $p < 0.05$, ** $p < 0.01$.

4.3. FUNCTIONAL ALTERATIONS OF CA1 NEURONS

4.3.1. Spontaneous activity under anaesthesia

Imaging neurons under isoflurane anaesthesia pose a unique opportunity to assess their spontaneous activity under baseline conditions, without confounding factors such as ongoing cognitive processes or locomotor activity. Imaging of spontaneous activity was performed at the beginning (day 0, baseline) and at the end of the experiment (day 18, peak of antibody deposits; Figure 9A).

The same FOVs were imaged before and after the antibody infusion and activity rates of pyramidal neurons were quantified (Figure 9B). In total, 2,222 (day 0) and 1,524 (day 18) cells in the control group and 2,219 (day 0) and 2,069 (day 18) cells in the NMDAR group were analysed. Fluorescence traces of these neurons were scored for amplitude and frequency of Ca^{2+} events (Figure 9C) and pairwise correlations between traces of simultaneously recorded neurons (Figure 9D). At day 0, the amplitude of calcium transients was 0.41 and 0.42 for control and NMDAR groups, respectively. At day 18, there was a significant increase in transient amplitude in the NMDAR group when compared to controls (control: 0.38 and NMDAR: 0.46, $p < 0.001$; Figure 9E). Moreover, frequency of calcium transients increased at day 18 in the NMDAR group (0.21 Hz) when compared to the control group (0.15 Hz, $p < 0.01$; Figure 9F). Baseline transient frequency was 0.16 Hz and 0.18 Hz for the control and NMDAR group, respectively. Mean pairwise correlation between neurons in each FOV was 0.04 (control) and 0.05 (NMDAR) at baseline. At the end of the infusion, there was a significant decrease in mean pairwise correlations in the NMDAR group (0.03) when compared to the control group (0.04, $p < 0.001$). These results indicate that NMDAR antibodies cause an increase in spontaneous activity of CA1 pyramidal neurons.

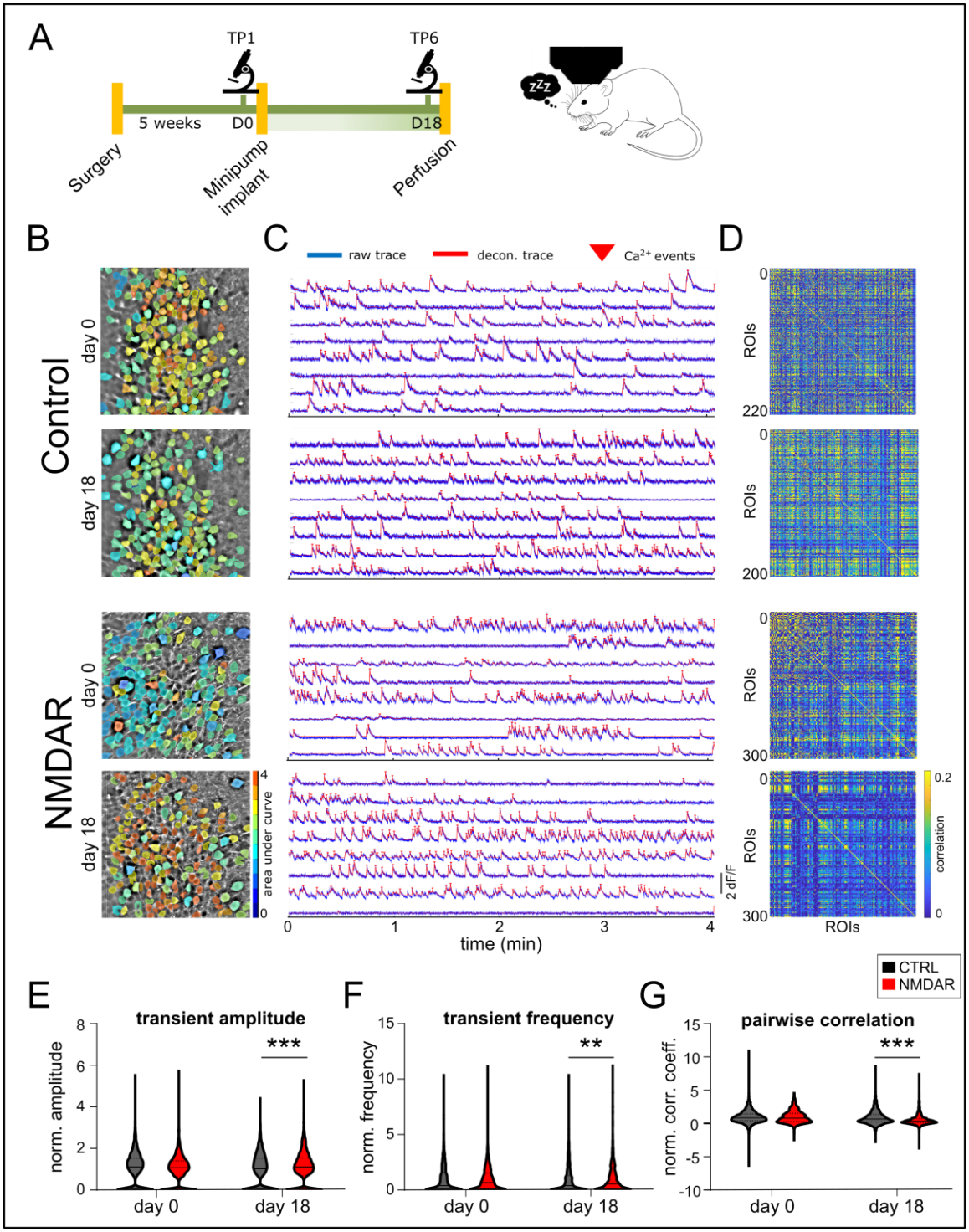

Figure 9. **Spontaneous activity of pyramidal neurons under isoflurane anaesthesia. A**, Timeline of the experiment. Imaging under anaesthesia was done at day 0 (before) and day 18 (after). The same mice were used for awake imaging. **B**, Example FOVs for control (upper two rows) and NMDAR (lower two rows) groups with neurons colour coded based on integral of the trace (area under curve) representing the overall activity. **C**, Corresponding fluorescence traces of neurons in B. **D**, Pairwise correlation matrix for neurons in B. **E**, Amplitude of Ca^{2+} transients. Effect of time: $F_{(1,\ 8030)} = 1.2$, $p = 0.3$; effect of treatment: $F_{(1,\ 8030)} = 14.9$, $p < 0.001$; interaction: $F_{(1,\ 8030)} = 14.9$, $p < 0.001$. **F**, Frequency of Ca^{2+} transients. Effect of time: $F_{(1,\ 8030)} = 0.1$, $p = 0.7$; effect of treatment: $F_{(1,\ 8030)} = 5.3$, $p = 0.02$; interaction: $F_{(1,\ 8030)} = 5.3$, $p = 0.02$. **G**, Pairwise correlation between neurons. Effect of time: $F_{(1,\ 8030)} = 171$, $p < 0.001$; effect of treatment: $F_{(1,\ 8030)} = 60$, $p < 0.001$; interaction: $F_{(1,\ 8030)} = 60$, $p < 0.001$. Significance was evaluated with two-way ANOVA followed by Šidák multiple comparisons test. ** $p < 0.01$, *** $p < 0.001$. $n_{(Control)} = 2{,}222$ (day 0) and 1,524 (day 18) cells from 5 animals, $n_{(NMDAR)} = 2{,}219$ (day 0) and 2,069 (day 18) cells from 4 animals. Data is shown as mean ± SEM.

4.3.2. *In vivo* two-photon imaging in behaving mice

In order to understand the impact of NMDAR antibodies on neuronal function, I investigated response properties of hippocampal neurons *in vivo* in behaving mice. To this end, I developed a hippocampal window preparation combined with delayed intracerebroventricular infusion.

To perform *in vivo* imaging of hippocampal neurons, mice were implanted with a hippocampal window consisting of a 1.5 mm long stainless-steel cannula with a 3 mm glass coverslip glued to one end (Figure 10A). A single intracerebroventricular catheter was implanted on the hemisphere opposite to the hippocampal window (Figure 10B). After baseline imaging was acquired, osmotic minipump was implanted subcutaneously and connected to the intracerebroventricular catheter through a piece of plastic tubing. A total of 100 μg of recombinant control or NMDAR antibody was delivered through the brain catheter. Animals that received NMDAR antibody but not controls showed clear human IgG staining throughout the brain, most prominently in the hippocampus (Figure 10C).

A total of 9 PV-cre mice and 4 SST-cre mice underwent the surgery at the age of approximately 2 months (see Table 2). Mice were left to recover 3-4 weeks, after which training and screening began. By the end of the training period mice were proficient at the task and achieved at least 1 trial per minute. Two-photon imaging was conducted at days -5, 0, 5, 10, 14 and 18. Timepoints 1 and 2 represent the baseline (i.e., before antibody administration), timepoints 3 and 4 represent the early symptomatic stage and timepoints 5 and 6 represent the late symptomatic stage (Figure 10D).

Two photon fluorescence data was collected at each session, while the animals performed the virtual spatial navigation task. The imaging data was corrected for motion artifacts with image registration procedure based on rigid transformation. ROIs corresponding to individual neuron bodies were extracted from motion-corrected data (Figure 10E). ROIs corresponding to the same neurons were drawn (Figure 10F).

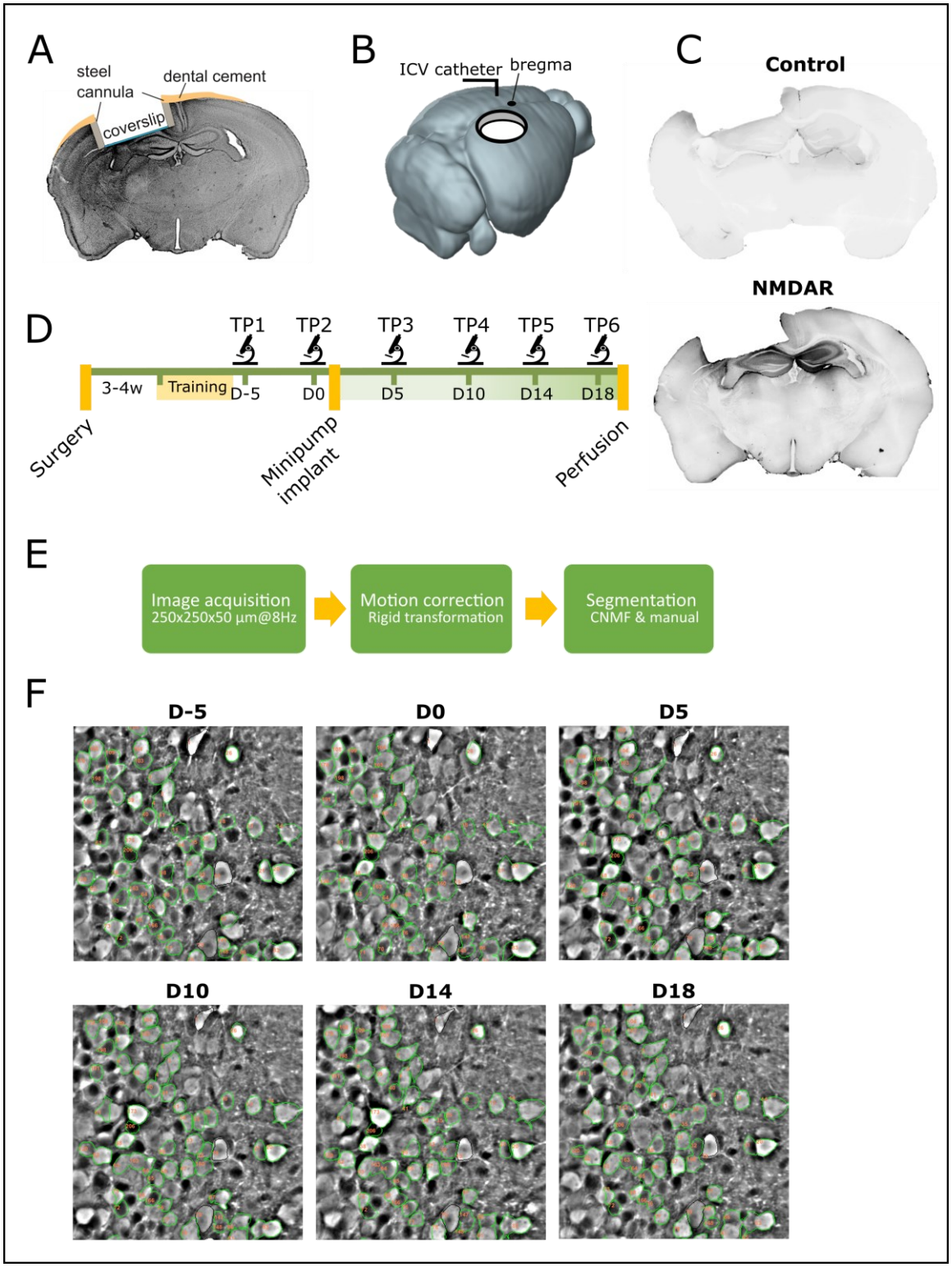

Figure 10. ***In vivo*** **imaging in the hippocampus combined with intracerebroventricular infusion.** **A**, Schematic of a hippocampal window consisting of 1.5 mm long stainless-steel cannula with a 3 mm glass coverslip glued to one end. **B**, Position of the hippocampal window and the intracerebroventricular catheter on the skull. **C**, Representative brain sections of mice infused with the control (top) and NMDAR (bottom) antibody. Anti-human IgG staining (inverted). **D**, Timeline of the experiment with key procedures highlighted. Gradual increase in antibody concentration is depicted in colour gradient. **E**, Simplified imaging data processing scheme. **F**, Representative example of a single FOV for all imaging timepoints for a PV-cre mouse. Excitatory neurons are segmented in green colour and inhibitory PV interneurons in black colour.

At each imaging session, mice performed a head-fixed spatial navigation task in a virtual reality setup (Figure 11A). During this task, mice ran on the familiar and novel tracks and collected water rewards (Figure 11B). Familiar and novel contexts were alternated in a random fashion after each completed trial. While mice performed the spatial navigation task, the position of the animal on the virtual track was recorded (Figure 11C). At the same time, licking (Figure 11D) and pupil diameter (Figure 11E) were tracked.

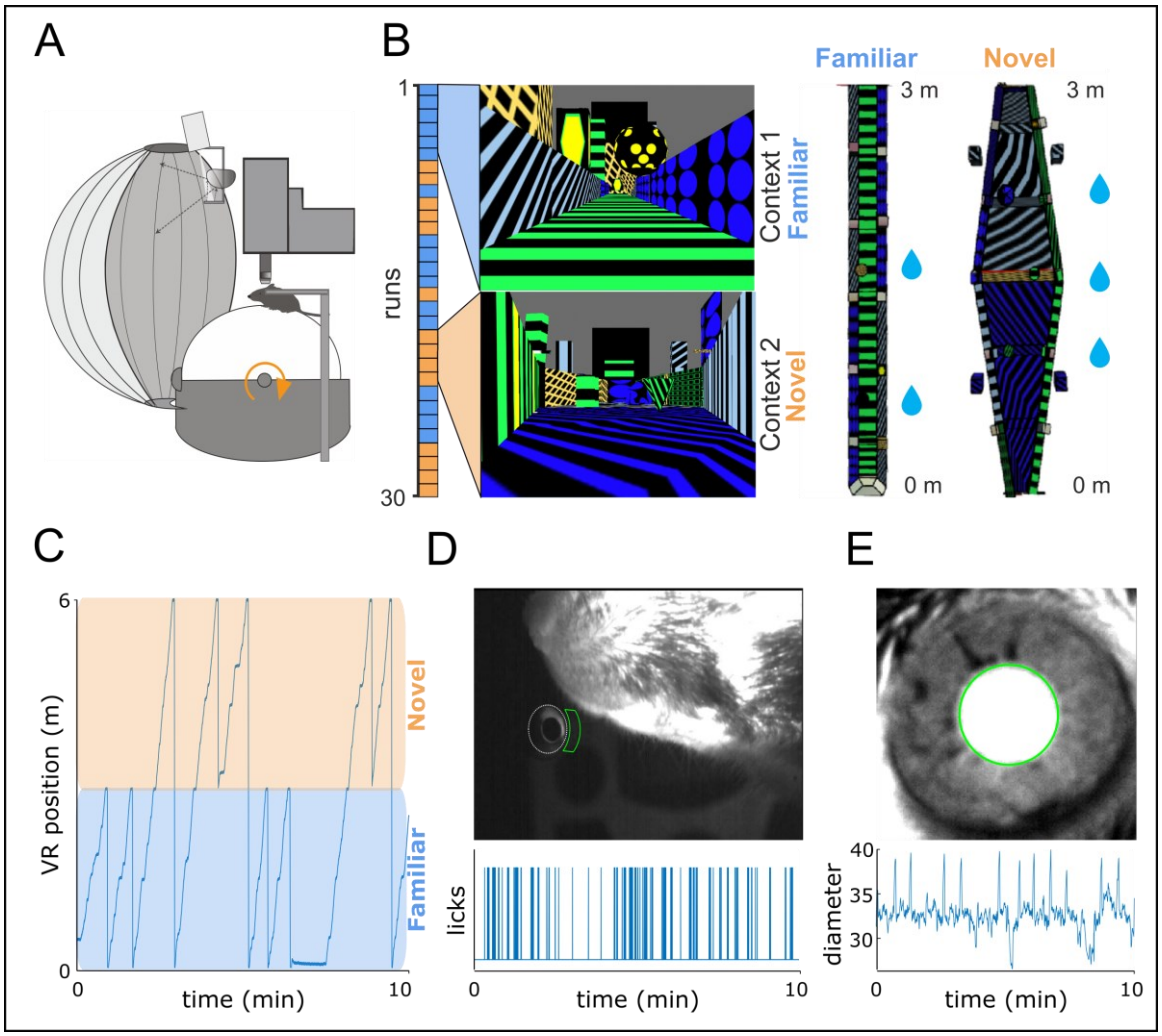

Figure 11. **Head-fixed spatial navigation task in a virtual reality. A**, Virtual reality setup consisting of an air-supported styrofoam ball, toroidal screen with a top-mounted projector, and a two-photon microscope. Movement of the ball rotation was restrained with a pin to forward and backward rotations. **B**, Design of the virtual linear track. Two linear tracks were presented to the mouse in a randomly alternating fashion. The same context 1 was used on each imaging session (familiar context) and a new context 2 was used on each imaging session (novel context). **C**, Example position trace showing random alternation between contexts. **D**, Licking detection. Top, an infrared camera image of the mouse's snout with the lick port used for water rewards delivery (highlighted with a dashed ellipse). Licks were detected through thresholding (green area). Bottom, example licking binary trace. **E**, Pupil tracking. Top, an infrared camera image of the mouse's eye with pupil diameter depicted with green circle. Bottom, example pupil diameter trace. Peaks correspond to pupil dilation in response to screen blanking between individual trials.

4.3.3. Virtual spatial navigation task

Three behavioural readouts were recorded to monitor the animal's performance on the virtual navigation task and to quantify the learning: running speed, licking and pupil diameter (proxy for arousal). Behavioural readouts binned along the virtual tracks showed typical behaviour in the spatial navigation task: the animals consistently run through the virtual linear track until they approached the reward location, which was marked by prominent visual and auditory cues. The animals tended to slow down ~20 cm before the reward location (Figure 12A) and increased licking in reward anticipation (Figure 12D), accompanied by increase in pupil diameter (Figure 12G). The performance in the familiar environment was constant throughout individual trials of a single imaging session as well as throughout the entire experiment. However, animal's behaviour in the novel environment was characterized by a relatively poor performance in the five initial trials, as indicated by the absence of running speed reduction (Figure 12B), increase in licking (Figure 12E) and pupil dilation (Figure 12H) prior to reward delivery. In later trials (11-15 trials), the performance on the novel track was similar to the familiar track, indicating that the mice learned to associate the reward with a new location during the imaging session, which typically lasted 10 minutes and 20 trials per track. Behaviour was quantified as the difference between the beginning of each reward trial and just before the reward delivery (illustrated in Figure 12E), and learning performance (i.e., reward expectation) was expressed as a ratio of these differences in trials 1-5 versus trials 11-15 (Figure 12C, F, I). Although the learning performance was consistently greater in the novel environment than in the familiar environment, there was no difference in behavioural performance between the control and NMDAR groups.

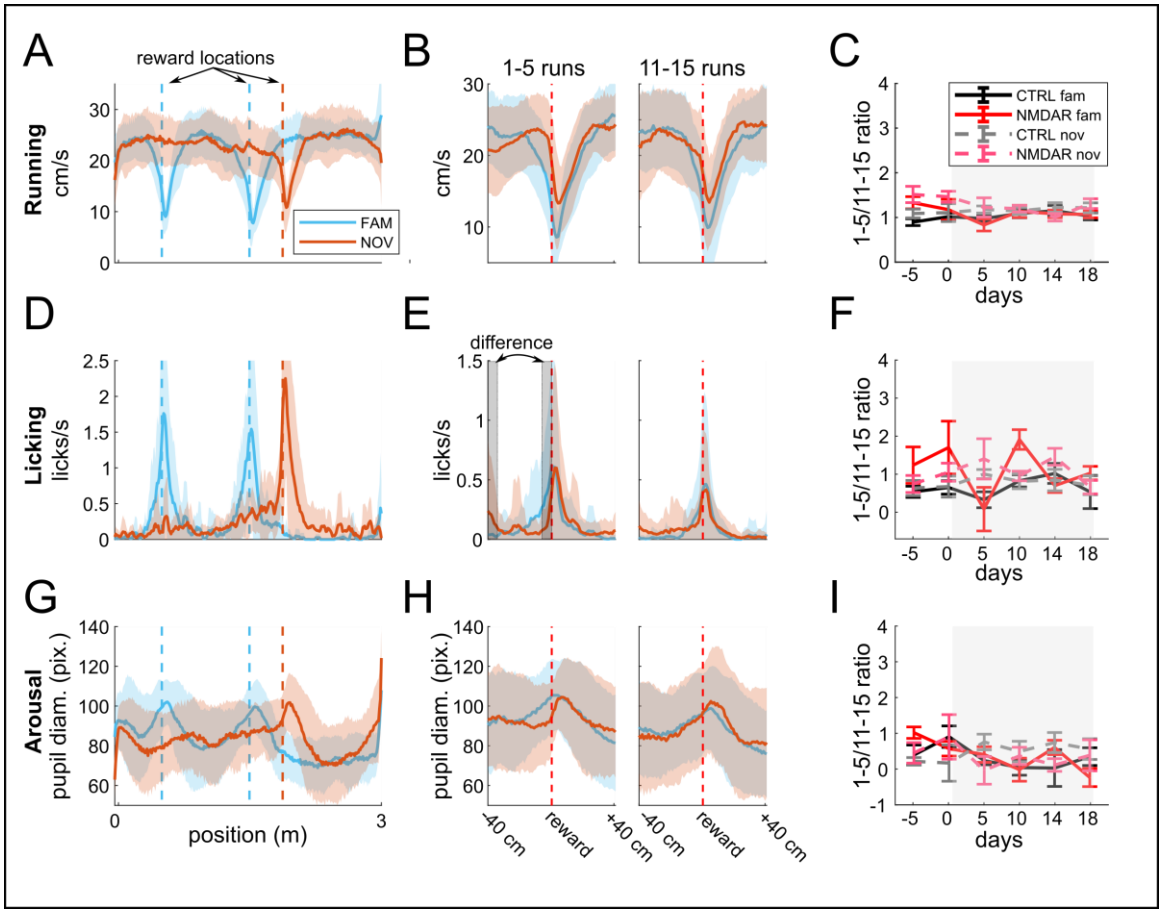

Figure 12. **Behavioural readouts during head-fixed spatial navigation task in virtual reality.** Three variables were assessed: running speed (A-C), licking (D-F) and arousal state through pupil diameter tracking (G-I). **A**, **D**, **G**, Behavioural readouts binned along the entire track for familiar (FAM, blue) and novel (NOV, orange) environments. Location of reward delivery is marked for both environments by dashed lines. **B**, **E**, **H**, Evaluation of the behavioural performance for 1-5 runs and 11-15 runs for snips of 80 cm (reward trials) centred on reward location (red dashed line) for each run. Performance (i.e., reward expectation) can be measured by reduced running, increased licking and pupil dilation prior to the reward delivery. **C**, **F**, **I**, Quantification of the behavioural performance over the entire experiment. Behaviour was quantified as the difference between the beginning of each reward trial (no reward expectation; mean of -40 to -34 cm) and just prior to reward delivery (immediate reward expectation; mean of -6 to -1 cm). Area is highlighted in E. Performance is expressed as a ratio of these differences in trials 1-5 versus 11-15 trials. Data is expressed as mean ± SD (A, B, E, F, G, H) or mean ± SEM (C, F, I). Significance was evaluated with two-way ANOVA with Bonferroni correction. Running, familiar; effect of time: $F_{(5, 301)} = 1.0$, $p = 0.9$; effect of treatment: $F_{(1, 301)} = 1.3$, $p = 0.5$; interaction: $F_{(5, 301)} = 1.5$, $p = 0.4$. Novel; effect of time: $F_{(5, 303)} = 0.7$, $p = 1$; effect of treatment: $F_{(1, 303)} = 3.0$, $p = 0.2$; interaction: $F_{(5, 303)} = 1.6$, $p = 0.3$. Licking, familiar; effect of time: $F_{(5, 267)} = 2.4$, $p = 0.1$; effect of treatment: $F_{(1, 267)} = 5.0$, $p = 0.06$; interaction: $F_{(5, 267)} = 1.5$, $p = 0.4$. Novel; effect of time: $F_{(5, 266)} = 1.7$, $p = 0.3$; effect of treatment: $F_{(1, 266)} = 3.3$, $p = 0.1$; interaction: $F_{(5, 266)} = 0.5$, $p = 1$. Arousal, familiar; effect of time: $F_{(5, 287)} = 2.3$, $p = 0.1$; effect of treatment: $F_{(1, 287)} = 0.2$, $p = 1$; interaction: $F_{(5, 287)} = 1.4$, $p = 0.5$. Novel; effect of time: $F_{(5, 291)} = 0.1$, $p = 1$; effect of treatment: $F_{(1, 291)} = 0.4$, $p = 1$; interaction: $F_{(5, 291)} = 1.2$, $p = 0.6$. Binned behavioural readouts were smoothed with a Gaussian kernel (σ = 12 cm). Behavioural data of mice with insufficient imaging data quality were also included in this analysis. $n_{(Control)} = 8$ mice, $n_{(NMDAR)} = 7$ mice.

4.3.4. Activity rates of pyramidal neurons

Calcium traces corresponding to activity of individual neurons were extracted from two-photon imaging data (see Section 3.4.5). Frames containing Ca^{2+} events, which correspond to action potentials or action potential trains, were identified on entire traces (Figure 13A) and amplitude and frequency of Ca^{2+} transients were quantified. Pyramidal neurons were found to have significantly lower Ca^{2+} transient amplitudes at timepoint 5 (0.68 and 0.62 a.u. for control and NMDAR groups, $p < 0.001$) and timepoint 6 (0.67 and 0.62 a.u. for control and NMDAR groups, $p < 0.01$) when compared to control (Figure 13B). Frequency of Ca^{2+} transients of pyramidal neurons was on average 0.22 and 0.20 Hz for the control and NMDAR group and there were no significant differences (Figure 13C, $p = 0.18$). Pairwise correlations between Ca^{2+} traces of neurons in a given FOV were computed next (Figure 13D). Mean pairwise correlation was 0.026 and 0.023 for the control and NMDAR group and there were no significant differences (Figure 13E, $p = 0.7$).

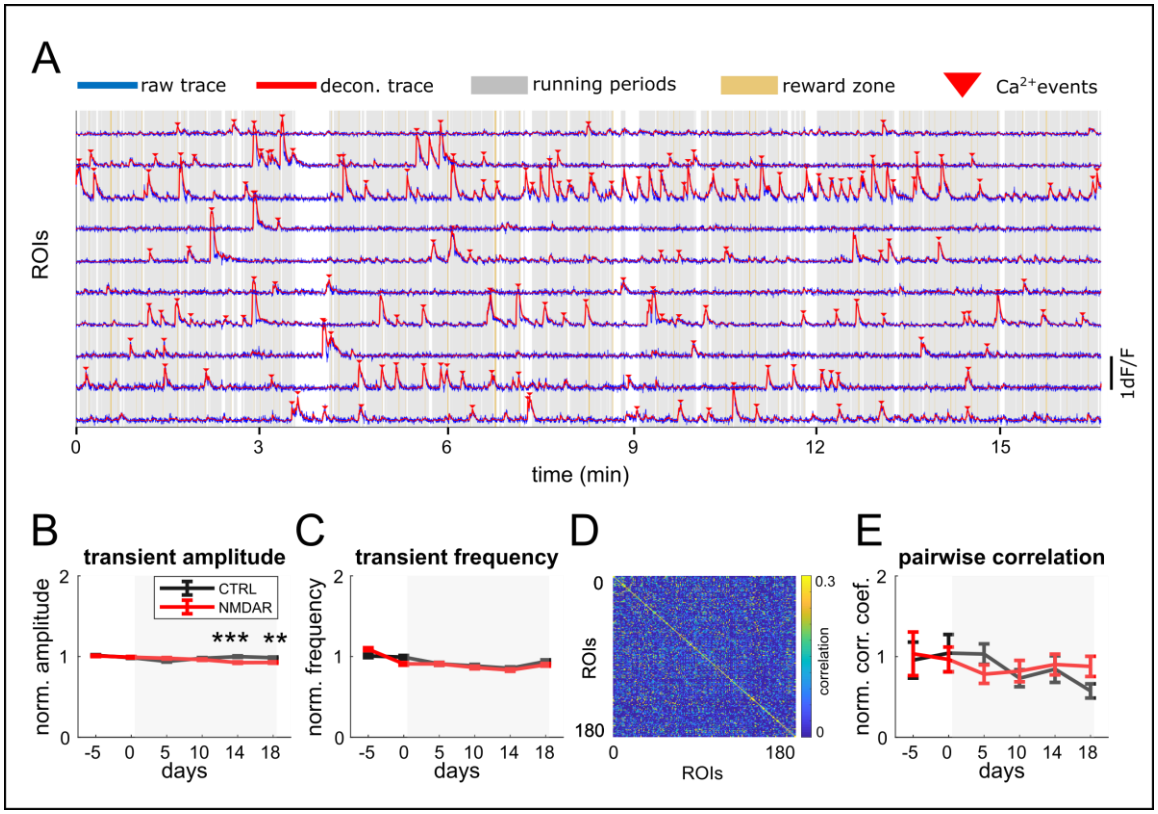

Figure 13. **Activity rates of CA1 pyramidal neurons. A**, example Ca^{2+} traces. **B**, Amplitude of Ca^{2+} transients; effect of time: $F_{(5,\ 24270)} = 10.9$, $p < 0.001$; effect of treatment: $F_{(1,\ 24270)} = 12.1$, $p < 0.001$; interaction: $F_{(5,\ 24270)} = 10.3$, $p < 0.001$. **C**, Frequency of Ca^{2+} transients; effect of time: $F_{(5,\ 24270)} = 30.9$, $p < 0.001$; effect of treatment: $F_{(1,\ 24270)} = 1.8$, $p = 0.18$; interaction: $F_{(5,\ 24270)} = 4.6$, $p < 0.001$. **D**, example cross-correlation matrix for a single FOV. **E**, Pairwise correlations of neuronal Ca^{2+} traces; effect of time: $F_{(5,\ 24270)} = 0.9$, $p = 0.5$; effect of treatment: $F_{(1,\ 24270)} = 0.1$, $p = 0.7$; interaction: $F_{(5,\ 24270)} = 0.6$, $p = 0.7$. Significance was evaluated with two-way ANOVA. Multiple comparisons were performed with Šidák test. $n_{(Control)} = 1895$ cells, $n_{(NMDAR)} = 2152$ cells. ** $p < 0.01$, *** $p < 0.001$.

4.3.5. Spatially tuned neurons

Spatially tuned cells (place cells) are characterized by bursts of activity when the animal is in a particular location of the virtual linear track (place field). Neurons with spatial tuning above chance levels were identified using a bootstrapping procedure (see Section 3.5.2), while only considering periods where the animal was running (Figure 14A). Activity rate maps, which represent spatially binned activity, were computed for each trial and each place cell separately. Place cells typically showed stereotyped patterns of activity in majority of trials (Figure 14B). On average, 20-25 % of CA1 pyramidal cells were place cells, and these seemed randomly distributed throughout the CA1 (Figure 14C). Place fields of CA1 place cells lined up the entire lengths of both familiar and novel tracks and collectively formed distinct spatial tuning maps (place maps) that were specific for each of the environments (Figure 14D).

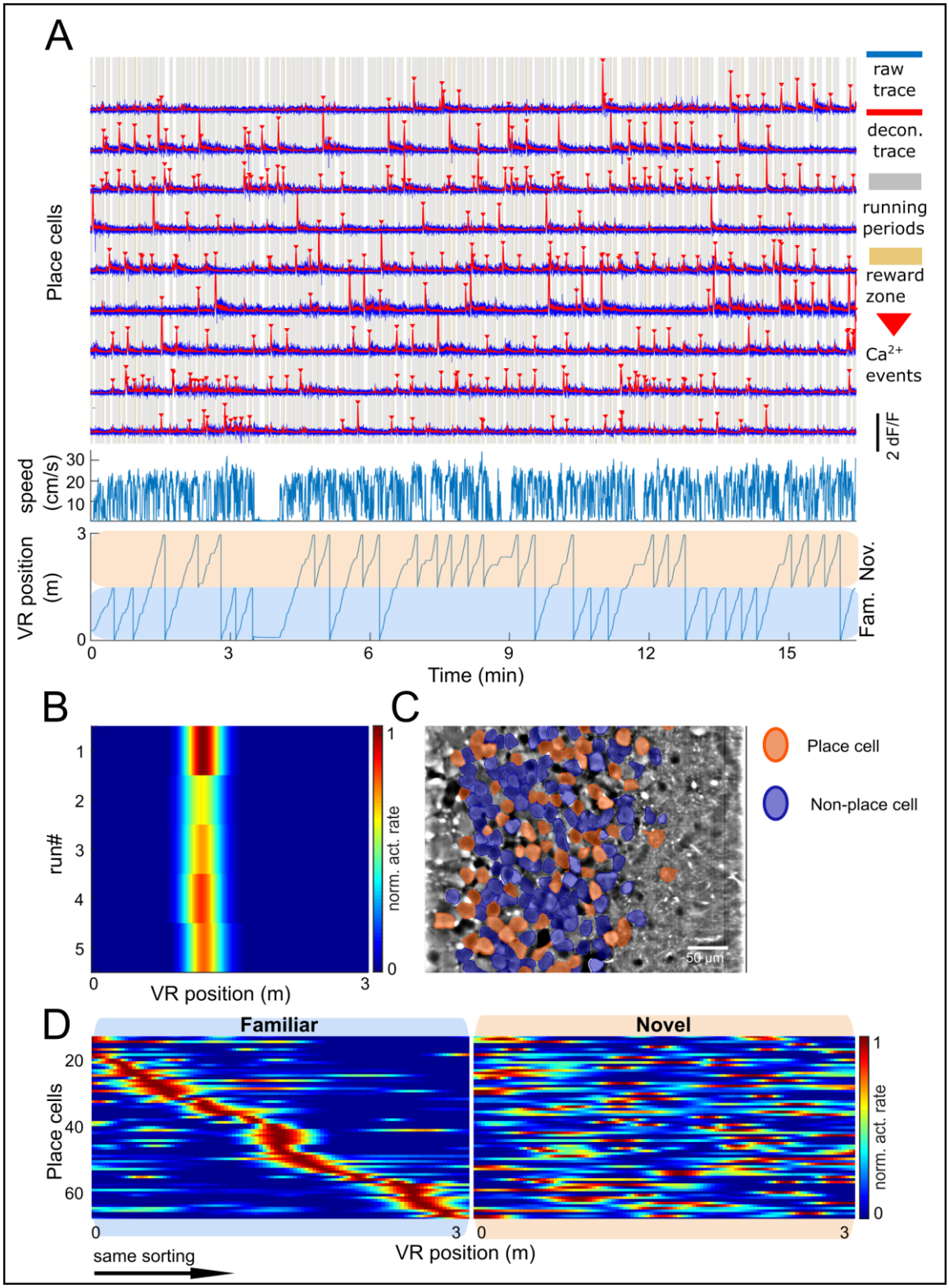

Figure 14. **Ca²⁺ traces of spatially tuned cells. A**, Example Ca²⁺ traces of spatially tuned cells (place cells). Blue, raw trace; red, deconvolved trace; red triangles, Ca²⁺ events. Below, running speed. Bottom, position on the virtual linear track. **B**, Activity rate map of a single place cell for individual trials (track traversals). **C**, FOV depicting place cells (red) and non-place cells (blue). **D**, Spatial map for all place cells for familiar (left) and novel (right) environments from a single experiment, sorted to maximum activity rate on the familiar track.

Next, pyramidal cells were categorized based on their activity levels into silent cells, place cells (significant spatial tuning) and non-place cells (without spatial tuning). A threshold of 0.3 transients per minute was chosen to categorize cells as silent or active (Figure 15A). On average, 35.6 % and 37.3 % of neurons were classified as silent in the control and NMDAR group, respectively. From active cells, 25.3 % (control group) and 21.6 % (NMDAR group) were place cells. The remainder of cells did not display spatially tuned activity or was spatially tuned only weakly (non-place cells). Next, I asked the question whether place fields are uniformly distributed in the familiar and novel tracks (Figure 15B). Considering active cells only, most cells had a place field only in the familiar environment (22.3 % of active cells in control and 20 % in NMDAR group). There was a significant difference in the fraction of active cells having a place field in familiar track only at day -5 (20 % and 15 % for the control and NMDAR group, respectively; $p = 0.034$). Fewer place cells had a place field in the novel track only. On average, 11.2 % and 10.0 % of active cells had a place field in the novel environment only for control and NMDAR group, respectively. There was a significant decrease in in the fraction of active cells having a place field in the novel track only at day 10 (9.5 % and 6.4 % for the control and NMDAR group, respectively; $p = 0.034$). From active cells, 6.0 % in control and 5.0 % in NMDAR groups had a place field in both familiar and novel tracks.

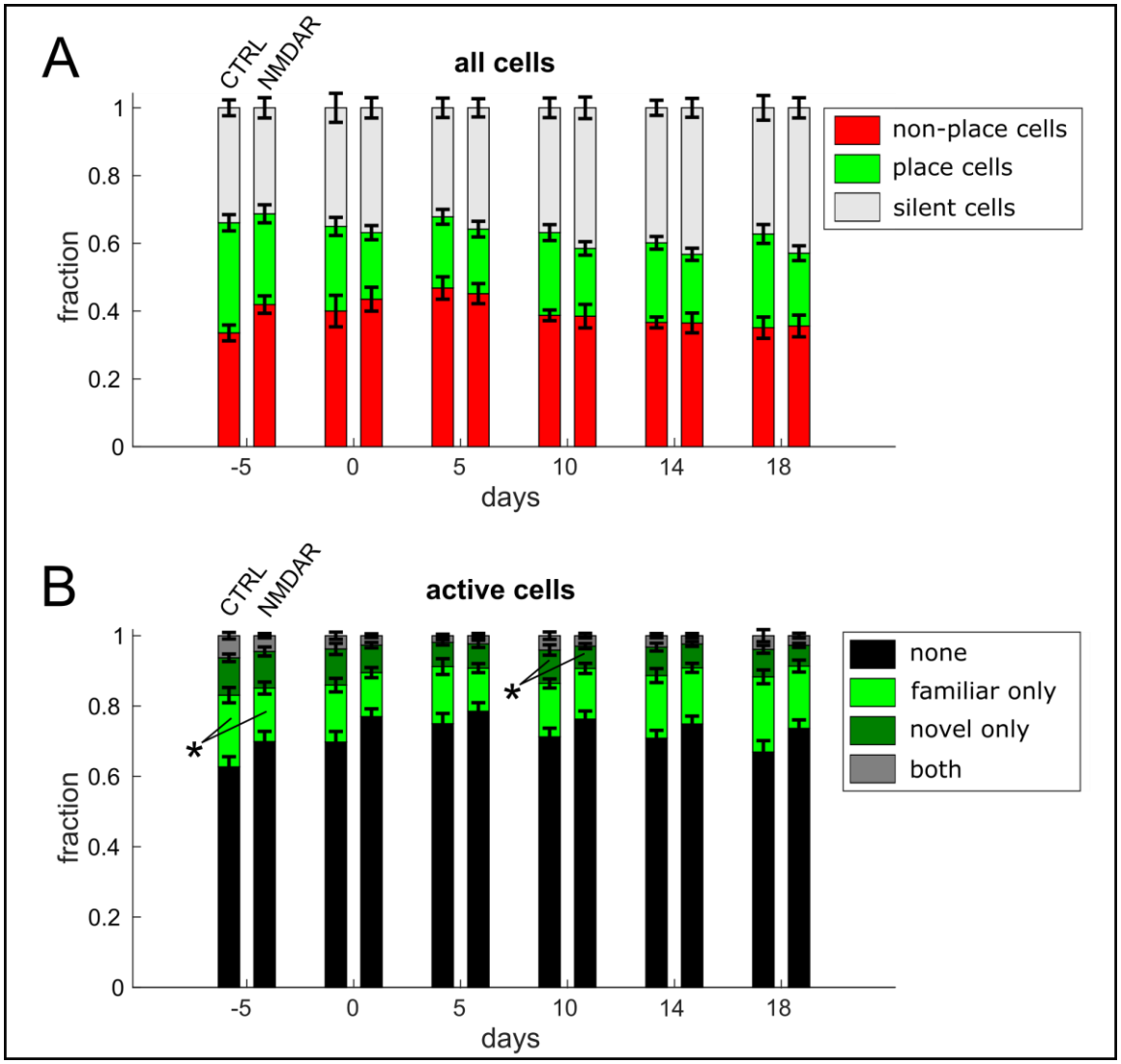

Figure 15. **CA1 pyramidal cell proportions. A**, Proportions of non-place cells, place cells and silent cells out of all recorded cells. Effect of time: $F_{(5, 144)} = 4.4$, $p = 0.001$; effect of treatment: $F_{(1, 144)} = 5.7$, $p = 0.004$; interaction: $F_{(5, 144)} = 0.7$, $p = 0.6$. **B**, Proportions of active cells having a place field in familiar environment only, novel environment only, both or none. Effect of time: $F_{(5, 144)} = 4.4$, $p = 0.001$; effect of treatment: $F_{(1, 144)} = 4.9$, $p = 0.003$; interaction: $F_{(5, 144)} = 1.2$, $p = 0.3$. Significance was evaluated with two-way multivariate ANOVA. Multiple comparisons were performed with Šidák test. $n_{(Control)} = 1895$ cells, $n_{(NMDAR)} = 2152$ cells. * $p < 0.05$.

4.3.6. Place cell properties

The ability to navigate spatial environments is one of the best characterized cognitive processes of rodents and is enabled by a dedicated network, the most prominent part of which is the hippocampus. Spatially tuned cells, also known as place cells, constitute a large fraction of hippocampal neurons with clearly defined properties. The following section focuses on characterization of properties of individual CA1 place cells, which are defined by one or more place fields.

First, place field properties were analysed, focusing on the number and width of individual place fields (schematized in Figure 16A). Mean place field width was 42.0 cm

and 41.0 cm for control and NMDAR groups, respectively, and there was no difference between the groups (Figure 16B). However, the average number of place fields per place cell was significantly lower in the NMDAR group (1.4 and 1.3 place fields per place cell for control and NMDAR groups, effect of treatment: $F_{(1, 7524)} = 18.0$, $p < 0.001$), with a significant difference between the groups at timepoint 6 (Figure 16C; $p < 0.001$).

Spatial information content is a measure of spatial firing selectivity and was on average 3.47 and 3.44 bits per Ca^{2+} event for control and NMDAR groups, respectively. There were no differences in spatial information content at any timepoints (Figure 16D).

Place cell reliability is expressed as the mean cross-correlation of individual traversal rate maps and measures how reliably will a place cell fire in its place field. Mean reliability of place cells in the control group was 0.46 and 0.46 in the NMDAR group and none of the timepoints were significantly different (Figure 16E).

Next, I looked at the long-term stability of place cells in the first recording session. Figure 16F shows activity rates of place cells that had a place field on day -5 for all imaging timepoints (only familiar track is shown, sorted to the first session). Place cells were sorted based on the place field location on the first imaging session in descending order, and place maps present on day -5 were visually appreciable in all subsequent timepoints. However, majority of place cells lost their place field between the first and the second imaging sessions, and there was relatively little change between the subsequent timepoints.

I then asked the question whether there was any change in long-term stability of activity rate maps of individual place cells. To that end, I investigated correlation of rate maps between individual timepoints (Figure 16G). Focusing on place cells that had a place field on two consecutive timepoints, I found a significant increase in mean place field correlations of the NMDAR group when compared to the control group (effect of treatment: $F_{(1, 1475)} = 17.7$, $p < 0.001$). Moreover, place cells that had a place field on both day 0 and day 5 were significantly more correlated in the NMDAR group than the control group ($p < 0.001$).

In the next step, mean rate maps of place cells that had a place field in a given timepoint (vertical axis) were correlated to rate maps of the same cells on all the other timepoints (horizontal axis), regardless of whether they had a place field in these timepoints or not. There was a progressive decrease and increase in rate map correlations for timepoints moving forward and backward in time, respectively. However, there was a marked

increase in rate map correlations for timepoints 5 and 6 in the NMDAR group (Figure 16H).

To quantify the stability of place field locations between the timepoints, I calculated the COM shift (see Section 3.5.3). When analysing place cells that had a place field on two consecutive timepoints, the average COM shift was 31.0 cm and 27.4 cm for the control and NMDAR group, respectively, and there was no difference between the groups (Figure 16I). When looking only at COM shift of place cells that had a place field on timepoint 1 (quantification of place maps in Figure 16F), the mean COM shift was 49.7 cm for the control group and 50.8 cm for the NMDAR group.

Next, I analysed the similarity between spatial maps, that contain place fields of all place cells. For this, POV correlations were calculated to quantify the stability of the neural representation of the familiar environment on different imaging sessions. POVs for a given session, representing activity rates for all place cells in a single location (position bin), were correlated to matching locations in the target session, yielding a cross-correlation matrix (Figure 16J). POV correlation to day -5 decreased with an exponential decay and there was no difference between control and NMDAR groups (Figure 16K). However, POV correlations to timepoint 6 were significantly increased in the NMDAR group for day 10 (control: 0.43, NMDAR: 0.51; $p < 0.001$) and day 14 (control: 0.56, NMDAR: 0.64; $p < 0.001$) when compared to controls, suggesting that spatial representations in the later timepoints became progressively more stable in the NMDAR group.

Together, these results indicate that CA1 spatial coding in mice infused with the NMDAR antibody was relatively intact with levels of spatial information, reliability, COM shift and place field width comparable to controls. However, place cells in the NMDAR group became significantly more stable as indicated by increased POV correlations and place field correlations, and these changes were associated with progressive antibody infusion into the brain.

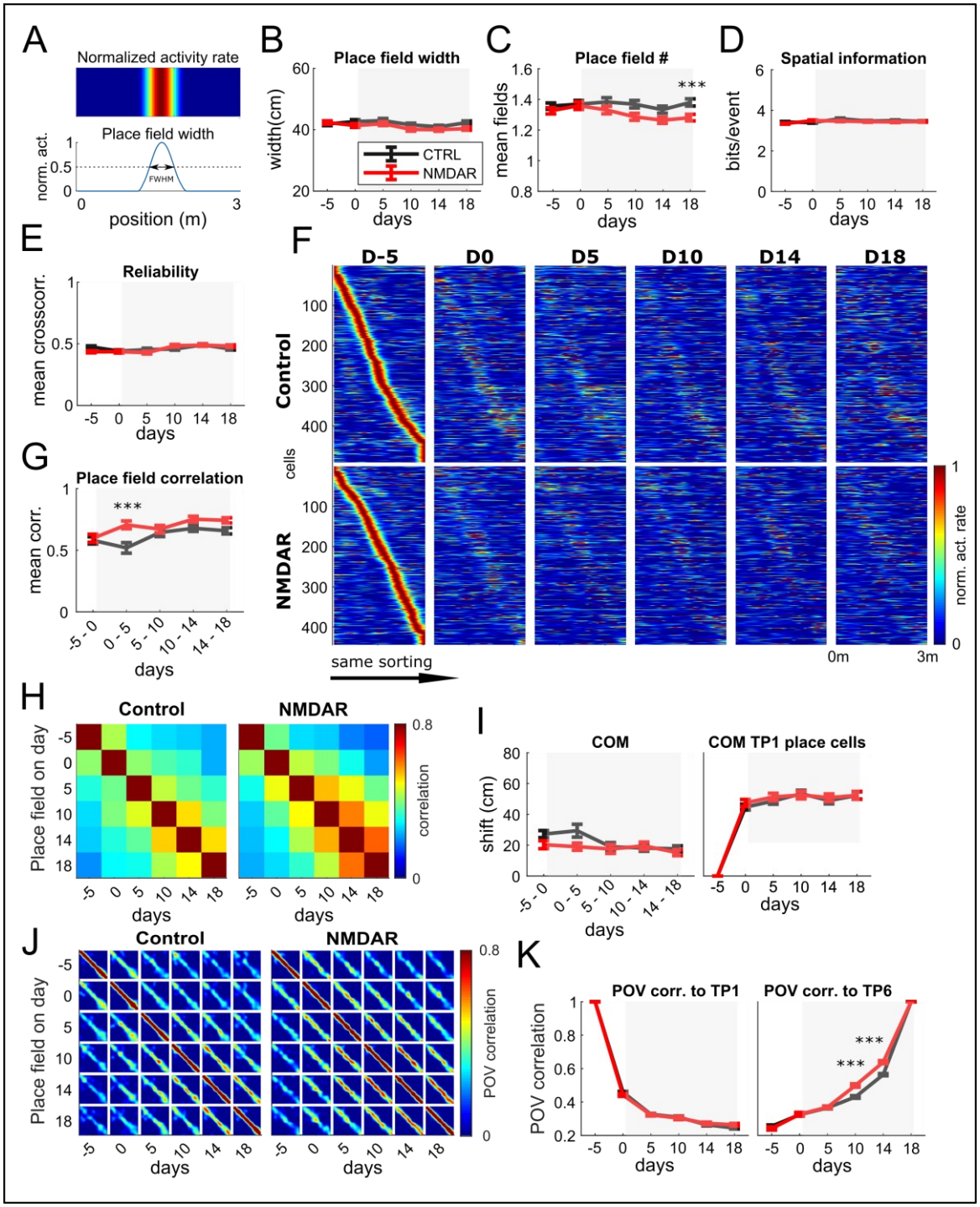

Figure 16. **Spatial tuning maps and place cell properties. A**, Schematic of place field properties quantification. **B**, Place field width. Effect of time: $F_{(5,\ 10061)} = 3.7$, $p = 0.003$; effect of treatment: $F_{(1,\ 10061)} = 9.7$, $p = 0.002$; interaction: $F_{(5,\ 10061)} = 1.3$, $p = 0.3$. **C**, Mean number of place fields per place cell. Effect of time: $F_{(5,\ 7524)} = 2.0$, $p = 0.08$; effect of treatment: $F_{(1,\ 7524)} = 18.0$, $p < 0.001$; interaction: $F_{(5,\ 7524)} = 1.1$, $p = 0.4$. **D**, Spatial information content of all cells for each timepoint. Effect of time: $F_{(5,\ 48552)} = 4.7$, $p < 0.001$; effect of treatment: $F_{(1,\ 48552)} = 4.2$, $p = 0.04$; interaction: $F_{(5,\ 48552)} = 3.2$, $p = 0.008$. **E**, Reliability of place cells for each timepoint. Effect of time: $F_{(5,\ 7524)} = 8.1$, $p < 0.001$; effect of treatment: $F_{(1,\ 7524)} = 0.4$, $p = 0.5$; interaction: $F_{(5,\ 7524)} = 3.9$, $p = 0.002$. **F**, Normalized activity rates for cells that had a place field on the familiar track on the first imaging session (day -5). Cells are sorted according to day -5, only familiar track is shown. **G**, Place field correlation of place cells having a place field on two consecutive timepoints. Effect of time: $F_{(5,\ 1475)} = 7.3$, $p < 0.001$; effect of treatment: $F_{(1,\ 1475)} = 17.7$, $p < 0.001$; interaction: $F_{(5,\ 1475)} = 2.2$, $p = 0.07$. **H**, Mean place field correlation for control (left) and NMDAR (right) antibody infused mice. **I**, COM shift. Left, COM shift of place cells having a place field on two consecutive timepoints. Effect of time: $F_{(5,\ 1475)} = 2.5$, $p = 0.04$; effect of treatment: $F_{(1,\ 1475)} = 5.2$, $p = 0.02$; interaction: $F_{(5,\ 1475)} = 2.5$, $p = 0.04$. Right, COM

shift of cells having a place field on TP1. Effect of time: $F_{(5, 5592)} = 196.2$, $p < 0.001$; effect of treatment: $F_{(1, 5592)} = 0.8$, $p = 0.4$; interaction: $F_{(5, 5592)} = 0.3$, $p = 0.93$. **J**, POV correlations for control (left) and NMDAR (right) antibody treated mice. **K**, Quantification of POV correlations to timepoint 1 (left) and timepoint 6 (right). POV corr. to TP1; effect of time: $F_{(5, 132)} = 3.8*e^3$, $p < 0.001$; effect of treatment: $F_{(1, 132)} = 0.01$, $p = 0.9$; interaction: $F_{(5, 132)} = 1.8$, $p = 0.1$. POV corr. to TP6; effect of time: $F_{(5, 132)} = 2.5*e^3$, $p < 0.001$; effect of treatment: $F_{(1, 132)} = 26.1$, $p < 0.001$; interaction: $F_{(5, 132)} = 12.6$, $p < 0.001$. Data is shown as mean ± SEM. Statistical comparisons were performed with two-way ANOVA. Multiple comparisons were performed with Šidák test. $n_{(Control)} = 1{,}895$ cells from 6 animals, $n_{(NMDAR)} = 2{,}152$ cells from 7 animals. * $p < 0.05$, ** $p < 0.01$, *** $p < 0.001$.

Place cells are dynamic features and retain their spatial tuning for variable periods of time. The CA1 population of place cells turns over within several days, the speed of which has important implications for spatial coding. For this reason, I next investigated place cell dynamics. Recurrence of place cells is defined as the fraction of cells remaining place cells within a given time interval, irrespective of place field location. Around 35 % of place cells survived from an initial timepoint to the next, while around 15 % of place cells survived over the span of thee timepoints (Figure 17A). While the survival rates of place cells from control and NMDAR groups remained undistinguishable under baseline conditions (timepoints 1 and 2), there was an overall trend towards higher survival rates for place cells of later timepoints in the NMDAR infused group. Furthermore, timepoint 3 place cells survived significantly longer in the NMDAR group than in the control group (mean survival: 22 % and 29 % for the control and NMDAR group, respectively; effect of treatment: $F_{(1, 96)} = 5.1$, $p = 0.026$).

CA1 cells undergo dynamic changes in response properties, whereby gaining or losing spatial tuning (Figure 17B). I found the ratios of lost place cells to be significantly lower in the NMDAR group with mean ratios of lost cells 0.07 and 0.05 for control and NMDAR groups, respectively (effect of treatment: $F_{(1, 120)} = 11.3$, $p = 0.002$). Similarly, ratios of gained place cells were significantly lower in the NMDAR group when compared to the control group (0.06 and 0.05 in control and NMDAR group, respectively; effect of treatment: $F_{(1, 120)} = 8.2$, $p = 0.005$). These results suggest that place cell turnover is slower following the antibody infusion in the NMDAR group, resulting in increased survival rates of existing place cells.

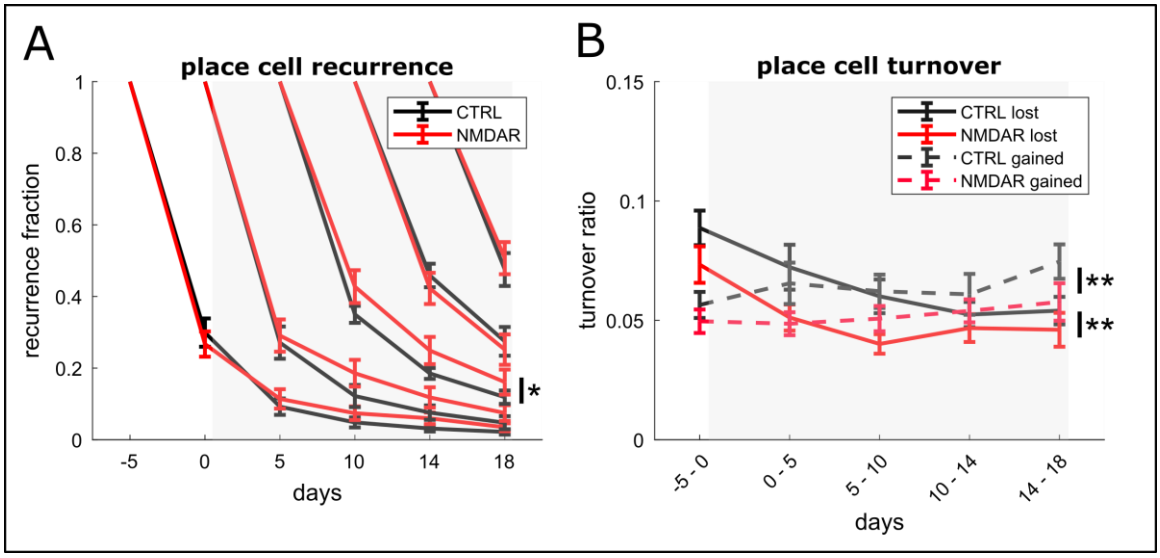

Figure 17. **Place cell dynamics. A**, Place cell recurrence for individual timepoints. Day 5 place cells: effect of time: $F_{(3, 96)} = 370.1$, $p < 0.001$; effect of treatment: $F_{(1, 96)} = 5.1$, $p = 0.026$; interaction: $F_{(3, 96)} = 0.7$, $p = 0.6$. **B**, Place cell turnover between consecutive timepoints. Lost, effect of time: $F_{(4, 120)} = 8.5$, $p < 0.001$; effect of treatment: $F_{(1, 120)} = 11.3$, $p = 0.002$; interaction: $F_{(4, 120)} = 0.6$, $p = 0.7$. Gained, effect of time: $F_{(4, 120)} = 1.1$, $p = 0.4$; effect of treatment: $F_{(1, 120)} = 8.2$, $p = 0.005$; interaction: $F_{(4, 120)} = 0.3$, $p = 0.9$. Significance was evaluated with two-way ANOVA with Bonferroni correction. $n_{(Control)} = 12$ FOVs from 6 animals, $n_{(NMDAR)} = 14$ FOVs from 7 animals. * $p < 0.05$, ** $p < 0.01$.

4.3.7. Network spatial coding

Analysis of single place cells has proven informative and straightforward, however information in the brain is not encoded by single neurons but rather by a distributed neural code, where neurons cooperate to encode information about position, motion direction or velocity (Stefanini et al., 2020). Therefore, I measured how well neurons encoded position by making predictions about the animal's position based on the neuronal activity recorded. For this, the Maximum Correlation Classifier was trained using data from all place cells in a given experiment with 70 % of data used for training and 30 % for testing (see Section 3.5.6). The classifier accurately predicted the animal's position on the familiar track for both control and NMDAR groups (Figure 18A). The decoding error for the familiar environment was on average 32 cm and 36 cm (effect of treatment: $F_{(1, 132)} = 3.3$, $p = 0.15$), for the novel environment 61 cm and 64 cm (effect of treatment: $F_{(1, 108)} = 0.1$, $p = 1$) for the control and NMDAR group, respectively (Figure 18B). The decoding error obtained by chance rate was estimated on shuffled data and was 100 cm for both groups. There were no significant differences in position encoding between the control and NMDAR group at any timepoint.

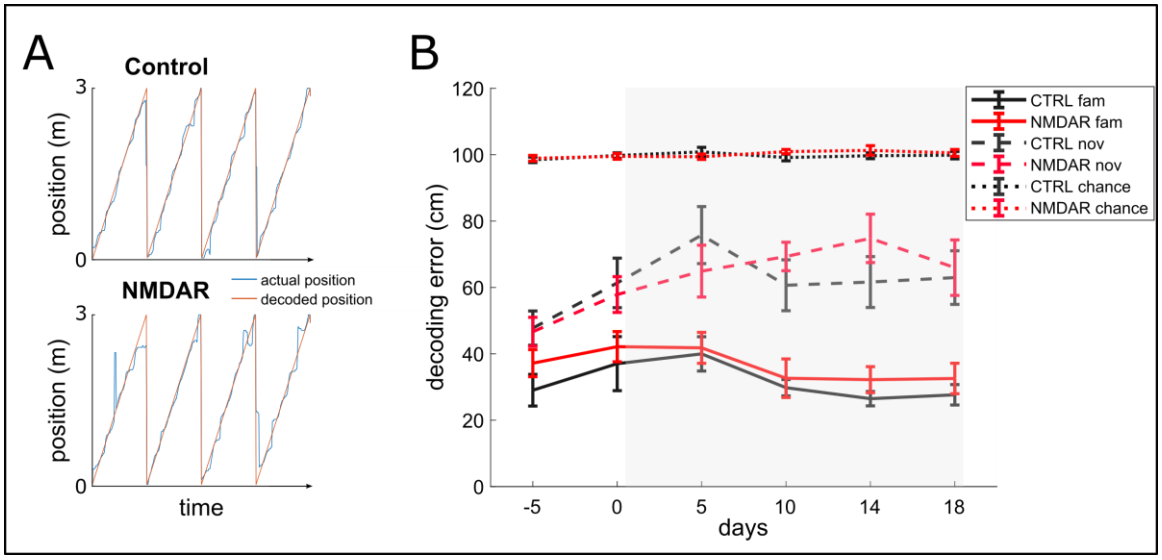

Figure 18. **Decoding of the animal's position from the neuronal activity. A**, Maximum Correlation Classifier used for position decoding. Examples of decoder performance on day 18 data for control (top) and NMDAR (bottom) group using activity from all place cells. **B**, Quantification of decoder performance for all FOVs for familiar (solid lines), novel (dashed lines) and shuffled data (dotted line). $n_{(Control)}$ = 12 FOVs, $n_{(NMDAR)}$ = 14 FOVs. Significance was evaluated with two-way ANOVA with Bonferroni correction; Familiar: effect of time: $F_{(5,\ 132)} = 2.5$, $p = 0.07$; effect of treatment: $F_{(1,\ 132)} = 3.3$, $p = 0.15$; interaction: $F_{(5,\ 132)} = 0.16$, $p = 1$. Novel: effect of time: $F_{(5,\ 108)} = 3.3$, $p = 0.02$; effect of treatment: $F_{(1,\ 108)} = 0.1$, $p = 1$; interaction: $F_{(5,\ 108)} = 0.8$, $p = 1$.

To probe neuronal discrimination between contexts, consistency of rate maps was determined between the first 10 consecutive runs versus the second 10 consecutive runs in the familiar environment. Similarly, the remapping of place cells between the familiar and novel contexts was quantified by comparing all runs in the familiar contexts to all runs in the novel context (Figure 19A). This analysis was performed for each experiment (i.e., FOV), and place cells were identified as cells with a significant place field in either or both of the contexts. To quantify the similarity between the contexts, POV correlation analysis was performed (Figure 19B). Spatial map consistency in the familiar environment was high (0.7 both groups, POV correlation between first and second blocks). The same measure of trial-to-trial consistency for runs in novel environment was generally lower, indicating initially less stable representation (0.4, data not shown). Consistency between familiar and novel environments was low (0.1, POV correlation between familiar and novel runs), indicating that animals perceived the environments as different.

To quantify the animal's ability to discriminate between familiar and novel contexts, a discrimination index was calculated (Figure 19C). Discrimination index values range between 0 and 1; low discrimination index indicates high similarity of spatial maps in the two environments and high discrimination index indicates that spatial maps are very different. The mean discrimination index was 0.79 and 0.78 for the control and NMDAR

group, respectively, and there were no significant differences between the groups (effect of treatment: $F_{(1, 132)} = 0.3$, $p = 0.6$). These results suggest that mice from both control and NMDAR groups are able to discriminate between familiar and novel environments equally well.

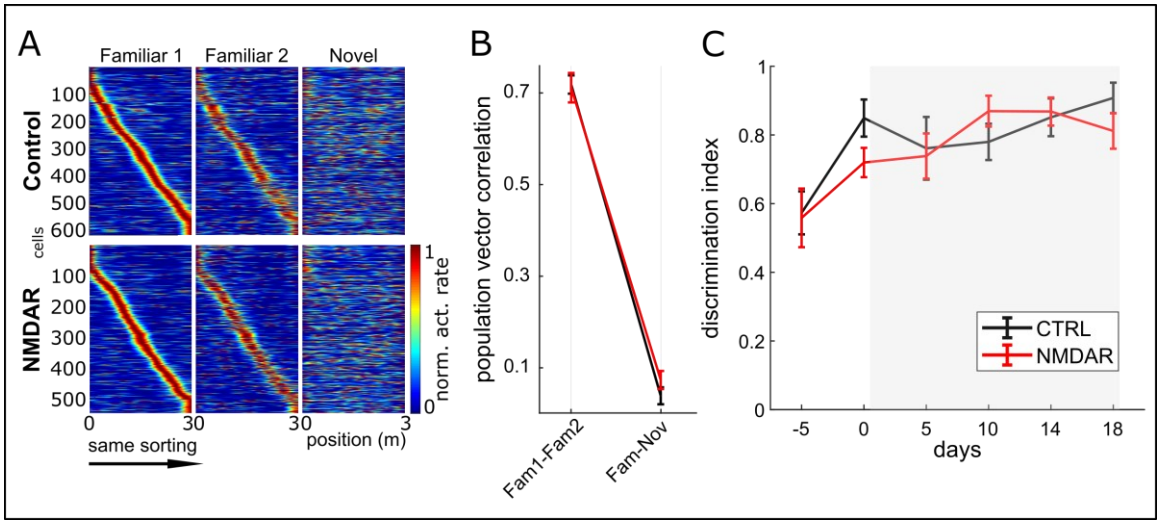

Figure 19. **Discrimination between familiar and novel contexts. A**, Rate maps for the first 10 (Familiar 1) and the second 10 (Familiar 2) runs in the familiar environment and 20 runs in the novel environment. Place cells having a place field in any of the contexts are shown, sorted according to Familiar 1. Data for day 18 are shown. **B**, POV correlations for the data presented in A. Significance was evaluated with a t-test ($p = 0.3$). **C**, Discrimination index for all timepoints. Significance was evaluated with two-way ANOVA. Effect of time: $F_{(5, 132)} = 6.4$, $p < 0.001$; effect of treatment: $F_{(1, 132)} = 0.3$, $p = 0.6$; interaction: $F_{(5, 132)} = 1.3$, $p = 0.3$.

4.3.8. Neuronal ensembles

Monitoring large numbers of neurons with Ca^{2+} imaging enables examination of the functional relationships between neurons and to investigate recurrent patterns of activity in local neuronal populations. Rather than acting alone, neurons are organized into functional units that fire in synchrony. *In vivo*, neuronal circuits cycle between periods of quiescence and periods of highly synchronized activity. Ensemble activations, or distinct groups of coactive neurons, represent recurrent activity states and form computational building blocks of neuronal circuits (Carrillo-Reid et al., 2015).

I next asked the question whether NMDAR antibodies affect neuronal function on the ensemble level, disregarding of the spatial tuning. Ensemble activations corresponding to significant population coactivity states were statistically identified for each imaging experiment, and these were primarily driven by a number of highly coactive neurons (Figure 20A). This analysis indicated that such population-wide activation events occur well above chance levels and neurons participating in an ensemble activation were randomly distributed in the CA1 pyramidal cell population (Figure 20B). To characterize whether ensemble activations represent recurring patterns or one-off events (Figure

20C), ensemble activation frames were cross-correlated within each single imaging session (Figure 20D). This revealed that ensemble activations are indeed recurring events and several possible states existed in each session.

Neuronal network state is characterized by instantaneous patterns of activity across all cells which can be represented in n-dimensional space, where n is the number of recorded neurons (typical FOV contained 150-200 neurons). Following principal component dimensionality reduction, k-means clustering was performed on the first 3 principal components. This analysis revealed that ensemble activations consist of a small number of unique states (Figure 20E). Neuronal ensemble similarity, defined as mean ensemble frame cross-correlation, was progressively increased in the NMDAR group compared to the control group (Figure 20F). On average, the ensemble similarity was 0.17 and 0.2 for the control and NMDAR group, respectively (effect of treatment: $F_{(1, 144)} = 4.2$, $p = 0.04$).

The number of neuronal ensembles was defined for each experiment through k-means clustering (best number of clusters; Figure 20G). The average best number of clusters was 4.3 and 4.6 clusters for the control and NMDAR group, respectively, and there was no difference between the groups. The quality of clustering, representing the distinctness of neuronal ensemble activations, was further evaluated by Euclidean distance comparison (Figure 20H). The mean Euclidean distance within the clusters was 8.2 and 6.7 a.u. for the control and NMDAR group, respectively, and there was no difference between the groups.

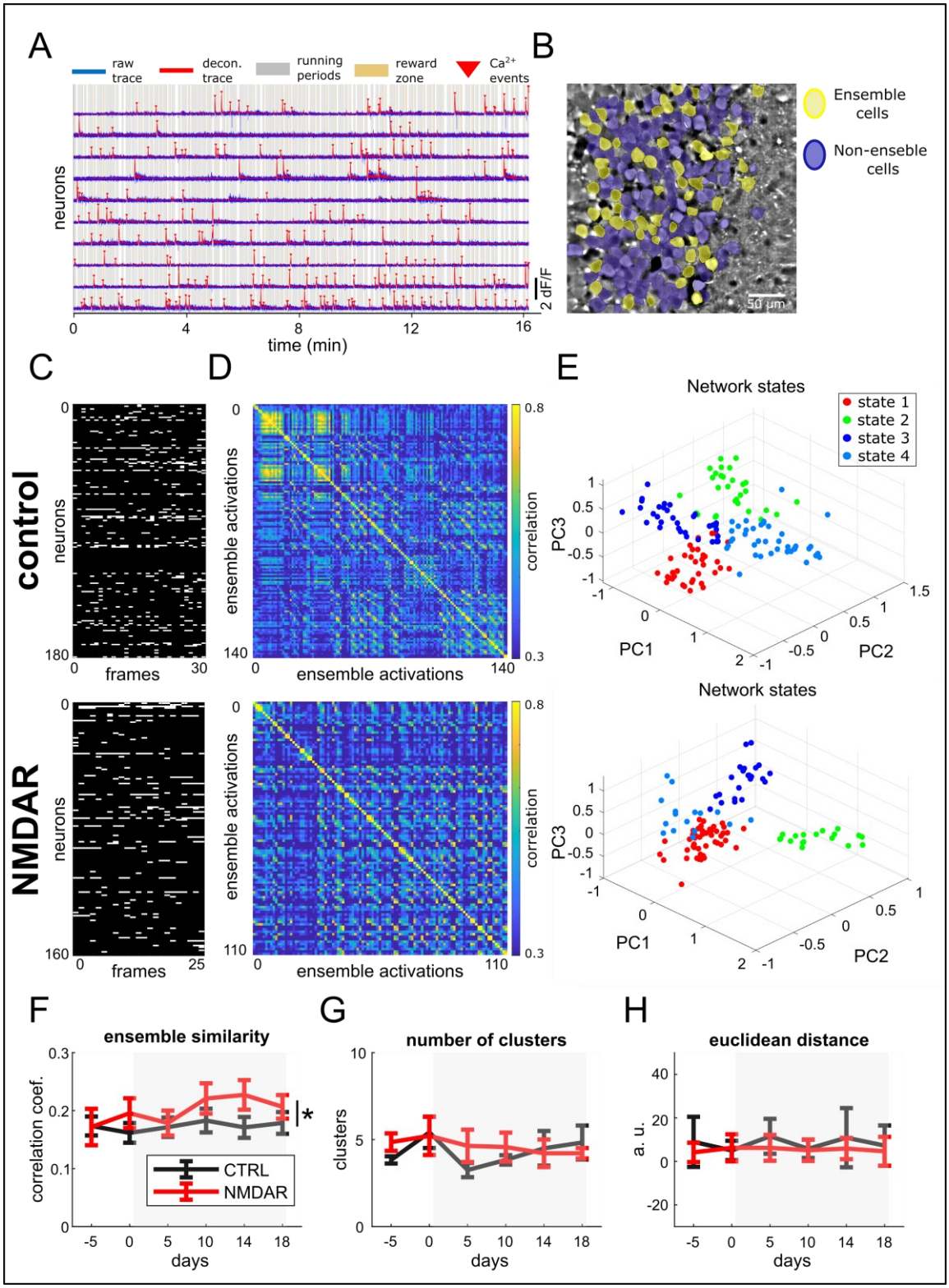

Figure 20. **Neuronal ensembles.** **A**, Example traces of neurons with correlated activity. **B**, FOV depicting neurons belonging to a single neuronal ensemble (yellow) or no ensemble (blue). **C**, Raster plots of control (top) and NMDAR (bottom) of all neurons in the given FOV for a single ensemble. **D**, Frame-frame correlation matrix for ensemble activations. **E**, Network states in principal component space. k-means clustering for k = 4 was performed. **F**, Neuronal ensemble similarity (correlation). Effect of time: $F_{(5,\ 144)} = 0.6$, $p = 0.7$; effect of treatment: $F_{(1,\ 144)} = 4.2$, $p = 0.04$; interaction: $F_{(5,\ 144)} = 0.4$, $p = 0.8$. **G**, Number of distinct ensembles (clusters in PCA space) identified with k-means clustering. Clustering was repeated for values of k between 2 and 15. Significance was evaluated with two-way ANOVA. Effect of time: $F_{(5,\ 144)} = 0.7$, $p = 0.6$; effect of treatment: $F_{(1,\ 144)} = 0.6$, $p = 0.4$; interaction: $F_{(5,\ 144)} = 0.6$, $p = 0.7$. **H**, Mean Euclidean distance within clusters. Effect of time: $F_{(5,}$

$_{144)}$ = 1.0, p = 0.4; effect of treatment: $F_{(1, 144)}$ = 2.7, p = 0.06; interaction: $F_{(5, 144)}$ = 0.8, p = 0.5. For analyses in C-E data from day 18 were used. Data is shown as mean ± SEM. * p < 0.05.

4.3.1. Activity rates of CA1 interneurons

Interneurons form an integral part of CA1 circuits and are essential for correct functioning of the hippocampus. I next asked the question whether interneurons are differentially affected by NMDAR antibodies. PV-positive and SST-positive interneurons were identified in two-photon images based on the expression of the red fluorescence molecule tdTomato, in addition to the green calcium indicator GCaMP7s. Validity of this approach was confirmed with immunohistochemistry, when brain sections from animals used for *in vivo* imaging were stained with commercial anti-PV and anti-SST antibody and imaged with a confocal microscope (Figure 21A). A total 99 PV interneurons (43 cells control group, 56 cells NMDAR group) and 128 SST interneurons (68 cells control group, 60 cells NMDAR group) were identified. Ca^{2+} transients in traces of PV and SST interneurons were processed as described previously (Figure 21B).

For PV interneurons, transient amplitude was on average 0.21 a.u. and 0.15 a.u. (Figure 21C), transient frequency was 0.8 Hz and 0.3 Hz (Figure 21D) for the control and NMDAR group, respectively. PV interneurons displayed a high degree of correlated activity (Figure 21E) and the mean pairwise correlation was 0.35 and 0.26 for the control and NMDAR group, respectively (Figure 21F). Although none of the differences were statistically significant, there was a trend towards lower amplitude and frequency in NMDAR group, indicating a possible decrease in activity of PV interneurons.

For SST interneurons, transient amplitude was on average 0.55 a.u. and 0.62 a.u. (Figure 21G) and transient frequency was 0.012 Hz and 0.010 Hz (Figure 21H). Pairwise correlations of SST interneurons were markedly lower than that of PV interneurons (Figure 21I) and was 0.08 and 0.09 for the control and NMDAR group, respectively (Figure 21J). There were no significant differences.

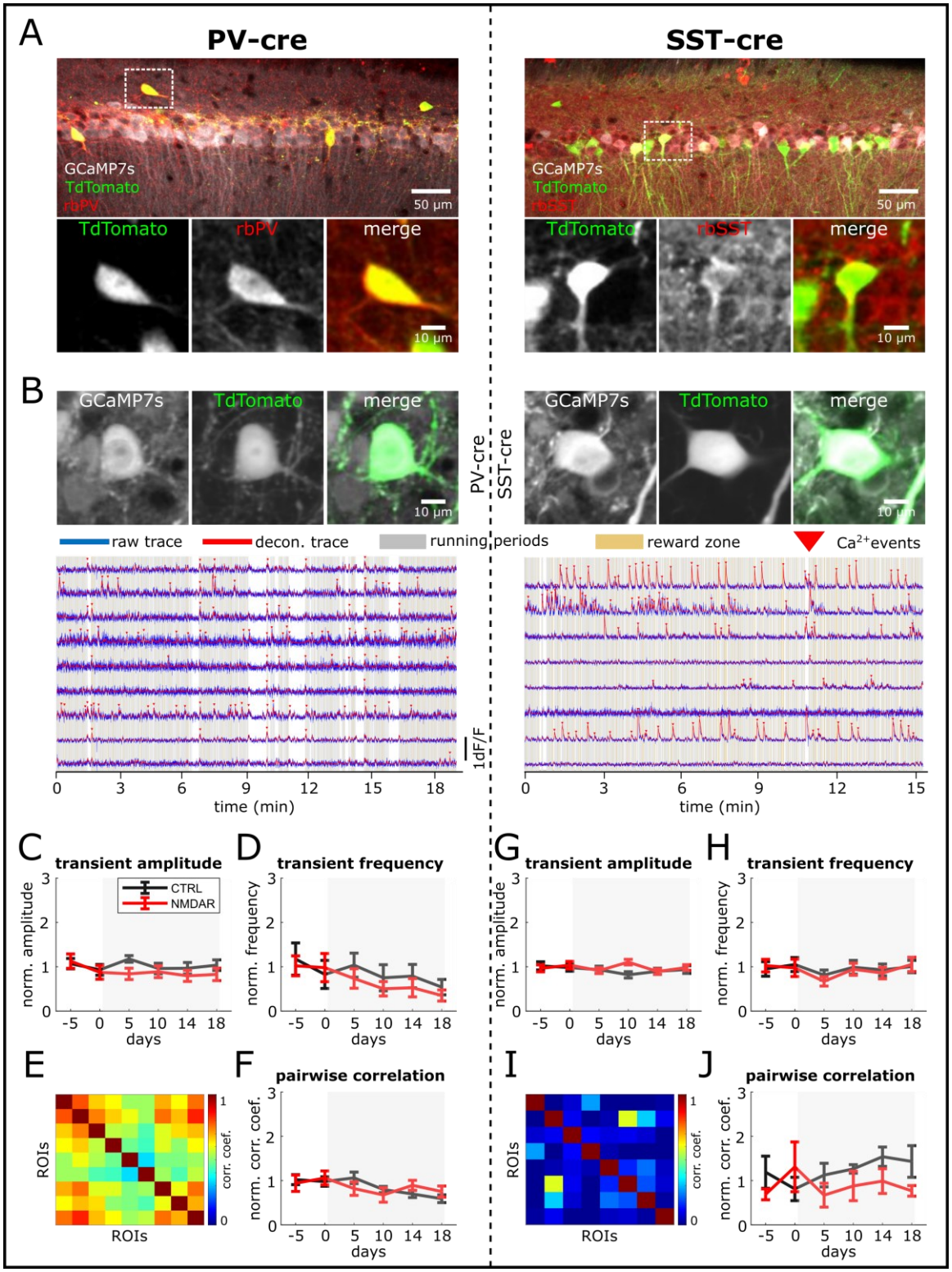

Figure 21. **Activity rates of pyramidal neurons and PV and SST interneurons. A**, Immunostaining for PV (left) and SST (right) interneurons in CA1. Bottom, overlay of endogenous flex-tdTomato expression with immunostaining for PV (left) or SST (right) antibody. **B**, *In vivo* images of PV (left) and SST (right) interneurons with example traces below. **C**, Transient amplitude of PV interneurons. Effect of time: $F_{(5,\ 590)} = 0.7$, $p = 0.6$; effect of treatment: $F_{(1,\ 590)} = 2.9$, $p = 0.09$; interaction: $F_{(5,\ 590)} = 0.5$, $p = 0.8$. **D**, Transient frequency of PV interneurons; effect of time: $F_{(5,\ 590)} = 1.8$, $p = 0.1$; effect of treatment: $F_{(1,\ 590)} = 1.3$, $p = 0.2$; interaction: $F_{(5,\ 590)} = 0.1$, $p = 1$. **E**, Example cross-correlation matrix of PV interneurons in B. **F**, Pairwise correlation of PV interneurons; effect of time: $F_{(5,\ 590)} = 2.2$, $p = 0.5$; effect of treatment: $F_{(1,\ 590)} = 1.9*e^{-4}$, $p = 1$; interaction: $F_{(5,\ 590)} = 0.8$, $p = 0.5$. **G**, Transient amplitude of SST interneurons; effect of time: $F_{(5,\ 778)} = 0.6$, $p = 0.7$; effect of treatment: $F_{(1,}$

$_{778)}$ = 1.3, p = 0.3; interaction: $F_{(5, 778)}$ = 1.3, p = 0.3. **H**, Transient frequency of SST interneurons; effect of time: $F_{(5, 778)}$ = 1.1, p = 0.4; effect of treatment: $F_{(1, 778)}$ = 0.2, p = 0.7; interaction: $F_{(5, 778)}$ = 0.2, p = 1. **I**, Example cross-correlation matrix of SST interneurons in B. **J**, Pairwise correlation of SST interneurons; effect of time: $F_{(5, 778)}$ = 0.4, p = 0.9; effect of treatment: $F_{(1, 778)}$ = 4.0, p = 0.05; interaction: $F_{(5, 778)}$ = 1.0, p = 0.4. Data was normalized to the mean of the two baseline sessions. $n_{(PV)}$ = 99 cells (43 control, 56 NMDAR); $n_{(SST)}$ = 128 cells (68 control, 60 NMDAR).

5. DISCUSSION

In this PhD work, I show how recombinant NMDAR antibodies affect structure and function of CA1 neurons in the mouse model of NMDAR encephalitis. I first investigated neuronal morphology in *ex vivo* preparations. I was able to show that in excitatory pyramidal neurons, NMDAR antibodies cause morphological alterations (lengthening) of dendritic spines without affecting their density. On the other hand, spine density in inhibitory interneurons is increased and spines tend to be smaller.

To probe the effect of NMDAR antibodies on neuronal function *in vivo*, I developed a hippocampal window preparation combined with intracerebroventricular infusion. This allowed me to assess the activity of the same neurons before and after administration of NMDAR antibodies. Under anaesthesia, CA1 pyramidal cells displayed increased amplitude and frequency of Ca^{2+} transients at the end of the infusion (day 18), reflecting an increase in spontaneous firing activity, while coordination of neuronal activity was impaired, as indicated by decreased pairwise correlations between simultaneously recorded neurons. In awake, behaving mice NMDAR antibodies decreased activity rates on pyramidal neurons, as indicated by decreased amplitude of Ca^{2+} transients at days 14 and 18.

Mice that received NMDAR antibodies performed the virtual spatial navigation task equally well as mice receiving control antibodies, as indicated by equal changes in running speed, licking and arousal in reward anticipation. Focusing on place cells, the cellular basis of spatial navigation, I found that spatial coding in mice infused with the NMDAR antibody was relatively intact with levels of spatial information, reliability, COM shift and place field width comparable to mice infused with the control antibody. However, there was a selective loss of place cells with multiple place fields in the NMDAR group, as indicated by lower mean number of place fields per place cell. Furthermore, place cells in the NMDAR group became more stable after NMDAR antibody infusion (days 5 – 18), as indicated by increased place field correlations and POV correlations, and recurrence of place cells from one session to the next. These differences in single place cell properties were not reflected at the population level, since mice that received NMDAR antibodies encoded space equally well as controls and were able to discriminate equally well between the familiar and novel contexts.

To further scrutinize the impact of NMDAR antibodies on neuronal network function, I focused my analysis on neuronal ensembles, the computational building blocks of

neuronal networks. At the level of neuronal ensembles, NMDAR antibodies were associated with increased ensemble similarity while the number and distinctness of ensembles remained unchanged. Finally, I investigated the impact of NMDAR antibodies on CA1 interneurons, which are an essential part of hippocampal circuits. There was a trend toward decreased amplitude and frequency of Ca^{2+} transients in PV interneurons and a trend towards lower coordination of SST interneurons. Together, these results indicate a phenotype of NMDAR encephalitis associated with increased stability of spatial representations in CA1 layer of the hippocampus.

5.1. ANIMAL MODELS OF NMDAR ENCEPHALITIS

Passive transfer of NMDAR antibodies using intracerebroventricular infusion has proven straightforward and informative. However, this approach was associated with several difficulties in this study. First, the time gap between implantation of the brain catheter and infusion of the antibody solution led to catheter clogging, resulting in a reduced transfer efficiency. For this reason, the antibody dose was increased from 20 μg for immediate infusion (data in Section 4.2) to 100 μg for delayed infusion (data in Section 4.3) to compensate for the lower efficiency. Second, bilateral intracerebroventricular infusion using two minipumps resulted in enlargement of the ventricles due to the volume of infused solution. This posed a problem for *in vivo* imaging experiments, where the same set of cells was tracked throughout the experiment. The brain tissue shift associated with intracerebroventricular infusion resulted in warping of the CA1 layer and rendered locating the same cells in a single focal plane impossible. Therefore, an alternative approach was chosen for *in vivo* imaging experiments, employing a single minipump with increased antibody concentration.

Intracerebroventricular infusion of recombinant monoclonal NMDAR antibodies represent a convenient way of studying isolated antibody effects. However, brain catheter insertion is associated with significant brain damage and inflammation of adjacent cortical areas. Furthermore, the surgical intervention associated with the minipump implantation on day 0 had adverse effects on animal's performance of the task on the following imaging session (day 5). General anaesthesia required for this resulted in drowsiness and reduction in locomotor activity for several days following the intervention. Thus, a mouse model that eliminates these issues would be a great asset to future experiments. A prospective model of NMDAR encephalitis is adoptive transfer of B cells, engineered to secrete the recombinant NMDAR antibody. In such a model, B cells

(murine or human) could be cultured *in vitro* and administered into the mouse ventricular system through a single stereotactic injection. In this way, a defined number of B cells would colonize the ventricular system and secrete antibodies into the CSF in a controlled way. An advantage of the intrathecal injection of B cells is the bypass of the BBB, which would otherwise hinder the transfer of B cells and antibodies from blood to CSF in a scenario where the B cells were injected intravenously. Moreover, the B cells could be engineered to express a fluorescent marker, such as GFP. Consequently, the efficiency of NMDAR encephalitis induction could be monitored in CSF samples collected serially through cisterna magna puncture and proliferation of B cells could be monitored with fluorescence-associated cell sorting and the antibody concentration could be assessed with ELISA assay. The number of injected B cells could be optimized to achieve a defined antibody dose over a specific period of time, and B cells could be reinjected if necessary. If successful, such a model would have two advantages over existing models of NMDAR encephalitis: first, compared to brain infusion, it would be minimally invasive and eliminate the need for bulky and problematic minipump setup. Second, it would be considerably more straightforward without the need for strict biosafety, as is the case of the HSV1 model (Linnoila et al., 2019), or expertise in protein synthesis in case of the holoreceptor model (Jones et al., 2019).

Although a more complete picture of NMDAR encephalitis is painted by models employing active immunization, the adoptive B cell transfer model could be used to study isolated roles of recombinant antibodies and B cells in pathophysiology of NMDAR encephalitis.

5.2. DENDRITIC SPINES IN NMDAR ENCEPHALITIS

The data presented in my thesis suggest that NMDAR antibodies alter dendritic spines, with interneurons affected differentially than pyramidal neurons in CA1. While dendritic spine density of pyramidal cells remained unchanged, these spines were affected morphologically. Both dendritic spine density and morphology of CA1 interneurons was affected, suggesting that interneurons may be more sensitive to NMDAR signalling perturbations. Since dendritic spines are known to morphologically respond to synaptic plasticity events (see Section 1.2.4), morphological changes in dendritic spines may be associated with LTP reduction caused by NMDAR antibodies (Hughes et al., 2010). However, the opposite effects were observed in pyramidal cells and interneurons: lengthening and shortening of spines, respectively. The reason for this differential effect

of NMDAR antibodies remains unknown. The finding of unchanged dendritic spine density of pyramidal neurons is consistent with previous reports, where dendritic spine density was found not to be affected by NMDAR antibodies when exposed in cell culture (Hughes et al., 2010). Structural analysis of interneurons revealed increased spine density in GAD67 mouse line, which expresses GFP mostly in SST interneurons. On the other hand, *in vivo* imaging revealed a trend towards decreased activity and synchrony of hippocampal interneurons. A possible explanation for this could be a homeostatic increase in dendritic spine density in response to decreased synaptic transmission caused by NMDAR antibodies. Furthermore, changes in dendritic spine morphology reported here are suggestive of dendritic spine plasticity changes. This could be investigated in a follow-up experiment, in which dynamics of CA1 dendritic spines would be investigated employing *in vivo* timelapse two-photon imaging in the mouse model of NMDAR encephalitis.

Given the above, it would be worthwhile to perform timelapse imaging of dendritic spines in stratum oriens of CA1 neurons, both excitatory pyramidal neurons (GFP-M mouse line) as well as inhibitory interneurons (GAD67 mouse line), to answer the question what the impact of NMDAR antibodies is on dendritic spine plasticity. If results of these experiments would confirm alterations of spine dynamics, such as spine survival and rates of spine elimination and formation, it would suggest that pathogenicity of NMDAR antibodies is mediated through altered neuronal circuit connectivity rather than through excitability changes of individual neurons. A timelapse *in vivo* study of CA1 dendritic spines showed a ~15 % decrease in spine density and corresponding increase in spine elimination rate in response to NMDAR antagonist MK-801 (Attardo et al., 2015). Given the superior potency of MK-801 over NMDAR antibodies in inhibiting NMDAR activity, a substantially smaller effect on spine turnover rates could be expected. Furthermore, spine size could be assessed before and after the NMDAR antibody infusion to provide a more conclusive evidence of spine morphological alterations. In addition, if these experiments were conducted at the same time scale as experiments in this study, it would enable a direct comparison between structural and functional changes associated with NMDAR encephalitis, such as temporal order of these changes.

5.3. NEURONAL ACTIVITY UNDER NMDAR ANTAGONISTS

There are mixed opinions on whether NMDAR antagonists affect activity rates of CA1 pyramidal neurons when administered *in vivo*. Interestingly, while NMDAR antagonists

consistently inhibit neuronal activity *in vitro* (Lowe et al., 1990), *in vivo* effects are less straightforward. Several studies reported no effect on activity rates by NMDAR antagonist CPP (Hayashi, 2019; Kentros et al., 1998; Silva et al., 2015) or MK-801 (Szczurowska et al., 2018) when applied *in vivo*. However, chronic treatment with NMDAR antagonist ketamine, which represents a mouse model of schizophrenia, resulted in increased activity rates when compared to saline treatment (Hamm et al., 2017). The origin of the discrepancy in effects of different NMDAR antagonists on neuronal activity *in vivo* is speculative, however a contributing factor could be the competitive and non-competitive mechanisms of NMDAR blockade of CPP and ketamine, respectively (Anis et al., 1983; Lowe et al., 1990).

Results of the present work suggest that spontaneous activity rates under anaesthesia (Ca^{2+} transient amplitude and frequency) increased after NMDAR antibodies treatment, in agreement with published literature (Hamm et al., 2017). Furthermore, correlation of neuronal activity decreased after treatment with NMDAR antibodies when compared to controls. However, this is in disagreement with results of the previous study, which found an increase in pairwise correlation after chronic ketamine treatment (Hamm et al., 2017). This discrepancy could be due to differences in experimental setup, particularly anesthetized (this study) vs. awake state of the animal. Furthermore, since high doses of isoflurane are known to affect synchrony of local ensembles (Lissek et al., 2016), the fluctuations in isoflurane levels could account for the observed differences in neuronal synchrony, despite best efforts to keep the anaesthesia level at a constant rate. The notion of spontaneous hyperactivity of neurons in neurodegenerative diseases has been described previously. In a mouse model of Alzheimer's disease (AD), spontaneous activity of CA1 neurons increased already well before the formation of plaques (Busche et al., 2012). Thus, neuronal hyperactivity is associated with cognitive deficits in neurodegenerative diseases, such as AD (Busche et al., 2012, 2008).

However, the effect of NMDAR antibodies on spontaneous neuronal activity was lost when recordings were performed in awake, behaving mice. There was no difference in frequency of Ca^{2+} transients or in pairwise correlations between the control and NMDAR group. However, there was a slight reduction in Ca^{2+} transient amplitudes at days 14 and 18. These results suggest that the increased inhibitory drive during wakefulness may be masking the excitability changes leading to altered spontaneous transmission under anaesthesia.

5.4. PLACE CELLS IN NMDAR HYPOFUNCTION

I found that animals that received NMDAR antibodies were not impaired in performance of the spatial navigation task when compared to control animals. Although there was evidence of reward location learning in the novel environment, the predominant strategy of the mice was associating the reward delivery with an audible clicking sound made by the water dispenser valve whenever water rewards were delivered. Furthermore, water rewards were delivered regardless of whether the mouse paused in the reward zone. Under such conditions, the most efficient strategy employed by the mice was running until they heard the click and then stopping to collect their rewards, without the necessity to associate the reward locations with spatial cues and wait time in the reward zone. Therefore, the task used in this study has minimal spatial learning demands and can thus be classified as spatial navigation task rather than spatial learning task. This has two implications for the results of this study: First, spatial navigation in mice is NMDAR independent (Morris et al., 2013), which could explain the absence of performance impairment in NMDAR antibody-infused animals, despite the mouse model of NMDAR encephalitis having well-established behavioural phenotype (Malviya et al., 2017; Planagumà et al., 2015). Indeed, animals receiving chronic systemic infusion of the NMDAR antagonist APV are impaired on spatial learning task but not on spatial navigation task (Morris et al., 2013). Moreover, basic behaviour such as running speed is not affected by NMDAR antagonists (Hayashi, 2019; Kentros et al., 1998; Silva et al., 2015). Second, the low cognitive demand of the task may account for the relatively low proportion of place cells in the present work (20-25 %) compared to published literature (30-50 %; Hainmueller and Bartos, 2018; Shuman et al., 2020). Place cell properties in CA1, such as reliability and proportion of spatially tuned cells, are influenced by the level of attention the mouse pays to the environment (Kinsky et al., 2018). Minimal learning demands of the task used in this study are suggested by the fact that location of the reward was not enriched in place fields, similarly to other studies employing spatial navigation task (Hayashi, 2019). On the other hand, place fields in spatial learning tasks accumulate around the goal or reward location (Gauthier and Tank, 2018; Zaremba et al., 2017). Moreover, place cell properties have been shown to be impaired on spatial learning task in a mouse model of schizophrenia, whereas place cells were not impaired on the spatial navigation version of the task in the same animals (Zaremba et al., 2017). Therefore, the choice of the task has critical implications for place cell properties and their dependence on NMDAR signalling.

Several other studies investigated CA1 place cells and spatial representations under NMDAR antagonists. Kentros et al. (1998) investigated long-term stability and plasticity of place cells in rats using familiar and novel open field arenas. The authors report that NMDAR blockade had no effect on spatial information content, reliability and long-term stability of place cells in the familiar environment. Furthermore, the stability of familiar environment spatial maps was unchanged after the NMDAR antagonist administration (Kentros et al., 1998; Morris et al., 2013; Silva et al., 2015), suggesting that NMDAR blockade does not interfere with previously formed place maps. A more recent study investigating the impact of chronic pharmacological blockade of NMDARs on place cell function using Ca^{2+} imaging in mice performing a spatial navigation task in a virtual reality reported no effect on place field properties or spatial information content of place cells. However, place cell recurrence was increased upon administration of NMDAR antagonist CPP (Hayashi, 2019), a result replicated in the present study.

A study by Zaremba et al. (2017) investigating place cells in the 22q11.2 deletion mouse model of schizophrenia found a 25 % decrease in fraction of place cells, 6 % decrease in average place fields per place cell and 15 % increase in COM shift between sessions when compared to controls. In the present study, a comparable decrease in average place fields per place cell was found. However, the decrease in place cell fraction and increase in COM shift was not replicated in this study. This discrepancy may be due to different mouse models used and the differences in behavioural tasks. Indeed, differences in virtual reality designs can influence properties of place cells, such as place field width. Place fields on a virtual track 1.8 m long were 16 cm wide on average (Hayashi, 2019), whereas on a 3 m long track used in this study the mean place field width was 42 cm. Although significant differences in fraction of familiar environment place cells were observed at day -5 and novel environment place cells at day 10, these changes are likely due to intrinsic variability and individual mouse differences and do not represent a robust NMDAR antibody effect. Indeed, relatively large baseline variability in place cell fraction (up to 25 %) has been reported by other authors (Shuman et al., 2020).

Curiously, NMDA receptor blockade did not prevent remapping when animals alternated between the familiar and novel environments. This result is consistent with published reports, which also found intact ability of CA1 neurons to remap, despite the NMDAR antagonist CPP completely abolishing the LTP in CA1 (Kentros et al., 1998; Silva et al., 2015). Therefore, NMDAR antagonists seem to have no effect on place field formation in novel environments. However, NMDAR blockade resulted in long-term instability of

novel maps, leading to a new remapping upon a second visit to the novel environment one day later (Kentros et al., 1998). This could be the result of the novel environment representation formed on the first encounter failing to stabilize overnight and being recalled on the second visit. Instead, the previously seen environment is perceived as a different environment on the second visit on the following day. The mechanism behind this failure to retain a memory could be dysregulation of SWR, which is essential for memory consolidation in the hippocampus (Zaremba et al., 2017). Long-term stability of novel place cells could not be investigated in this study, since a new novel environment was presented on each imaging session. These data suggest that there may be NMDAR independent mechanisms of place field formation and maintenance. Despite NMDAR antagonist CPP sparing individual place field properties, Bayesian decoding of animal's position from neuronal activity revealed a higher error between reconstructed and actual position suggesting a degraded place cell coding under NMDAR blockade (Silva et al., 2015). Although properties of individual place cells were found to be affected by NMDAR antibodies in this study, there was no difference in position reconstruction error between the control and NMDAR group.

Breakdown of spatial coding and interneuron synchronization is associated with epilepsy in a pilocarpine treatment mouse model of epilepsy. Epileptic mice have altered timing of inhibition in the DG, leading to a decrease in synchronization between CA1 and DG. As a result of this desynchronization, place cells have reduced information content, reduced place cell reliability, reduced place cell proportion and increased position decoding error when compared to controls. Furthermore, place cells in epileptic mice completely remapped within a week. Strikingly, this place cell instability emerged only 6 weeks after epileptogenesis and was dissociated from interneuron death and seizure onset. This temporal dissociation suggests that place cell instability is mediated by an unknown circuit mechanism that is independent of seizure onset and interneuron loss (Shuman et al., 2020). Although these results on place cell instability were not replicated in this study, most likely owing to differences in disease models, these findings could however have an implication for the present study: given the 6-week time lag between the onset of epileptic seizures and the onset of spatial coding instability, the timeline of experiments in this work may not have been sufficiently long to capture more dramatic effects of NMDAR antibodies. Even though the mice begin to experience behavioural symptoms 10 days into the NMDAR antibody infusion (Planagumà et al., 2015), place cell instability may take longer to manifest.

The role of place cells in memory retention was long debated. According to the original theory, place cells should retain stable place fields to encode long-term memory of familiar environments (O'Keefe and Nadel, 1978). Indeed, evidence emerged that place cells are extremely stable entities with stable place fields for up to 153 days (Thompson and Best, 1990). With the advent of large-scale recordings however, an alternative hypothesis emerged that dynamic aspects of place coding may facilitate distinct memory traces of events occurring in the same environment (Leutgeb et al., 2005). Mounting evidence supports the latter hypothesis. A study by Ziv et al. (2013) was the first to observe long-term dynamics of CA1 place cells *in vivo* and reported that place cell coding is highly dynamic. Specifically, there is only 25 % overlap in subset of cells with statistically significant place fields between sessions 5 days apart. Thus, cells come in and out of the place coding ensemble leading to a spatial representation decaying in time. However, a small fraction of place cells retain their spatial tuning for long periods of time. Although spatial maps have a fluctuating membership, the place cell overlap in sessions 30 days apart was sufficient to accurately predict mouse's location using a decoder trained on data recorded 30 days prior (Ziv et al., 2013). Data in this work show that CA1 place cell coding is indeed dynamic, with ~30 % overlap in place cell subsets over 5-day intervals. Nevertheless, a fraction of place cells retained stable place fields over the entire length of the experiment (23 days). NMDAR antibodies decreased the dynamics of place cell coding, as indicated by lower turnover rates when compared to controls.

It has long been known that NMDAR blockade impairs memory acquisition and LTP (Morris et al., 1986). However, NMDARs are also involved in memory retention. LTP is a long-lasting phenomenon which decays within weeks of its induction (Barnes, 1979). Interestingly, spatial memory retention can be enhanced by blocking the LTP decay, achieved by chronic administration of NMDAR antagonist CPP (Villarreal et al., 2002). These data suggest that LTP is involved in maintaining spatial memory and is actively reversed by NMDAR activation. Therefore, the rate of change of place cell activity could also be an NMDAR activation-dependent process, which could be slowed down through reduced NMDAR activity. The data presented in this study suggest that NMDAR antibodies indeed reduced the speed of change in place cell activity, as indicated by increase in place field correlation and increase in place cell recurrence accompanied by reduced place cell turnover rates.

An important question is what could be the link between long-term memory deficits observed in patients (Kayser and Dalmau, 2016) and decreased place cell dynamics

observed in this study. One possibility is that altered place cell dynamics could interfere with the cortical transfer and therefore hamper long-term memory formation.

5.5. NEURONAL ENSEMBLES

Analysis of single neurons tuned to single features (e.g., place cells) has proven informative and straightforward. However, focusing analyses to only a fraction of cells begs the question what is the role of the other neurons in encoding a specific feature, such as physical space. That question can be answered twofold: First, neurons deemed as feature-unresponsive may be encoding other variables that are not measured in a particular experiment, such as time or nonspatial dimensions. Moreover, individual neurons may be only weakly tuned to a given stimulus and thus not pass the statistical thresholding step. Second, all neurons may participate in encoding of multiple variables through nonlinear responses. Indeed, there is evidence that information is not carried by individual cells, place cells or time cells, but rather through a diffuse, distributed neural code, where neurons cooperate to encode information about position, motion direction or velocity. Individual neuron responses are only weakly predictive of their contribution to network code, that is, the neurons with clearly identifiable responses might not necessarily be the most important ones. In addition, even non-place cells encode position through their activity correlated with place cells (Stefanini et al., 2020).

Neuronal ensemble analysis in this work revealed presence of neuronal ensembles in both the control and NMDAR group, with intact number and distinctness of ensembles occurring in each session. There was however and increase in ensemble similarity as indicated by higher correlation of ensemble activation frames. This contrasts with results of a previous study, which reported a decrease in ensemble similarity in a ketamine model of schizophrenia (Hamm et al., 2017). This discrepancy may partly originate in the fact that ensemble analysis in this study was performed on data from mice performing the spatial navigation task, as opposed to spontaneously occurring ensembles investigated by Hamm et al. (2017). Furthermore, this increase in ensemble stability may reflect the decrease in diffusivity of place cell firing (i.e., lower number of place fields per place cell).

A study by Poll et al. (2020) investigated the neural mechanisms underlying memory deficits in a mouse model of AD (APP/PS1) using time-lapse *in vivo* imaging of c-Fos reporter system of neuronal activity. By exposing the mice to familiar and novel contexts associated with fear conditioning, they were able to observe neuronal ensembles

encoding the experience in each context. Interestingly, baseline as well as learning induced changes in neuronal activity of AD mice were comparable to those of control mice, indicating CA1 network per se was not disturbed. The fact that the memory trace is intact in AD mice is in striking contrast to the learning deficit of these mice, and it indicates that the memory engram is present regardless of memory performance. Strikingly, the novel ensemble (an ensemble encoding the novel environment) interfered with the recall of the familiar ensemble during memory retrieval. Although the neuronal ensembles are intact, the interference between them impedes memory recall. This suggests that AD mice perceived the familiar environment as novel on repeated visits. Furthermore, pharmacological silencing of the novel ensemble during re-exposure to familiar context rescued memory deficits in AD mice. The presence of a novel ensemble in a familiar environment indicated a possible defect in pattern separation and pattern completion functions of the hippocampus, resulting in a mismatch between contextual experiences in AD (Poll et al., 2020). Moreover, a similar misclassification phenotype was reported in aged mice, where visits of the same environment resulted in less similar representations and visits to a novel environment resulted in more similar CA1 representations compared with young mice (Attardo et al., 2018). These results suggest that cognitive impairments may not be manifested as absent or corrupted neuronal ensembles, but rather errors in hippocampal integration and experience mismatch.

5.6. ROLE OF CA1 INTERNEURONS IN SPATIAL CODING

Interneuron dysfunction has been implicated in cognitive and spatial coding deficits in rodent models of neurodegenerative diseases, such as AD (Mably et al., 2017), schizophrenia (Zaremba et al., 2017) or Down's syndrome (Raveau et al., 2018). However, different studies suggest that CA1 interneuron inhibition impairs spatial coding (Shuman et al., 2020) or have no effect on spatial coding (Royer et al., 2012). These seemingly contradictory findings could be explained by relatively robust resistance of place cell coding to input perturbation. Indeed, modelling suggests that the amount of suppression may be the critical factor in determining whether perturbation of hippocampal interneurons alter CA1 spatial coding. While modest (25 %) loss of PV and SST interneurons has no discernible effect on spatial coding, high levels of interneuron loss can lead to impaired spatial coding. Interestingly, loss of majority of PV interneurons (75 %) can lead to increased place cell stability. Such increase in stability may be a result of

increased reliance on inputs that are more consistent than inhibition (Shuman et al., 2020).

In data presented in this work, there was a trend towards decreased activity of PV interneurons and a trend towards lower pairwise correlations between SST interneurons. Given the above, the reduction in PV interneuron activity could be a contributing factor in the increased stability of spatial representations described in this study. However, interneurons exhibit high firing rates that far exceed Ca^{2+} indicator kinetics (Lin and Schnitzer, 2016) as well as the sampling rate of the imaging system used in this study (Varga et al., 2012). Activity rates of CA1 interneurons presented here are thus only a coarse approximation of the true firing rates. However, Ca^{2+} traces of interneurons can still be used to approximate average firing rates over time (Hainmueller and Bartos, 2018). Nevertheless, it is possible that changes in CA1 interneurons activity rates are seriously underestimated in this study.

5.7. CONCLUDING REMARKS

Taken together the results of my PhD work, I show the effect of NMDAR antibodies on structure of hippocampal dendritic spines and on function of hippocampal place cell ensembles. They reveal differential effects of NMDAR antibodies on hippocampal dendritic spines, with interneurons being more susceptible to NMDAR antibodies than pyramidal neurons. Whether NMDAR antibodies also affect dynamic properties of hippocampal dendritic spines, such as turnover rates, remains unknown. However, morphological changes in dendritic spines associated with NMDAR antibodies are suggestive of this possibility. Thus, further experiments are needed to confirm the results of this study.

Behavioural task used in this study represent a convenient and adequate paradigm for investigations of place cells, particularly for relatively short training period (7 days) compared to more demanding spatial learning tasks (15 days; Hainmueller and Bartos, 2018) as well as overall high rate of trials thereby reducing the length of the imaging session. A follow-up experiment could be designed to investigate the long-term stability of novel environment place cells. Furthermore, specific aspects of spatial learning could be investigated next, such as transmission of information stored in the hippocampus to other brain areas involved in spatial learning, such as the prefrontal cortex. Indeed, it has been shown that an intact memory engram could exist in the hippocampus, but downstream areas failed to retrieve this information (Poll et al., 2020).

As a result of chronic infusion of NMDAR antibodies, place cells were more confined, as indicated by a lower number of place fields per place cell, and were more stable, as indicated by higher correlation of place fields between sessions and higher recurrence. Interestingly, the overall effect of NMDAR antibodies on hippocampal spatial processing was relatively mild, despite the cognitive symptoms the mice present with already at day 10 (Planagumà et al., 2015). This suggests place cells themselves might not be faithfully reporting on the cognitive state of the animals. These findings are consistent with literature, reporting little (Silva et al., 2015) or no effect (Kentros et al., 1998) of NMDAR antagonists on place cell function. Remarkably, there was an increase in place cell stability associated with NMDAR antibodies, an effect similar to other NMDAR antagonists (Hayashi, 2019). The mechanism behind this change could be decreased LTP decay, which is known to be a NMDAR-dependent process (Villarreal et al., 2002). The rate of change in place cell coding was slowed down in this study, possibly as a result of this LTP decay inhibition. This hypothesis could be answered with electrophysiology experiments, investigating the LTP decay within a week of continuous NMDAR antibodies treatment. Furthermore, decrease in PV interneuron activity could contribute to increased place cell stability (Shuman et al., 2020).

Given the effects on structure and function of hippocampal neurons, the next question is how do these changes translate into connectivity of local neurons and their long-range projections. White matter changes are associated with NMDAR encephalitis in patients (Finke et al., 2013), further suggesting that this disease affects the whole brain and is not limited to the hippocampus. Moreover, connectivity changes following NMDAR encephalitis could explain the persistent cognitive symptoms that some patients experience long after the acute phase subsided. More research is needed to better understand brain changes pertinent to this debilitating disease the NMDAR encephalitis is.

6. REFERENCES

Abbas AK, Lichtman AH, Pillai S. 2021. Cellular and Molecular Immunology - 10th Edition 600.

Allegra M, Posani L, Gómez-Ocádiz R, Schmidt-Hieber C. 2020. Differential Relation between Neuronal and Behavioral Discrimination during Hippocampal Memory Encoding. *Neuron* **108**:1103-1112.e6. doi:10.1016/j.neuron.2020.09.032

Anis NA, Berry SC, Burton NR, Lodge D. 1983. The dissociative anaesthetics, ketamine and phencyclidine, selectively reduce excitation of central mammalian neurones by N-methyl-aspartate. *Br J Pharmacol* **79**:565–575. doi:10.1111/J.1476-5381.1983.TB11031.X

Armangue T, Spatola M, Vlagea A, Mattozzi S, Cárceles-Cordon M, Martinez-Heras E, Llufriu S, Muchart J, Erro ME, Abraira L, Moris G, Monros-Giménez L, Corral-Corral Í, Montejo C, Toledo M, Bataller L, Secondi G, Ariño H, Martínez-Hernández E, Juan M, Marcos MA, Alsina L, Saiz A, Rosenfeld MR, Graus F, Dalmau J, Aguilera-Albesa S, Amado-Puentes A, Arjona-Padillo A, Arrabal L, Arratibel I, Aznar-Laín G, Bellas-Lamas P, Bermejo T, Boyero-Durán S, Camacho A, Campo A, Campos D, Cantarín-Extremera V, Carnero C, Conejo-Moreno D, Dapena M, Dacruz-Álvarez D, Delgadillo-Chilavert V, Deyà A, Estela-Herrero J, Felipe A, Fernández-Cooke E, Fernández-Ramos J, Fortuny C, García-Monco JC, Gili T, González-Álvarez V, Guerri R, Guillén S, Hedrera-Fernández A, López M, López-Laso E, Lorenzo-Ruiz M, Madruga M, Málaga-Diéguez I, Martí-Carrera I, Martínez-Lacasa X, Martín-Viota L, Martín Gil L, Martínez-González MJ, Moreira A, Miranda-Herrero MC, Monge L, Muñoz-Cabello B, Navarro-Morón J, Neth O, Noguera-Julian A, Nuñez-Enamorado N, Pomar V, Portillo-Cuenca JC, Poyato M, Prieto L, Querol L, Rodríguez-Rodríguez E, Sarria-Estrada S, Sierra C, Soler-Palacín P, Soto-Insuga V, Toledo-Bravo L, Tomás M, Torres-Torres C, Turón E, Zabalza A. 2018. Frequency, symptoms, risk factors, and outcomes of autoimmune encephalitis after herpes simplex encephalitis: a prospective observational study and retrospective analysis. *Lancet Neurol* **17**:760–772. doi:10.1016/S1474-4422(18)30244-8

Aronov D, Nevers R, Tank DW, D A, R N, DW T. 2017. Mapping of a non-spatial dimension by the hippocampal-entorhinal circuit. *Nature* **543**:719–722. doi:10.1038/nature21692

Attardo A, Fitzgerald JE, Schnitzer MJ. 2015. Impermanence of dendritic spines in live adult CA1 hippocampus. *Nature* **523**:592–596. doi:10.1038/nature14467

Attardo A, Lu J, Kawashima T, Okuno H, Fitzgerald JE, Bito H, Schnitzer MJ. 2018. Long-Term Consolidation of Ensemble Neural Plasticity Patterns in Hippocampal Area CA1. *Cell Rep* **25**:640-650.e2. doi:10.1016/j.celrep.2018.09.064

Balu DT. 2016. The NMDA Receptor and Schizophrenia. From Pathophysiology to Treatment.Advances in Pharmacology. Academic Press. pp. 351–382. doi:10.1016/bs.apha.2016.01.006

Balu DT, Li Y, Puhl MD, Benneyworth MA, Basu AC, Takagi S, Bolshakov VY, Coyle JT. 2013. Multiple risk pathways for schizophrenia converge in serine racemase knockout mice, a mouse model of NMDA receptor hypofunction. *Proc Natl Acad Sci U S A* **110**. doi:10.1073/pnas.1304308110

Bannerman DM, Bus T, Taylor A, Sanderson DJ, Schwarz I, Jensen V, Hvalby Ø, Rawlins JNP, Seeburg PH, Sprengel R. 2012. Dissecting spatial knowledge from spatial choice by hippocampal NMDA receptor deletion. *Nat Neurosci* **15**:1153–1159. doi:10.1038/nn.3166

Barnes CA. 1979. Memory deficits associated with senescence: A neurophysiological and behavioral study in the rat. *J Comp Physiol Psychol* **93**:74–104. doi:10.1037/h0077579

Belforte JE, Zsiros V, Sklar ER, Jiang Z, Yu G, Li Y, Quinlan EM, Nakazawa K. 2010. Postnatal NMDA receptor ablation in corticolimbic interneurons confers schizophrenia-like phenotypes. *Nat Neurosci* **13**:76–83. doi:10.1038/nn.2447

Bien CG, Rohleder C, Mueller JK, Bien CI, Koethe D, Leweke FM. 2021. Neural Autoantibodies

in Cerebrospinal Fluid and Serum in Clinical High Risk for Psychosis, First-Episode Psychosis, and Healthy Volunteers. *Front Psychiatry* **12**:382. doi:10.3389/fpsyt.2021.654602

Bird CM, Capponi C, King JA, Doeller CF, Burgess N. 2010. Establishing the boundaries: The hippocampal contribution to imagining scenes. *J Neurosci* **30**:11688–11695. doi:10.1523/JNEUROSCI.0723-10.2010

Bootman MD, Berridge MJ. 1995. The elemental principles of calcium signaling. *Cell* **83**:675–678. doi:10.1016/0092-8674(95)90179-5

Bosch M, Hayashi Y. 2012. Structural plasticity of dendritic spines. *Curr Opin Neurobiol*. doi:10.1016/j.conb.2011.09.002

Brandon NJ, Sawa A. 2011. Linking neurodevelopmental and synaptic theories of mental illness through DISC1. *Nat Rev Neurosci*. doi:10.1038/nrn3120

Brigman JL, Wright T, Talani G, Prasad-Mulcare S, Jinde S, Seabold GK, Mathur P, Davis MI, Bock R, Gustin RM, Colbran RJ, Alvarez VA, Nakazawa K, Delpire E, Lovinger DM, Holmes A. 2010. Loss of GluN2B-containing NMD A receptors in CA1 hippocampus and cortex impairs long-term depression, reduces dendritic spine density, and disrupts learning. *J Neurosci* **30**:4590–4600. doi:10.1523/JNEUROSCI.0640-10.2010

Brilot F, Dale RC, Selter RC, Grummel V, Kalluri SR, Aslam M, Phil M, Busch V, Zhou D, Cepok S, Hemmer B. 2009. Antibodies to native myelin oligodendrocyte glycoprotein in children with inflammatory demyelinating central nervous system disease. *Ann Neurol* **66**:833–842. doi:10.1002/ana.21916

Busche MA, Chen X, Henning HA, Reichwald J, Staufenbiel M, Sakmann B, Konnerth A. 2012. Critical role of soluble amyloid-β for early hippocampal hyperactivity in a mouse model of Alzheimer's disease. *Proc Natl Acad Sci U S A* **109**:8740–8745. doi:10.1073/pnas.1206171109

Busche MA, Eichhoff G, Adelsberger H, Abramowski D, Wiederhold KH, Haass C, Staufenbiel M, Konnerth A, Garaschuk O. 2008. Clusters of hyperactive neurons near amyloid plaques in a mouse model of Alzheimer's disease. *Science (80-)* **321**:1686–1689. doi:10.1126/science.1162844

Butler WN, Hardcastle K, Giocomo LM. 2019. Remembered reward locations restructure entorhinal spatial maps. *Science (80-)* **363**:1447–1452. doi:10.1126/science.aav5297

Carceles-Cordon M, Mannara F, Aguilar E, Castellanos A, Planagumà J, Dalmau J. 2020. NMDAR Antibodies Alter Dopamine Receptors and Cause Psychotic Behavior in Mice. *Ann Neurol* **88**:603–613. doi:10.1002/ana.25829

Carrillo-Reid L, Miller JK, Hamm JP, Jackson J, Yuste R. 2015. Endogenous Sequential Cortical Activity Evoked by Visual Stimuli. *J Neurosci* **35**:8813–8828. doi:10.1523/JNEUROSCI.5214-14.2015

Carrillo-Reid L, Yang W, Bando Y, Peterka DS, Yuste R. 2016. Imprinting and recalling cortical ensembles. *Science (80-)* **353**:691–694. doi:10.1126/science.aaf7560

Castillo-Gómez E, Oliveira B, Tapken D, Bertrand S, Klein-Schmidt C, Pan H, Zafeiriou P, Steiner J, Jurek B, Trippe R, Prüss H, Zimmermann WH, Bertrand D, Ehrenreich H, Hollmann M. 2017. All naturally occurring autoantibodies against the NMDA receptor subunit NR1 have pathogenic potential irrespective of epitope and immunoglobulin class. *Mol Psychiatry* **22**:1776–1784. doi:10.1038/mp.2016.125

Chen W, Hobbs JP, Tang A, Beggs JM. 2010. A few strong connections: Optimizing information retention in neuronal avalanches. *BMC Neurosci* **11**. doi:10.1186/1471-2202-11-3

Corkin S. 1968. Acquisition of motor skill after bilateral medial temporal-lobe excision. *Neuropsychologia* **6**:255–265. doi:10.1016/0028-3932(68)90024-9

Cossell L, Iacaruso MF, Muir DR, Houlton R, Sader EN, Ko H, Hofer SB, Mrsic-Flogel TD. 2015. Functional organization of excitatory synaptic strength in primary visual cortex. *Nature* **518**:399–403. doi:10.1038/nature14182

Cui L, Sun W, Yu M, Li N, Guo L, Gu H, Zhou Y. 2016. Disrupted-in-schizophrenia1 (DISC1) L100P mutation alters synaptic transmission and plasticity in the hippocampus and

causes recognition memory deficits. *Mol Brain* **9**:1–13. doi:10.1186/s13041-016-0270-y

Dale RC, Church AJ, Surtees RAH, Lees AJ, Adcock JE, Harding B, Neville BGR, Giovannoni G. 2004. Encephalitis lethargica syndrome: 20 New cases and evidence of basal ganglia autoimmunity. *Brain* **127**:21–33. doi:10.1093/brain/awh008

Dalmau J. 2020. Pregnancy, N-Methyl-D-Aspartate Receptor Antibodies, and Neuropsychiatric Diseases. *Ann Neurol*. doi:10.1002/ana.25654

Dalmau J, Armangué T, Planagumà J, Radosevic M, Mannara F, Leypoldt F, Geis C, Lancaster E, Titulaer MJ, Rosenfeld MR, Graus F. 2019. An update on anti-NMDA receptor encephalitis for neurologists and psychiatrists: mechanisms and models. *Lancet Neurol* **18**:1045–1057. doi:10.1016/S1474-4422(19)30244-3

Dalmau J, Gleichman AJ, Hughes EG, Rossi JE, Peng X, Lai M, Dessain SK, Rosenfeld MR, Balice-Gordon R, Lynch DR. 2008. Anti-NMDA-receptor encephalitis: case series and analysis of the effects of antibodies. *Lancet Neurol* **7**:1091–1098. doi:10.1016/S1474-4422(08)70224-2

Dalmau J, Tüzün E, Wu HY, Masjuan J, Rossi JE, Voloschin A, Baehring JM, Shimazaki H, Koide R, King D, Mason W, Sansing LH, Dichter MA, Rosenfeld MR, Lynch DR. 2007. Paraneoplastic anti-N-methyl-D-aspartate receptor encephalitis associated with ovarian teratoma. *Ann Neurol* **61**:25–36. doi:10.1002/ana.21050

Dalva MB, Takasu MA, Lin MZ, Shamah SM, Hu L, Gale NW, Greenberg ME. 2000. EphB receptors interact with NMDA receptors and regulate excitatory synapse formation. *Cell* **103**:945–956. doi:10.1016/S0092-8674(00)00197-5

Danielson NB, Zaremba JD, Kaifosh P, Bowler J, Ladow M, Losonczy A. 2016. Sublayer-Specific Coding Dynamics during Spatial Navigation and Learning in Hippocampal Area CA1. *Neuron* **91**:652–665. doi:10.1016/j.neuron.2016.06.020

Dao LM, Machule ML, Bacher P, Hoffmann J, Ly LT, Wegner F, Scheffold A, Prüss H. 2021. Decreased inflammatory cytokine production of antigen-specific CD4+ T cells in NMDA receptor encephalitis. *J Neurol* **268**:2123–2131. doi:10.1007/s00415-020-10371-y

Davis B, Christie J, Rorden C. 2009. Temporal order judgments activate temporal parietal junction. *J Neurosci* **29**:3182–3188. doi:10.1523/JNEUROSCI.5793-08.2009

Denk W, Strickler JH, Webb WW. 1990. Two-photon laser scanning fluorescence microscopy. *Science (80-)* **248**:73–76. doi:10.1126/science.2321027

Diba K, Buzsáki G. 2007. Forward and reverse hippocampal place-cell sequences during ripples. *Nat Neurosci* **10**:1241–1242. doi:10.1038/nn1961

Ding Y, Zhou Z, Chen J, Peng Y, Wang Haitao, Qiu W, Xie W, Zhang J, Wang Honghao. 2021. Anti-NMDAR encephalitis induced in mice by active immunization with a peptide from the amino-terminal domain of the GluN1 subunit. *J Neuroinflammation* **18**. doi:10.1186/s12974-021-02107-0

Dombeck DA, Khabbaz AN, Collman F, Adelman TL, Tank DW. 2019. Imaging large-scale neural activity with cellular resolution in awake, mobile mice. - PubMed - NCBI, Neuron. doi:10.1016/J.NEURON.2007.08.003

Dubey D, Pittock SJ, Kelly CR, McKeon A, Lopez-Chiriboga AS, Lennon VA, Gadoth A, Smith CY, Bryant SC, Klein CJ, Aksamit AJ, Toledano M, Boeve BF, Tillema JM, Flanagan EP. 2018. Autoimmune encephalitis epidemiology and a comparison to infectious encephalitis. *Ann Neurol* **83**:166–177. doi:10.1002/ana.25131

Dupret D, O'Neill J, Pleydell-Bouverie B, Csicsvari J. 2010. The reorganization and reactivation of hippocampal maps predict spatial memory performance. *Nat Neurosci* **13**:995–1002. doi:10.1038/nn.2599

Dvorkin R, Ziv NE. 2016. Relative Contributions of Specific Activity Histories and Spontaneous Processes to Size Remodeling of Glutamatergic Synapses. *PLoS Biol* **14**:e1002572. doi:10.1371/journal.pbio.1002572

Ehrenreich H. 2018. Autoantibodies against N -methyl- d -aspartate receptor 1 in health and disease. *Curr Opin Neurol*. doi:10.1097/WCO.0000000000000546

Ehrenreich H. 2017. Autoantibodies against the N-Methyl-d-Aspartate Receptor Subunit NR1: Untangling Apparent Inconsistencies for Clinical Practice. *Front Immunol* **8**:181. doi:10.3389/fimmu.2017.00181

Eichenbaum H. 2015. The Hippocampus as a Cognitive Map ... of Social Space. *Neuron*. doi:10.1016/j.neuron.2015.06.013

Eichenbaum H. 2014. Time cells in the hippocampus: a new dimension for mapping memories. *Nat Rev Neurosci* **15**:732–744. doi:10.1038/nrn3827

Eichenbaum H. 2013. Memory on time. *Trends Cogn Sci*. doi:10.1016/j.tics.2012.12.007

Ekstrom AD, Kahana MJ, Caplan JB, Fields TA, Isham EA, Newman EL, Fried I. 2003. Cellular networks underlying human spatial navigation. *Nature* **425**:184–187. doi:10.1038/nature01964

Finke C, Kopp UA, Scheel M, Pech L-M, Soemmer C, Schlichting J, Leypoldt F, Brandt AU, Wuerfel J, Probst C, Ploner CJ, Prüss H, Paul F. 2013. Functional and structural brain changes in anti-N-methyl-D-aspartate receptor encephalitis. *Ann Neurol* **74**:284–296. doi:10.1002/ana.23932

Freund TF, Buzsáki G. 1996. Interneurons of the Hippocampus. *Hippocampus* **6**:347–470. doi:10.1002/(sici)1098-1063(1996)6:4<347::aid-hipo1>3.0.co;2-i

Friedrich J, Zhou P, Paninski L. 2017. Fast online deconvolution of calcium imaging data. *PLOS Comput Biol* **13**:e1005423. doi:10.1371/journal.pcbi.1005423

Fyhn M, Hafting T, Treves A, Moser MB, Moser EI. 2007. Hippocampal remapping and grid realignment in entorhinal cortex. *Nature* **446**:190–194. doi:10.1038/nature05601

Garner AR, Rowland DC, Hwang SY, Baumgaertel K, Roth BL, Kentros C, Mayford M. 2012. Generation of a synthetic memory trace. *Science (80-)* **335**:1513–1516. doi:10.1126/science.1214985

Gauthier JL, Tank DW. 2018. A Dedicated Population for Reward Coding in the Hippocampus. *Neuron* **99**:179-193.e7. doi:10.1016/j.neuron.2018.06.008

Goode TD, Tanaka KZ, Sahay A, McHugh TJ. 2020. An Integrated Index: Engrams, Place Cells, and Hippocampal Memory. *Neuron* **107**:805–820. doi:10.1016/j.neuron.2020.07.011

Göppert-Mayer M. 1931. Über Elementarakte mit zwei Quantensprüngen. *Ann Phys* **401**:273–294. doi:10.1002/andp.19314010303

Graus F, Dalmau J. 2021. Autoimmune encephalitis or autoimmune psychosis? *Eur Neuropsychopharmacol*. doi:10.1016/j.euroneuro.2021.05.004

Gréa H, Bouchet D, Rogemond V, Hamdani N, Le Guen E, Tamouza R, Darrau E, Passerieux C, Honnorat J, Leboyer M, Groc L. 2019. Human Autoantibodies Against N-Methyl-D-Aspartate Receptor Modestly Alter Dopamine D1 Receptor Surface Dynamics. *Front Psychiatry* **10**. doi:10.3389/fpsyt.2019.00670

Gresa-Arribas N, Titulaer MJ, Torrents A, Aguilar E, McCracken L, Leypoldt F, Gleichman AJ, Balice-Gordon R, Rosenfeld MR, Lynch D, Graus F, Dalmau J. 2014. Antibody titres at diagnosis and during follow-up of anti-NMDA receptor encephalitis: A retrospective study. *Lancet Neurol* **13**:167–177. doi:10.1016/S1474-4422(13)70282-5

Groc L, Bard L, Choquet D. 2009. Surface trafficking of N-methyl-d-aspartate receptors: Physiological and pathological perspectives. *Neuroscience*. doi:10.1016/j.neuroscience.2008.05.029

Groc L, Heine M, Cognet L, Brickley K, Stephenson FA, Lounis B, Choquet D. 2004. Differential activity-dependent regulation of the lateral mobilities of AMPA and NMDA receptors. *Nat Neurosci* **7**:695–696. doi:10.1038/nn1270

Gu L, Kleiber S, Schmid L, Nebeling F, Chamoun M, Steffen J, Wagner J, Fuhrmann M. 2014. Long-Term In Vivo Imaging of Dendritic Spines in the Hippocampus Reveals Structural Plasticity. *J Neurosci* **34**:13948–13953. doi:10.1523/JNEUROSCI.1464-14.2014

Guzman SJ, Schlögl A, Frotscher M, Jonas P. 2016. Synaptic mechanisms of pattern completion in the hippocampal CA3 network. *Science (80-)* **353**:1117–1123. doi:10.1126/science.aaf1836

Hainmueller T, Bartos M. 2018. Parallel emergence of stable and dynamic memory engrams

in the hippocampus. *Nature* **558**:292–296. doi:10.1038/s41586-018-0191-2

Hamm JP, Peterka DS, Gogos JA, Yuste R. 2017. Altered cortical ensembles in mouse models of schizophrenia. *Neuron* **94**:153. doi:10.1016/j.neuron.2017.03.019

Hammer C, Stepniak B, Schneider A, Papiol S, Tantra M, Begemann M, Sirén A-LL, Pardo LA, Sperling S, Mohd Jofrry S, Gurvich A, Jensen N, Ostmeier K, Lühder F, Probst C, Martens H, Gillis M, Saher G, Assogna F, Spalletta G, Stöcker W, Schulz TF, Nave K-AA, Ehrenreich H. 2014. Neuropsychiatric disease relevance of circulating anti-NMDA receptor autoantibodies depends on blood-brain barrier integrity. *Mol Psychiatry* **19**:1143–1149. doi:10.1038/mp.2013.110

Hara M, Martinez-Hernandez E, Ariño H, Armangué T, Spatola M, Petit-Pedrol M, Saiz A, Rosenfeld MR, Graus F, Dalmau J. 2018. Clinical and pathogenic significance of IgG, IgA, and IgM antibodies against the NMDA receptor. *Neurology* **90**:E1386–E1394. doi:10.1212/WNL.0000000000005329

Hassabis D, Kumaran D, Vann SD, Maguire EA. 2007. Patients with hippocampal amnesia cannot imagine new experiences. *Proc Natl Acad Sci U S A* **104**:1726–1731. doi:10.1073/pnas.0610561104

Hayama T, Noguchi J, Watanabe S, Takahashi N, Hayashi-Takagi A, Ellis-Davies GCR, Matsuzaki M, Kasai H. 2013. GABA promotes the competitive selection of dendritic spines by controlling local Ca 2+ signaling. *Nat Neurosci* **16**:1409–1416. doi:10.1038/nn.3496

Hayashi Y. 2019. NMDA receptor-dependent dynamics of hippocampal place cell ensembles. *J Neurosci* **39**:5173–5182. doi:10.1523/JNEUROSCI.0243-19.2019

Hebb D. 1949. The organization of behavior. New York, NY: Wiley.

Hodgkin AL, Huxley AF. 1952. A quantitative description of membrane current and its application to conduction and excitation in nerve. *J Physiol* **117**:500. doi:10.1113/JPHYSIOL.1952.SP004764

Horton NG, Wang K, Kobat D, Clark CG, Wise FW, Schaffer CB, Xu C. 2013. In vivo three-photon microscopy of subcortical structures within an intact mouse brain. *Nat Photonics* **7**:205–209. doi:10.1038/nphoton.2012.336

Hu W, Macdonald ML, Elswick DE, Sweet RA. 2015. The glutamate hypothesis of schizophrenia: Evidence from human brain tissue studies. *Ann N Y Acad Sci* **1338**:38–57. doi:10.1111/nyas.12547

Hughes EG, Peng X, Gleichman AJ, Lai M, Zhou L, Tsou R, Parsons TD, Lynch DR, Dalmau J, Balice-Gordon RJ. 2010. Cellular and synaptic mechanisms of anti-NMDA receptor encephalitis. *J Neurosci Off J Soc Neurosci* **30**:5866–5875. doi:10.1523/JNEUROSCI.0167-10.2010

Hung AY, Futai K, Sala C, Valtschanoff JG, Ryu J, Woodworth MA, Kidd FL, Sung CC, Miyakawa T, Bear MF, Weinberg RJ, Sheng M. 2008. Smaller dendritic spines, weaker synaptic transmission, but enhanced spatial learning in mice lacking Shank1. *J Neurosci* **28**:1697–1708. doi:10.1523/JNEUROSCI.3032-07.2008

Irani SR, Alexander S, Waters P, Kleopa KA, Pettingill P, Zuliani L, Peles E, Buckley C, Lang B, Vincent A. 2010. Antibodies to Kv1 potassium channel-complex proteins leucine-rich, glioma inactivated 1 protein and contactin-associated protein-2 in limbic encephalitis, Morvan's syndrome and acquired neuromyotonia. *Brain* **133**:2734–2748. doi:10.1093/brain/awq213

Jayakumar RP, Madhav MS, Savelli F, Blair HT, Cowan NJ, Knierim JJ. 2019. Recalibration of path integration in hippocampal place cells. *Nature* **566**:533–537. doi:10.1038/s41586-019-0939-3

Jézéquel J, Johansson EM, Dupuis JP, Rogemond V, Gréa H, Kellermayer B, Hamdani N, Le Guen E, Rabu C, Lepleux M, Spatola M, Mathias E, Bouchet D, Ramsey AJ, Yolken RH, Tamouza R, Dalmau J, Honnorat J, Leboyer M, Groc L. 2017. Dynamic disorganization of synaptic NMDA receptors triggered by autoantibodies from psychotic patients. *Nat Commun* **8**. doi:10.1038/s41467-017-01700-3

Johnson A, Redish AD. 2007. Neural ensembles in CA3 transiently encode paths forward of the animal at a decision point. *J Neurosci* **27**:12176–12189. doi:10.1523/JNEUROSCI.3761-07.2007

Jones BE, Tovar KR, Goehring A, Jalali-Yazdi F, Okada NJ, Gouaux E, Westbrook GL. 2019. Autoimmune receptor encephalitis in mice induced by active immunization with conformationally stabilized holoreceptors. *Sci Transl Med* **11**. doi:10.1126/scitranslmed.aaw0044

Jurek B, Chayka M, Kreye J, Lang K, Kraus L, Fidzinski P, Kornau HC, Dao LM, Wenke NK, Long M, Rivalan M, Winter Y, Leubner J, Herken J, Mayer S, Mueller S, Boehm-Sturm P, Dirnagl U, Schmitz D, Kölch M, Prüss H. 2019. Human gestational N-methyl-d-aspartate receptor autoantibodies impair neonatal murine brain function. *Ann Neurol* **86**:656–670. doi:10.1002/ana.25552

Kasai H, Matsuzaki M, Noguchi J, Yasumatsu N, Nakahara H. 2003. Structure-stability-function relationships of dendritic spines. *Trends Neurosci*. doi:10.1016/S0166-2236(03)00162-0

Kasai H, Ziv NE, Okazaki H, Yagishita S, Toyoizumi T. 2021. Spine dynamics in the brain, mental disorders and artificial neural networks, Nature Reviews Neuroscience. Nat Rev Neurosci. doi:10.1038/s41583-021-00467-3

Kay K, Chung JE, Sosa M, Schor JS, Karlsson MP, Larkin MC, Liu DF, Frank LM. 2020. Constant Sub-second Cycling between Representations of Possible Futures in the Hippocampus. *Cell* **180**:552-567.e25. doi:10.1016/j.cell.2020.01.014

Kayser MS, Dalmau J. 2016. Anti-NMDA receptor encephalitis, autoimmunity, and psychosis. *Schizophr Res* **176**:36–40. doi:10.1016/j.schres.2014.10.007

Kelleher E, McNamara P, Dunne J, Fitzmaurice B, Heron EA, Whitty P, Walsh R, Mooney C, Hogan D, Conlon N, Gill M, Vincent A, Doherty CP, Corvin A. 2020. Prevalence of N-Methyl-D-Aspartate Receptor antibody (NMDAR-Ab) encephalitis in patients with first episode psychosis and treatment resistant schizophrenia on clozapine, a population based study. *Schizophr Res* **222**:455–461. doi:10.1016/j.schres.2019.11.023

Kentros C, Hargreaves E, Hawkins RD, Kandel ER, Shapiro M, Muller R V. 1998. Abolition of long-term stability of new hippocampal place cell maps by NMDA receptor blockade. *Science (80-)*. doi:10.1126/science.280.5372.2121

Kinsky NR, Sullivan DW, Mau W, Hasselmo ME, Eichenbaum HB. 2018. Hippocampal Place Fields Maintain a Coherent and Flexible Map across Long Timescales. *Curr Biol* **28**:3578-3588.e6. doi:10.1016/j.cub.2018.09.037

Knierim JJ, Neunuebel JP. 2016. Tracking the flow of hippocampal computation: Pattern separation, pattern completion, and attractor dynamics. *Neurobiol Learn Mem*. doi:10.1016/j.nlm.2015.10.008

Kobat D, Horton NG, Xu C. 2011. In vivo two-photon microscopy to 1.6-mm depth in mouse cortex. *J Biomed Opt* **16**:106014. doi:10.1117/1.3646209

Kreye J, Wenke NK, Chayka M, Leubner J, Murugan R, Maier N, Jurek B, Ly L-TT, Brandl D, Rost BR, Stumpf A, Schulz P, Radbruch H, Hauser AE, Pache F, Meisel A, Harms L, Paul F, Dirnagl U, Garner C, Schmitz D, Wardemann H, Prüss H. 2016. Human cerebrospinal fluid monoclonal N-methyl-D-aspartate receptor autoantibodies are sufficient for encephalitis pathogenesis. *Brain A J Neurol* **139**:2641–2652. doi:10.1093/brain/aww208

Kwon HB, Sabatini BL. 2011. Glutamate induces de novo growth of functional spines in developing cortex. *Nature* **474**:100–104. doi:10.1038/nature09986

Lai M, Hughes EG, Peng X, Zhou L, Gleichman AJ, Shu H, Matá S, Kremens D, Vitaliani R, Geschwind MD, Bataller L, Kalb RG, Davis R, Graus F, Lynch DR, Dalmau J, Balice-Gordon R. 2009. AMPA receptor antibodies in limbic encephalitis alter synaptic receptor location. *Ann Neurol* **65**:424–434. doi:10.1002/ana.21589

Lai M, Huijbers MGM, Lancaster E, Graus F, Bataller L, Balice-Gordon R, Cowell JK, Dalmau J. 2010. Investigation of LGI1 as the antigen in limbic encephalitis previously attributed to

potassium channels: A case series. *Lancet Neurol* **9**:776–785. doi:10.1016/S1474-4422(10)70137-X

Lennon VA, Kryzer TJ, Pittock SJ, Verkman AS, Hinson SR. 2005. IgG marker of optic-spinal multiple sclerosis binds to the aquaporin-4 water channel. *J Exp Med* **202**:473–477. doi:10.1084/jem.20050304

Leutgeb S, Leutgeb JK, Barnes CA, Moser EI, McNaughton BL, Moser MB, JK L, CA B, EI M, BL M, M-B M. 2005. Independent Codes for Spatial and Episodic Memory in Hippocampal Neuronal Ensembles. *Science (80-)* **309**:619–623. doi:10.1126/science.1114037

Li Q, Clark S, Lewis D V., Wilson WA. 2002. NMDA receptor antagonists disinhibit rat posterior cingulate and retrosplenial cortices: A potential mechanism of neurotoxicity. *J Neurosci* **22**:3070–3080. doi:10.1523/jneurosci.22-08-03070.2002

Lin MZ, Schnitzer MJ. 2016. Genetically encoded indicators of neuronal activity. *Nat Neurosci* **19**:1142–1153. doi:10.1038/nn.4359

Linnoila J, Pulli B, Armangué T, Planagumà J, Narsimhan R, Schob S, Zeller MWG, Dalmau J, Chen J. 2019. Mouse model of anti-NMDA receptor post–herpes simplex encephalitis. *Neurol - Neuroimmunol Neuroinflammation* **6**:e529. doi:10.1212/NXI.0000000000000529

Lissek T, Obenhaus HA, Ditzel DAW, Nagai T, Miyawaki A, Sprengel R, Hasan MT. 2016. Frontiers | General Anesthetic Conditions Induce Network Synchrony and Disrupt Sensory Processing in the Cortex | Cellular Neuroscience. *Front Cell Neurosci* **10**. doi:10.3389/fncel.2016.00064

Lowe DA, Neijt HC, Aebischer B. 1990. D-CPP-ene (SDZ EAA 494), a potent and competitive N-methyl-D-aspartate (NMDA) antagonist: effect on spontaneous activity and NMDA-induced depolarizations in the rat neocortical slice preparation, compared with other CPP derivatives and MK-801. *Neurosci Lett* **113**:315–321. doi:10.1016/0304-3940(90)90604-8

Mably AJ, Gereke BJ, Jones DT, Colgin LL. 2017. Impairments in spatial representations and rhythmic coordination of place cells in the 3xTg mouse model of Alzheimer's disease. *Hippocampus* **27**:378–392. doi:10.1002/HIPO.22697

MacDonald ML, Alhassan J, Newman JT, Richard M, Gu H, Kelly RM, Sampson AR, Fish KN, Penzes P, Wills ZP, Lewis DA, Sweet RA. 2017. Selective loss of smaller spines in SchizophreniaAmerican Journal of Psychiatry. Am J Psychiatry. pp. 586–594. doi:10.1176/appi.ajp.2017.16070814

Maguire EA, Nannery R, Spiers HJ. 2006. Navigation around London by a taxi driver with bilateral hippocampal lesions. *Brain* **129**:2894–2907. doi:10.1093/brain/awl286

Malhotra AK, Pinals DA, Adler CM, Elman I, Clifton A, Pickar D, Breier A. 1997. Ketamine-induced exacerbation of psychotic symptoms and cognitive impairment in neuroleptic-free schizophrenics. *Neuropsychopharmacology* **17**:141–150. doi:10.1016/S0893-133X(97)00036-5

Malviya M, Barman S, Golombeck KS, Planagumà J, Mannara F, Strutz-Seebohm N, Wrzos C, Demir F, Baksmeier C, Steckel J, Falk KK, Gross CC, Kovac S, Bönte K, Johnen A, Wandinger K-PP, Martín-García E, Becker AJ, Elger CE, Klöcker N, Wiendl H, Meuth SG, Hartung H-PP, Seebohm G, Leypoldt F, Maldonado R, Stadelmann C, Dalmau J, Melzer N, Goebels N. 2017. NMDAR encephalitis: passive transfer from man to mouse by a recombinant antibody. *Ann Clin Transl Neurol* **4**:768–783. doi:10.1002/acn3.444

Manns JR, Howard MW, Eichenbaum H. 2007. Gradual changes in hippocampal activity support remembering the order of events. *Neuron* **56**:530–540. doi:10.1016/J.NEURON.2007.08.017

Manto M, Dalmau J, Didelot A, Rogemond V, Honnorat J. 2010. In vivo effects of antibodies from patients with anti-NMDA receptor encephalitis: Further evidence of synaptic glutamatergic dysfunction. *Orphanet J Rare Dis* **5**. doi:10.1186/1750-1172-5-31

Markus EJ, Barnes CA, McNaughton BL, Gladden VL, Skaggs WE. 1994. Spatial information content and reliability of hippocampal CA1 neurons: Effects of visual input.

Hippocampus **4**:410–421. doi:10.1002/hipo.450040404

Marquetand J, van Lessen M, Bender B, Reimold M, Elsen G, Stoecker W, Synofzik M. 2016. Slowly progressive LGI1 encephalitis with isolated late-onset cognitive dysfunction: A treatable mimic of Alzheimer's disease. *Eur J Neurol*. doi:10.1111/ene.12939

Masurkar A V., Srinivas K V., Brann DH, Warren R, Lowes DC, Siegelbaum SA. 2017. Medial and lateral entorhinal cortex differentially excite deep versus superficial CA1 pyramidal neurons. *Cell Rep* **18**:148–160. doi:10.1016/j.celrep.2016.12.012

Matsuzaki M, Honkura N, Ellis-Davies GCR, Kasai H. 2004. Structural basis of long-term potentiation in single dendritic spines. *Nature* **429**:761–766. doi:10.1038/nature02617

Matus A. 2000. Actin-based plasticity in dendritic spines. *Science (80-)*. doi:10.1126/science.290.5492.754

May C, Nordhoff E, Casjens S, Turewicz M, Eisenacher M, Gold R, Brüning T, Pesch B, Stephan C, Woitalla D, Penke B, Janáky T, Virók D, Siklós L, Engelhardt JI, Meyer HE. 2014. Highly immunoreactive IgG antibodies directed against a set of twenty human proteins in the sera of patients with amyotrophic lateral sclerosis identified by protein array. *PLoS One* **9**. doi:10.1371/journal.pone.0089596

McCall S, Vilensky JA, Gilman S, Taubenberger JK. 2008. The relationship between encephalitis lethargica and influenza: A critical analysis. *J Neurovirol*. doi:10.1080/13550280801995445

McDonald-McGinn DM, Sullivan KE, Marino B, Philip N, Swillen A, Vorstman JAS, Zackai EH, Emanuel BS, Vermeesch JR, Morrow BE, Scambler PJ, Bassett AS. 2015. 22q11.2 deletion syndrome. *Nat Rev Dis Prim* **1**. doi:10.1038/nrdp.2015.71

McHugh TJ, Blum KI, Tsien JZ, Tonegawa S, Wilson MA. 1996. Impaired hippocampal representation of space in CA1-specific NMDAR1 knockout mice. *Cell* **87**:1339–1349. doi:10.1016/S0092-8674(00)81828-0

McKeon A, Marnane M, O'Connell M, Stack JP, Kelly PJ, Lynch T. 2007. Potassium channel antibody-associated encephalopathy presenting with a frontotemporal dementia-like syndrome. *Arch Neurol* **64**:1528–1530. doi:10.1001/archneur.64.10.1528

McNaughton BL, Barnes CA, Meltzer J, Sutherland RJ. 1989. Hippocampal granule cells are necessary for normal spatial learning but not for spatially-selective pyramidal cell discharge. *Exp Brain Res* **76**:485–496. doi:10.1007/BF00248904

Mesbah-Oskui L, Georgiou J, Roder JC. 2015. Hippocampal place cell and inhibitory neuron activity in disrupted-in-schizophrenia-1 mutant mice: implications for working memory deficits. *npj Schizophr* **1**:1–7. doi:10.1038/npjschz.2015.11

Meshulam L, Gauthier JL, Brody CD, Tank DW, Bialek W. 2017. Collective Behavior of Place and Non-place Neurons in the Hippocampal Network. *Neuron* **96**:1178-1191.e4. doi:10.1016/j.neuron.2017.10.027

Meyers EM. 2013. The neural decoding toolbox. *Front Neuroinform* **7**:8. doi:10.3389/fninf.2013.00008

Mikasova L, De Rossi P, Bouchet D, Georges F, Rogemond V, Didelot A, Meissirel C, Honnorat J, Groc L. 2012. Disrupted surface cross-talk between NMDA and Ephrin-B2 receptors in anti-NMDA encephalitis. *Brain A J Neurol* **135**:1606–1621. doi:10.1093/brain/aws092

Mikasova L, Xiong H, Kerkhofs A, Bouchet D, Krugers HJ, Groc L. 2017. Stress hormone rapidly tunes synaptic NMDA receptor through membrane dynamics and mineralocorticoid signalling. *Sci Rep* **7**:1–12. doi:10.1038/s41598-017-08695-3

Mizrahi A, Crowley JC, Shtoyerman E, Katz LC. 2004. High-Resolution in Vivo Imaging of Hippocampal Dendrites and Spines. *J Neurosci* **24**:3147–3151. doi:10.1523/JNEUROSCI.5218-03.2004

Monyer H, Sprengel R, Schoepfer R, Herb A, Higuchi M, Lomeli H, Burnashev N, Sakmann B, Seeburg PH. 1992. Heteromeric NMDA receptors: Molecular and functional distinction of subtypes. *Science (80-)* **256**:1217–1221. doi:10.1126/science.256.5060.1217

Morris RGM, Anderson E, Lynch GS, Baudry M. 1986. Selective impairment of learning and blockade of long-term potentiation by an N-methyl-D-aspartate receptor antagonist,

AP5. *Nature* **319**:774–776. doi:10.1038/319774a0
Morris RGM, Steele RJ, Bell JE, Martin SJ. 2013. N-methyl-d-aspartate receptors, Learning and memory: Chronic intraventricular infusion of the NMDA receptor antagonist d-AP5 interacts directly with the neural mechanisms of spatial learning. *Eur J Neurosci* **37**:700–717. doi:10.1111/ejn.12086
Moscato EH, Peng X, Jain A, Parsons TD, Dalmau J, Balice-Gordon RJ. 2014. Acute mechanisms underlying antibody effects in anti-N-methyl-D-aspartate receptor encephalitis. *Ann Neurol* **76**:108–119. doi:10.1002/ana.24195
Murray RM, Van Os J. 1998. Predictors of outcome in schizophrenia. *J Clin Psychopharmacol* **18**. doi:10.1097/00004714-199804001-00002
Nagaoka A, Takehara H, Hayashi-Takagi A, Noguchi J, Ishii K, Shirai F, Yagishita S, Akagi T, Ichiki T, Kasai H. 2016. Abnormal intrinsic dynamics of dendritic spines in a fragile X syndrome mouse model in vivo. *Sci Rep* **6**:26651. doi:10.1038/srep26651
Nakai J, Ohkura M, Imoto K. 2001. A high signal-to-noise Ca2+ probe composed of a single green fluorescent protein. *Nat Biotechnol* **19**:137–141.
Nakazawa K, Sapkota K. 2020. The origin of NMDA receptor hypofunction in schizophrenia. *Pharmacol Ther*. doi:10.1016/j.pharmthera.2019.107426
Nakazawa K, Sun LD, Quirk MC, Rondi-Reig L, Wilson MA, Tonegawa S. 2003. Hippocampal CA3 NMDA Receptors Are Crucial for Memory Acquisition of One-Time Experience. *Neuron* **38**:305–315. doi:10.1016/S0896-6273(03)00165-X
Niewoehner B, Single FN, Hvalby, Jensen V, Meyer Zum Alten Borgloh S, Seeburg PH, Rawlins JNP, Sprengel R, Bannerman DM. 2007. Impaired spatial working memory but spared spatial reference memory following functional loss of NMDA receptors in the dentate gyrus. *Eur J Neurosci* **25**:837–846. doi:10.1111/j.1460-9568.2007.05312.x
Nishiyama M, Togashi K, Aihara T, Hong K. 2010. GABAergic activities control spike timing- and frequency-dependent long-term depression at hippocampal excitatory synapses. *Front Synaptic Neurosci* **2**. doi:10.3389/fnsyn.2010.00022
O'Keefe J, Dostrovsky J. 1971. The hippocampus as a spatial map. Preliminary evidence from unit activity in the freely-moving rat. *Brain Res* **34**:171–175. doi:10.1016/0006-8993(71)90358-1
O'Keefe J, Nadel L. 1978. The Hippocampus as a Cognitive Map. Oxford University Press.
O'Keefe J, Recce ML. 1993. Phase relationship between hippocampal place units and the EEG theta rhythm. *Hippocampus* **3**:317–330. doi:10.1002/hipo.450030307
Oheim M, Beaurepaire E, Chaigneau E, Mertz J, Charpak S. 2001. Two-photon microscopy in brain tissue: Parameters influencing the imaging depth. *J Neurosci Methods* **111**:29–37. doi:10.1016/S0165-0270(01)00438-1
Okamoto KI, Nagai T, Miyawaki A, Hayashi Y. 2004. Rapid and persistent modulation of actin dynamics regulates postsynaptic reorganization underlying bidirectional plasticity. *Nat Neurosci* **7**:1104–1112. doi:10.1038/nn1311
Okazaki H, Hayashi-Takagi A, Nagaoka A, Negishi M, Ucar H, Yagishita S, Ishii K, Toyoizumi T, Fox K, Kasai H. 2018. Calcineurin knockout mice show a selective loss of small spines. *Neurosci Lett* **671**:99–102. doi:10.1016/j.neulet.2018.02.006
Pan H, Oliveira B, Saher G, Dere E, Tapken D, Mitjans M, Seidel J, Wesolowski J, Wakhloo D, Klein-Schmidt C, Ronnenberg A, Schwabe K, Trippe R, Mätz-Rensing K, Berghoff S, Al-Krinawe Y, Martens H, Begemann M, Stöcker W, Kaup F-JJ, Mischke R, Boretius S, Nave K-AA, Krauss JK, Hollmann M, Lühder F, Ehrenreich H. 2018. Uncoupling the widespread occurrence of anti-NMDAR1 autoantibodies from neuropsychiatric disease in a novel autoimmune model. *Mol Psychiatry* **24**:1489–1501. doi:10.1038/s41380-017-0011-3
Papouin T, Ladépêche L, Ruel J, Sacchi S, Labasque M, Hanini M, Groc L, Pollegioni L, Mothet JP, Oliet SHR. 2012. Synaptic and extrasynaptic NMDA receptors are gated by different endogenous coagonists. *Cell* **150**:633–646. doi:10.1016/j.cell.2012.06.029
Pearce JM, Roberts ADL, Good M. 1998. Hippocampal lesions disrupt navigation based on cognitive maps but not heading vectors. *Nature* **396**:75–77. doi:10.1038/23941

Pelkey KA, Chittajallu R, Craig MT, Tricoire L, Wester JC, McBain CJ. 2017. Hippocampal gabaergic inhibitory interneurons. *Physiol Rev* **97**:1619–1747. doi:10.1152/physrev.00007.2017

Petit-Pedrol M, Groc L. 2021. Regulation of membrane NMDA receptors by dynamics and protein interactions. *J Cell Biol*. doi:10.1083/JCB.202006101

Pfeiffer BE, Foster DJ. 2013. Hippocampal place-cell sequences depict future paths to remembered goals. *Nature* **497**:74–79. doi:10.1038/nature12112

Phillips WA, Silverstein SM. 2003. Convergence of biological and psychological perspectives on cognitive coordination in schizophrenia. *Behav Brain Sci* **26**:65–82. doi:10.1017/S0140525X03000025

Pillow JW, Shlens J, Paninski L, Sher A, Litke AM, Chichilnisky EJ, Simoncelli EP. 2008. Spatio-temporal correlations and visual signalling in a complete neuronal population. *Nature* **454**:995–999. doi:10.1038/nature07140

Planagumà J, Haselmann H, Mannara F, Petit-Pedrol M, Grünewald B, Aguilar E, Röpke L, Martín-García E, Titulaer MJ, Jercog P, Graus F, Maldonado R, Geis C, Dalmau J. 2016. Ephrin-B2 prevents N-methyl-D-aspartate receptor antibody effects on memory and neuroplasticity. *Ann Neurol* **80**:388–400. doi:10.1002/ana.24721

Planagumà J, Leypoldt F, Mannara F, Gutiérrez-Cuesta J, Martín-García E, Aguilar E, Titulaer MJ, Petit-Pedrol M, Jain A, Balice-Gordon R, Lakadamyali M, Graus F, Maldonado R, Dalmau J. 2015. Human N-methyl D-aspartate receptor antibodies alter memory and behaviour in mice. *Brain* **138**:94–109. doi:10.1093/brain/awu310

Pnevmatikakis EA, Soudry D, Gao Y, Machado TA, Merel J, Pfau D, Reardon T, Mu Y, Lacefield C, Yang W, Ahrens M, Bruno R, Jessell TM, Peterka DS, Yuste R, Paninski L. 2016. Simultaneous Denoising, Deconvolution, and Demixing of Calcium Imaging Data. *Neuron* **89**:285. doi:10.1016/j.neuron.2015.11.037

Poels EMP, Kegeles LS, Kantrowitz JT, Javitt DC, Lieberman JA, Abi-Dargham A, Girgis RR. 2014. Glutamatergic abnormalities in schizophrenia: A review of proton MRS findings. *Schizophr Res*. doi:10.1016/j.schres.2013.12.013

Poll S, Mittag M, Musacchio F, Justus LC, Giovannetti EA, Steffen J, Wagner J, Zohren L, Schoch S, Schmidt B, Jackson WS, Ehninger D, Fuhrmann M. 2020. Memory trace interference impairs recall in a mouse model of Alzheimer's disease. *Nat Neurosci* **23**:952–958. doi:10.1038/s41593-020-0652-4

Prüss H. 2021. Autoantibodies in neurological disease. *Nat Rev Immunol*. doi:10.1038/s41577-021-00543-w

Prüss H, Finke C, Höltje M, Hofmann J, Klingbeil C, Probst C, Borowski K, Ahnert-Hilger G, Harms L, Schwab JM, Ploner CJ, Komorowski L, Stoecker W, Dalmau J, Wandinger KP. 2012. N-methyl-D-aspartate receptor antibodies in herpes simplex encephalitis. *Ann Neurol* **72**:902–911. doi:10.1002/ana.23689

Prüss H, Leubner J, Wenke NK, Czirják GÁ, Szentiks CA, Greenwood AD. 2015. Anti-NMDA Receptor Encephalitis in the Polar Bear (Ursus maritimus) Knut. *Sci Rep* **5**. doi:10.1038/srep12805

Ramon y Cajal S, Looie496. n.d. CajalHippocampus (modified).png. https://commons.wikimedia.org/wiki/File:CajalHippocampus_(modified).png

Raveau M, Polygalov D, Boehringer R, Amano K, Yamakawa K, McHugh TJ. 2018. Alterations of in vivo CA1 network activity in Dp(16)1Yey Down syndrome model mice. *Elife* **7**. doi:10.7554/ELIFE.31543

Ripke S, Neale BM, Corvin A, Walters JTR, Farh KH, Holmans PA, Lee P, Bulik-Sullivan B, Collier DA, Huang H, Pers TH, Agartz I, Agerbo E, Albus M, Alexander M, Amin F, Bacanu SA, Begemann M, Belliveau RA, Bene J, Bergen SE, Bevilacqua E, Bigdeli TB, Black DW, Bruggeman R, Buccola NG, Buckner RL, Byerley W, Cahn W, Cai G, Campion D, Cantor RM, Carr VJ, Carrera N, Catts S V., Chambert KD, Chan RCK, Chen RYL, Chen EYH, Cheng W, Cheung EFC, Chong SA, Cloninger CR, Cohen D, Cohen N, Cormican P, Craddock N, Crowley JJ, Curtis D, Davidson M, Davis KL, Degenhardt F, Del Favero J, Demontis D,

Dikeos D, Dinan T, Djurovic S, Donohoe G, Drapeau E, Duan J, Dudbridge F, Durmishi N, Eichhammer P, Eriksson J, Escott-Price V, Essioux L, Fanous AH, Farrell MS, Frank J, Franke L, Freedman R, Freimer NB, Friedl M, Friedman JI, Fromer M, Genovese G, Georgieva L, Giegling I, Giusti-Rodríguez P, Godard S, Goldstein JI, Golimbet V, Gopal S, Gratten J, De Haan L, Hammer C, Hamshere ML, Hansen M, Hansen T, Haroutunian V, Hartmann AM, Henskens FA, Herms S, Hirschhorn JN, Hoffmann P, Hofman A, Hollegaard M V., Hougaard DM, Ikeda M, Joa I, Julià A, Kahn RS, Kalaydjieva L, Karachanak-Yankova S, Karjalainen J, Kavanagh D, Keller MC, Kennedy JL, Khrunin A, Kim Y, Klovins J, Knowles JA, Konte B, Kucinskas V, Kucinskiene ZA, Kuzelova-Ptackova H, Kähler AK, Laurent C, Keong JLC, Lee SH, Legge SE, Lerer B, Li M, Li T, Liang KY, Lieberman J, Limborska S, Loughland CM, Lubinski J, Lönnqvist J, Macek M, Magnusson PKE, Maher BS, Maier W, Mallet J, Marsal S, Mattheisen M, Mattingsdal M, McCarley RW, McDonald C, McIntosh AM, Meier S, Meijer CJ, Melegh B, Melle I, Mesholam-Gately RI, Metspalu A, Michie PT, Milani L, Milanova V, Mokrab Y, Morris DW, Mors O, Murphy KC, Murray RM, Myin-Germeys I, Müller-Myhsok B, Nelis M, Nenadic I, Nertney DA, Nestadt G, Nicodemus KK, Nikitina-Zake L, Nisenbaum L, Nordin A, O'Callaghan E, O'Dushlaine C, O'Neill FA, Oh SY, Olincy A, Olsen L, Van Os J, Pantelis C, Papadimitriou GN, Papiol S, Parkhomenko E, Pato MT, Paunio T, Pejovic-Milovancevic M, Perkins DO, Pietiläinen O, Pimm J, Pocklington AJ, Powell J, Price A, Pulver AE, Purcell SM, Quested D, Rasmussen HB, Reichenberg A, Reimers MA, Richards AL, Roffman JL, Roussos P, Ruderfer DM, Salomaa V, Sanders AR, Schall U, Schubert CR, Schulze TG, Schwab SG, Scolnick EM, Scott RJ, Seidman LJ, Shi J, Sigurdsson E, Silagadze T, Silverman JM, Sim K, Slominsky P, Smoller JW, So HC, Spencer CCA, Stahl EA, Stefansson H, Steinberg S, Stogmann E, Straub RE, Strengman E, Strohmaier J, Stroup TS, Subramaniam M, Suvisaari J, Svrakic DM, Szatkiewicz JP, Söderman E, Thirumalai S, Toncheva D, Tosato S, Veijola J, Waddington J, Walsh D, Wang D, Wang Q, Webb BT, Weiser M, Wildenauer DB, Williams NM, Williams S, Witt SH, Wolen AR, Wong EHM, Wormley BK, Xi HS, Zai CC, Zheng X, Zimprich F, Wray NR, Stefansson K, Visscher PM, Adolfsson R, Andreassen OA, Blackwood DHR, Bramon E, Buxbaum JD, Børglum AD, Cichon S, Darvasi A, Domenici E, Ehrenreich H, Esko T, Gejman P V., Gill M, Gurling H, Hultman CM, Iwata N, Jablensky A V., Jönsson EG, Kendler KS, Kirov G, Knight J, Lencz T, Levinson DF, Li QS, Liu J, Malhotra AK, McCarroll SA, McQuillin A, Moran JL, Mortensen PB, Mowry BJ, Nöthen MM, Ophoff RA, Owen MJ, Palotie A, Pato CN, Petryshen TL, Posthuma D, Rietschel M, Riley BP, Rujescu D, Sham PC, Sklar P, St Clair D, Weinberger DR, Wendland JR, Werge T, Daly MJ, Sullivan PF, O'Donovan MC. 2014. Biological insights from 108 schizophrenia-associated genetic loci. *Nature* **511**:421–427. doi:10.1038/nature13595

Robinson AP, Harp CT, Noronha A, Miller SD. 2014. The experimental autoimmune encephalomyelitis (EAE) model of MS. utility for understanding disease pathophysiology and treatment.Handbook of Clinical Neurology. Handb Clin Neurol. pp. 173–189. doi:10.1016/B978-0-444-52001-2.00008-X

Robinson NTM, Descamps LAL, Russell LE, Buchholz MO, Bicknell BA, Antonov GK, Lau JYN, Nutbrown R, Schmidt-Hieber C, Häusser M. 2020. Targeted Activation of Hippocampal Place Cells Drives Memory-Guided Spatial Behavior. *Cell* **183**:1586-1599.e10. doi:10.1016/j.cell.2020.09.061

Rolls ET, O'Mara SM. 1995. View-responsive neurons in the primate hippocampal complex. *Hippocampus* **5**:409–424. doi:10.1002/hipo.450050504

Rosch RE, Wright S, Cooray G, Papadopoulou M, Goyal S, Lim M, Vincent A, Upton AL, Baldeweg T, Friston KJ. 2018. NMDA-receptor antibodies alter cortical microcircuit dynamics. *Proc Natl Acad Sci U S A*. doi:10.1073/pnas.1804846115

Royer S, Zemelman B V, Losonczy A, Kim J, Chance F, Magee JC, Buzsáki G. 2012. Control of timing, rate and bursts of hippocampal place cells by dendritic and somatic inhibition. *Nat Neurosci* **15**:769–775. doi:10.1038/nn.3077

Ryan TJ, Roy DS, Pignatelli M, Arons A, Tonegawa S. 2015. Engram cells retain memory under

retrograde amnesia. *Science (80-)* **348**:1007–1013. doi:10.1126/science.aaa5542

Sakimura K, Kutsuwada T, Ito I, Manabe T, Takayama C, Kushiya E, Yagi T, Shinichi A, Inoue Y, Sugiyama H, Mishina M, Aizawa S, Inoue Y, Sugiyama H, Mishina M. 1995. Reduced hippocampal LTP and spatial learning in mice lacking NMDA receptor ε1 subunit, Nature. Nature Publishing Group. doi:10.1038/373151a0

Sanderson NSR, Zimmermann M, Eilinger L, Gubser C, Schaeren-Wiemers N, Lindberg RLP, Dougan SK, Ploegh HL, Kappos L, Derfuss T. 2017. Cocapture of cognate and bystander antigens can activate autoreactive B cells. *Proc Natl Acad Sci U S A* **114**:734–739. doi:10.1073/pnas.1614472114

Schindelin J, Arganda-Carreras I, Frise E, Kaynig V, Longair M, Pietzsch T, Preibisch S, Rueden C, Saalfeld S, Schmid B, Tinevez JY, White DJ, Hartenstein V, Eliceiri K, Tomancak P, Cardona A. 2012. Fiji: An open-source platform for biological-image analysis. *Nat Methods*. doi:10.1038/nmeth.2019

Schneidman E, Berry MJ, Segev R, Bialek W. 2006. Weak pairwise correlations imply strongly correlated network states in a neural population. *Nature* **440**:1007–1012. doi:10.1038/nature04701

Schultz C, Engelhardt M. 2014. Anatomy of the hippocampal formation. *Front Neurol Neurosci* **34**:6–17. doi:10.1159/000360925

Schumacher H, Meyer T, Prüss H. 2019. GABAB receptor encephalitis in a patient diagnosed with amyotrophic lateral sclerosis. *BMC Neurol* **19**. doi:10.1186/s12883-019-1269-7

Scoville WB, Milner B. 1957. Loss of recent memory after bilateral hippocampal lesions. *J Neurol Neurosurg Psychiatry* **20**:11–21. doi:10.1136/jnnp.20.1.11

Sheffield MEJ, Dombeck DA. 2015. Calcium transient prevalence across the dendritic arbour predicts place field properties. *Nature* **517**:200–204. doi:10.1038/nature13871

Sheintuch L, Geva N, Baumer H, Rechavi Y, Rubin A, Ziv Y. 2020. Multiple Maps of the Same Spatial Context Can Stably Coexist in the Mouse Hippocampus. *Curr Biol* **0**:1–10. doi:10.1016/j.cub.2020.02.018

Shuman T, Aharoni D, Cai DJ, Lee CR, Chavlis S, Page-Harley L, Vetere LM, Feng Y, Yang CY, Mollinedo-Gajate I, Chen L, Pennington ZT, Taxidis J, Flores SE, Cheng K, Javaherian M, Kaba CC, Rao N, La-Vu M, Pandi I, Shtrahman M, Bakhurin KI, Masmanidis SC, Khakh BS, Poirazi P, Silva AJ, Golshani P. 2020. Breakdown of spatial coding and interneuron synchronization in epileptic mice. *Nat Neurosci* **23**:229–238. doi:10.1038/s41593-019-0559-0

Silva D, Feng T, Foster DJ. 2015. Trajectory events across hippocampal place cells require previous experience. *Nat Neurosci* **18**:1772–1779. doi:10.1038/nn.4151

Smitt PS, Kinoshita A, De Leeuw B, Moll W, Coesmans M, Jaarsma D, Henzen-Logmans S, Vecht C, De Zeeuw C, Sekiyama N, Nakanishi S, Shigemoto R. 2000. Paraneoplastic Cerebellar Ataxia Due to Autoantibodies against a Glutamate Receptor. *N Engl J Med* **342**:21–27. doi:10.1056/nejm200001063420104

Sosa M, Giocomo LM. 2021. Navigating for reward. *Nat Rev Neurosci*. doi:10.1038/s41583-021-00479-z

Spatola M, Sabater L, Planagumà J, Martínez-Hernandez E, Armangué T, Prüss H, Iizuka T, Caparó Oblitas RL, Antoine J-CC, Li R, Heaney N, Tubridy N, Munteis Olivas E, Rosenfeld MR, Graus F, Dalmau J. 2018. Encephalitis with mGluR5 antibodies: Symptoms and antibody effects. *Neurology* **90**:e1964–e1972. doi:10.1212/WNL.0000000000005614

Stefanini F, Kushnir L, Jimenez JC, Jennings JH, Woods NI, Stuber GD, Kheirbek MA, Hen R, Fusi S. 2020. A Distributed Neural Code in the Dentate Gyrus and in CA1. *Neuron* 703–716. doi:10.1016/j.neuron.2020.05.022

Steffens H, Mott AC, Li S, Wegner W, Švehla P, Kan VWY, Wolf F, Liebscher S, Willig KI. 2021. Stable but not rigid: Chronic in vivo STED nanoscopy reveals extensive remodeling of spines, indicating multiple drivers of plasticity. *Sci Adv* **7**:eabf2806. doi:10.1126/sciadv.abf2806

Szczurowska E, Ahuja N, Jiruška P, Kelemen E, Stuchlík A. 2018. Impairment of neural

coordination in hippocampal neuronal ensembles after a psychotomimetic dose of dizocilpine. *Prog Neuro-Psychopharmacology Biol Psychiatry* **81**:275–283. doi:10.1016/j.pnpbp.2017.09.013

Takahashi N, Kawamura M, Shiota J, Kasahata N, Hirayama K. 1997. Pure topographic disorientation due to right retrosplenial lesion. *Neurology* **49**:464–469. doi:10.1212/WNL.49.2.464

Tamminga CA, Stan AD, Wagner AD. 2010. The hippocampal formation in schizophrenia. *Am J Psychiatry*. doi:10.1176/appi.ajp.2010.09081187

Tavares RM, Mendelsohn A, Grossman Y, Williams CH, Shapiro M, Trope Y, Schiller D. 2015. A Map for Social Navigation in the Human Brain. *Neuron* **87**:231–243. doi:10.1016/j.neuron.2015.06.011

Theer P, Hasan MT, Denk W. 2003. Two-photon imaging to a depth of 1000 μm in living brains by use of a Ti:Al_2O_3 regenerative amplifier. *Opt Lett* **28**:1022. doi:10.1364/ol.28.001022

Thompson LT, Best PJ. 1990. Long-term stability of the place-field activity of single units recorded from the dorsal hippocampus of freely behaving rats. *Brain Res* **509**:299–308. doi:10.1016/0006-8993(90)90555-P

Titulaer MJ, McCracken L, Gabilondo I, Armangué T, Glaser C, Iizuka T, Honig LS, Benseler SM, Kawachi I, Martinez-Hernandez E, Aguilar E, Gresa-Arribas N, Ryan-Florance N, Torrents A, Saiz A, Rosenfeld MR, Balice-Gordon R, Graus F, Dalmau J. 2013. Treatment and prognostic factors for long-term outcome in patients with anti-NMDA receptor encephalitis: An observational cohort study. *Lancet Neurol* **12**:157–165. doi:10.1016/S1474-4422(12)70310-1

Tsien JZ, Huerta PT, Tonegawa S. 1996. The Essential Role of Hippocampal CA1 NMDA Receptor–Dependent Synaptic Plasticity in Spatial Memory. *Cell* **87**:1327–1338. doi:10.1016/S0092-8674(00)81827-9

Tsodyks M. 1999. Attractor neural network models of spatial maps in hippocampus. *Hippocampus*. doi:10.1002/(SICI)1098-1063(1999)9:4<481::AID-HIPO14>3.0.CO;2-S

Tüzün E, Zhou L, Baehring JM, Bannykh S, Rosenfeld MR, Dalmau J. 2009. Evidence for antibody-mediated pathogenesis in anti-NMDAR encephalitis associated with ovarian teratoma. *Acta Neuropathol* **118**:737–743. doi:10.1007/s00401-009-0582-4

Varga C, Golshani P, Soltesz I. 2012. Frequency-invariant temporal ordering of interneuronal discharges during hippocampal oscillations in awake mice. *Proc Natl Acad Sci* **109**:E2726–E2734. doi:10.1073/PNAS.1210929109

Villarreal DM, Do V, Haddad E, Derrick BE. 2002. NMDA receptor antagonists sustain ltp and spatial memory: Active processes mediate LTP decay. *Nat Neurosci* **5**:48–52. doi:10.1038/nn776

Vitaliani R, Mason W, Ances B, Zwerdling T, Jiang Z, Dalmau J. 2005. Paraneoplastic encephalitis, psychiatric symptoms, and hypoventilation in ovarian teratoma. *Ann Neurol* **58**:594–604. doi:10.1002/ana.20614

von Engelhardt J, Doganci B, Jensen V, Hvalby Ø, Göngrich C, Taylor A, Barkus C, Sanderson DJ, Rawlins JNP, Seeburg PH, Bannerman DM, Monyer H. 2008. Contribution of Hippocampal and Extra-Hippocampal NR2B-Containing NMDA Receptors to Performance on Spatial Learning Tasks. *Neuron* **60**:846–860. doi:10.1016/J.NEURON.2008.09.039

Vyklicky V, Korinek M, Smejkalova T, Balik A, Krausova B, Kaniakova M, Lichnerova K, Cerny J, Krusek J, Dittert I, Horak M, Vyklicky L. 2014. Structure, function, and pharmacology of NMDA receptor channels. *Physiol Res*. doi:10.33549/physiolres.932678

Wardemann H, Yurasov S, Schaefer A, Young JW, Meffre E, Nussenzweig MC. 2003. Predominant autoantibody production by early human B cell precursors. *Science (80-)* **301**:1374–1377. doi:10.1126/science.1086907

Wiegert JS, Pulin M, Gee CE, Oertner TG. 2019. The fate of hippocampal synapses depends on the sequence of plasticity-inducing events. *Elife* **7**:1–18. doi:10.7554/eLife.39151

Wilson MA, McNaughton BL. 1993. Dynamics of the hippocampal ensemble code for space. *Science (80-)* **261**:1055–1058. doi:10.1126/science.8351520

Yang Y, Liu N, He Y, Liu Y, Ge L, Zou L, Song S, Xiong W, Liu X. 2018. Improved calcium sensor GCaMP-X overcomes the calcium channel perturbations induced by the calmodulin in GCaMP. *Nat Commun* **9**. doi:10.1038/s41467-018-03719-6

Yasuda R. 2019. Biophysics of Biochemical Signaling in Dendritic Spines: Implications in Synaptic Plasticity - ScienceDirect. *Biophys J*. doi:10.1016/j.bpj.2017.07.029

Yuste R. 2010. Dendritic spines. The MIT press, Cambridge.

Zaremba JD, Diamantopoulou A, Danielson NB, Grosmark AD, Kaifosh PW, Bowler JC, Liao Z, Sparks FT, Gogos JA, Losonczy A. 2017. Impaired hippocampal place cell dynamics in a mouse model of the 22q11.2 deletion. *Nat Neurosci* **20**:1612–1623. doi:10.1038/nn.4634

Zierhut KC, Graßmann R, Kaufmann J, Steiner J, Bogerts B, Schiltz K. 2013. Hippocampal CA1 deformity is related to symptom severity and antipsychotic dosage in schizophrenia. *Brain* **136**:804–814. doi:10.1093/brain/aws335

Ziv Y, Burns LD, Cocker ED, Hamel EO, Ghosh KK, Kitch LJ, El Gamal A, Schnitzer MJ. 2013. Long-term dynamics of CA1 hippocampal place codes. *Nat Neurosci* **16**:264–266. doi:10.1038/nn.3329

Declaration of Author Contribution

All results in this work including experiment design, experimental data acquisition, and data analysis were performed by the author (for exceptions see below).

Sebastian Ehrt is hereby acknowledged for acquiring part of the data and for performing part of spine scoring for the pyramidal neuron dataset (Figure 7).

Anna Brauer is hereby acknowledged for acquiring part of the data, performing part of image acquisition, and performing all spine scoring for the interneuron dataset (Figure 8).

Evgeny Logunov is hereby acknowledged for performing the PV/SST staining and for the image acquisition (Figure 21A).

Acknowledgments

These pages are a result of countless drops of sweat and tears (sometimes of joy too) over four and a half years of my life. This endeavour would not have been possible without the support of many people inside and outside the lab. I am deeply grateful to all of you, who helped me to push through my PhD.

First and foremost, I would like to thank Dr. Dr. Sabine Liebscher for her supervision of this PhD. project. Thank you for the opportunity to work on this project and for giving me the freedom to follow my interests, develop my skills and grow as a scientist. Many thanks belong to past and present members of the Liebscher lab, namely Vanessa, Sebastian, Anna, Anna-Lena, Chris, Xiaoqian, Zeynep and Shenyi. Vanessa, thank you for organizing our events and putting your heart into it, without you the lab would not function as it did over the years. I also thank people from Kerschensteiner and Bareyre labs for helping us out and tolerating our occasional presence in the 'big' lab. Thanks especially to you Clara for offering a shoulder.

I would like to acknowledge members of my Thesis Advisory Committee, who helped me to keep my project on track: Dr. Ruben Portugues, Dr. Harald Prüß, and Dr. Alessio Attardo. A special thanks goes to Prof. Martin Kerschensteiner, who went beyond his responsibilities as an advisor. Thank you for those discussions and ideas as well as for those recommendation letters.

My gratitude goes also to the Graduate School of Systemic Neurosciences (GSN) for allowing me to be a part of this amazing scientific family. GSN office, you have always been very helpful and I appreciate that. Furthermore, I thank the GSN for providing financial means for my attendance of a summer school as well as for supporting me in a time of financial difficulties. Last but not least, I thank the GSN for all the delicious free food on those wonderful GSN events.

This research project/publication was supported by LMUexcellent, funded by the Federal Ministry of Education and Research (BMBF) and the Free State of Bavaria under the Excellence Strategy of the Federal Government and the Länder.